MULTI-AXIAL FATIGUE ANALYSIS

OF THERMITE RAIL WELDS

A Dissertation

by

MARYAM TAVAKOLI

Submitted to the Office of Graduate and Professional Studies of
Texas A&M University
in partial fulfillment of the requirements for the degree of

DOCTOR OF PHILOSOPHY

Chair of Committee,	Gary T. Fry
Committee Members,	David H. Allen
	Peter B. Keating
	Vikram Kinra
Head of Department,	Robin Autenrieth

December 2018

Major Subject: Civil Engineering

ABSTRACT

This dissertation aims to examine the high-cycle fatigue behavior of thermite-welded railroad rails. In particular, the occurrence of fatigue defects in web and base regions of the rail is addressed, as frequently reported by field surveys. Fatigue life estimates are made by means of a multi-axial critical-plane fatigue algorithm that computes the fatigue damage based on the time history of stress tensors. The finite element method is used to analyze a full-scale replica of the wheel-track system comprising axle, wheel, thermite-welded rail, tie plates, and ties. The time-dependent rolling of the wheel and thermal stresses caused by seasonal temperature variations are incorporated into the finite element simulation. In addition, the effects of the track foundation stiffness and thermite weld geometry are explored.

Fatigue crack nucleation is studied at three critical locations of the rail, where most reported weld service failures occur: web-to-base fillet, base center, and base corners. Under wheel loads, the results of the fatigue analysis indicate that it can take a long period of time for a fatigue crack to nucleate in the aforementioned regions of the rail if the material is nominally “defect-free”. Fatigue cracks tend to initiate in a transverse plane, next to the thermite weld, perpendicular to flexural tensile stresses that form in the rail base. The implementation of small planar surface defects at critical locations has shown to significantly reduce the fatigue nucleation life of thermite rail welds. Also, axial tensile stresses resulting from cold winter weather are found to considerably accelerate the fatigue nucleation process, especially in the web-to-base fillet region.

To my beloved parents and my wonderful sister

ACKNOWLEDGMENTS

I would like to give a special thank you to my advisor, Dr. Gary Fry, for providing invaluable guidance during the course of this study. His inspiration, kindness, and endless support helped me go through many difficult times along the way. The precious life lessons and professional mentorship that he passed on to me will live on always and forever.

I would like to acknowledge my other committee members, Dr. David Allen, Dr. Peter Keating, and Dr. Vikram Kinra for their insightful suggestions and comments. I thank Dr. Akram Abu-Odeh for his support during the early stages of this work. My appreciation also goes to my colleagues in the research group, especially Dr. Maysam Kiani, for their friendship and assistance.

My deepest gratitude extends to my parents whose love and encouragement have allowed me to follow my aspirations. Without their constant support and sacrifice, I could never reach this academic level. I am also very grateful to my sister, Maedeh, who kindly accompanied me through my journey at Texas A&M.

This project was conducted under the auspices of the Transportation Technology Center Inc. (a subsidiary of the Association of American Railroads) which provided technical and financial support. Center for Railway Research at Texas A&M Transportation Institute and Texas A&M Supercomputing Facility are also acknowledged for their generous allocation of facilities and computational resources.

CONTRIBUTORS AND FUNDING SOURCES

Contributors

This dissertation was supported by a committee comprising Dr. Gary Fry, Dr. David Allen, and Dr. Peter Keating of the Department of Civil Engineering and Dr. Vikram Kinra of the Department of Aerospace Engineering at Texas A&M University.

All the work presented in this dissertation was completed independently by the student.

Funding Sources

Funding for the project came from the Transportation Technology Center Inc. (a subsidiary of the Association of American Railroads) and the Center for Railway Research at Texas A&M Transportation Institute. Partial financial support was also provided by Zachry Endowed Fellowship and Troy Marceleno Fellowship from the Department of Civil Engineering.

TABLE OF CONTENTS

Page

Page

Page

LIST OF FIGURES

Page

Page

Page

Page

LIST OF TABLES

Page

1. INTRODUCTION

1.1 Background

Improvements in rail manufacturing and damage detection technologies have made it possible for the railway industry to extend the service life of rails significantly. However, broken rails are still a frequent cause of service interruptions and train derailments around the world (Dick et al. [1]).

In the past, bolting was the most common method to connect two adjoining rail sections. Through the development of rail thermite welding technology, continuously welded rails quickly replaced mechanical joints in the late 19th century (Hart [2]). Thermite welding is a highly exothermic process that utilizes chemical reactions of metallic oxides with aluminum powders to fuse large industrial components. Simplicity, portability, low equipment cost, and brief traffic interruption made thermite welding the first choice to join rails in the field (Gibert [3]). However, due to the casting nature of the process, various defects, such as pores and nonmetallic inclusions, can form in thermite welds (Cheesewright [4]). In addition, thermite rail welds often introduce a geometric stress concentration associated with the weld external shape. Therefore, thermite welds generally exhibit inferior mechanical properties (fracture toughness and fatigue strength), compared to the rail base metal, under repeated heavy axle loads (HAL) of train wheels.

Statistics show that most of the rail failures originated from fatigue cracks that were nucleated in thermite welds. According to the analysis of top five causes of major train derailments for U.S. class I freight railroads (Liu et al. [5]), shown in Figure 1.1,

broken rails/welds are the leading cause of train derailment accidents. Derailments caused by broken rails have been a safety and economic concern for over a century (Aldrich [6]). Severe consequences may occur as a result of each major train derailment, particularly the release of hazardous material, which can threaten people's lives and properties. Obviously, the increasing capacity of North American railroads will make the economic consequences of thermite weld service failures more drastic in the future (Kristan [7]). The increased tonnage carried over each piece of track results in an accelerated wear and degradation of existing track components, including rail welds. Therefore, improving the fatigue behavior of thermite rail welds under HAL operating conditions is highly demanded by the railway industry to ensure the safety and economic revenue of the track.

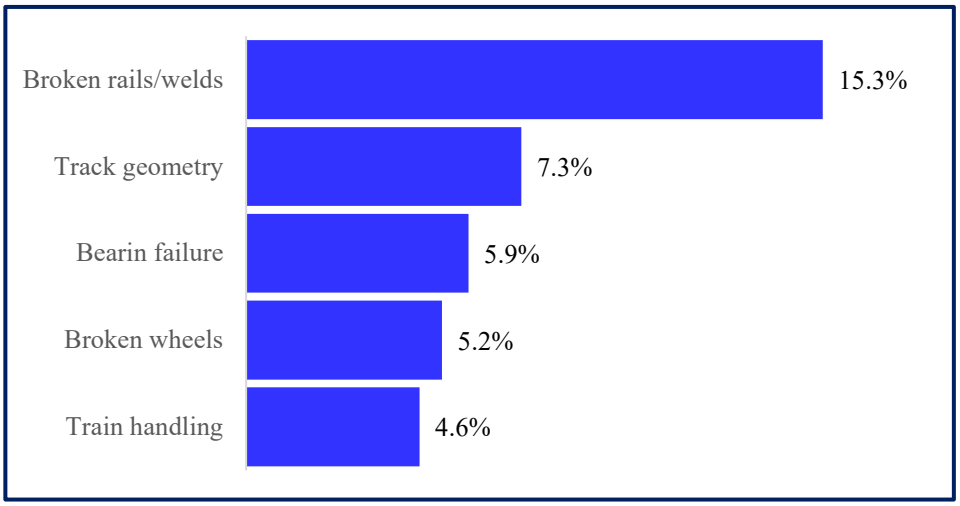

Figure 1.1. Analysis of major train derailments based on FRA data for U.S. Class I freight railroads (2001-2010)

In general, fatigue cracks tend to originate from imperfections across the thermite weld section. Railhead defects are more frequent due to the large contact forces at the wheel-rail interface. However, railhead defects and associated fatigue cracks can be eliminated by regular grinding, and thus, those defects generally do not impose failure. Field observations suggest that most of the service failures initiate at cracks in either web-to-base fillet or base region locations of the rail, right next to the thermite weld (Lawrence et al. [8]). Despite the importance of this issue, few studies have focused on understanding the mechanism of fatigue fracture in web-to-base and base regions of thermite rail welds. Therefore, there is a strong demand for more research in this area.

1.2 Scope and Objective

The main objective of this study is to estimate and improve the service life of field-welded rails with the aim to enhance the track safety and decrease the possibility of train derailments caused by broken rail welds. In this regard, a detailed computational model of a wheel-track system is developed and analyzed to interpret and understand the fatigue fracture failures of thermite rail welds that are observed in the field surveys. The time-dependent rolling of the wheel and thermal stresses caused by seasonal temperature variations are incorporated into the finite element simulation. In addition, the effects of track foundation stiffness are explored. An advanced multi-axial critical-plane fatigue algorithm is developed to quantify the fatigue damage in web and base regions of a "defect-free" rail weld where dynamic crack propagation has been frequently observed to originate. Additionally, the presence of planar imperfections is investigated by the

implementation of a small defect to critical spots of the weld. The stress field, as well as the fatigue performance, are assessed at the periphery of the implemented defect.

1.3 Organization

This dissertation comprises six sections. Section 1 provides the introduction and organization of the dissertation. Section 2 is devoted to the literature review on thermite rail welds. Section 3 presents a full-scale 3-D simulation of a wheel-track system which is analyzed by means of the finite element method to compute the time history of stress/strain tensors in various regions of the thermite rail weld. Section 4 presents a multi-axial critical plane fatigue model to predict the fatigue crack nucleation in railroad weldments, based on the results of the finite element analysis. In Section 5, the stress field at the periphery of a small pre-existing surface defect, located in the foot region of the thermite rail weld, is examined and the fatigue performance is assessed. Finally, Section 6 presents the main findings of this study as well as suggestions for the continuation of this research in the future.

2. LITERATURE REVIEW ON THERMITE RAIL WELDS

2.1 Introduction

Thermite welding is the most popular method to join and repair continuously welded rails (CWR) in the field. A brief history of thermite welding, as well as its unique application for the railway industry, are provided in this section. Different rail welding technologies are explained, and the general procedure of the thermite rail weld fabrication is addressed.

Simplicity, portability, and relative low cost are among the most important features of rail thermite welding. However, various types of weld defects and metallurgical discontinuities can form in thermite welds. Consequently, thermite welds are preferential sites of fatigue crack nucleation when compared to base metals or other rail plant-welds. In this section, the reliability of field-welded rails is explored based on the previous studies that are available in the literature. In addition, material properties of thermite rail welds are scrutinized to find potential causes that may result in the poor fatigue performance of thermite rail welds in service.

2.2 History of Thermite Welding

The thermite process refers to a set of exothermic chemical reactions that can reduce metals from their oxides, using an active agent (Ailes [9]). The first industrial application of the process was discovered in 1854 by a French chemist, Henri Sainte-

Claire Deville, who produced metallic aluminum by reduction with sodium using the following reaction (Habashi [10])

$$AlCl_3.NaCl + 3Na \rightarrow Al + 4NaCl \qquad (2.1)$$

It was realized from the start that aluminum is a strong deoxidizing agent, but the aluminum produced by this reaction was very costly and its application was limited to the laboratory studies. Many experiments have been carried by such metallurgists as Deville and others to reduce metals from their oxides using aluminum. All these experiments were confined with the obstacle that the reduction can only take place at very high temperature, and when the desired temperature was reached by external heating of the mixture, it proceeded with an explosion (Goldschmidt Thermit Company [11]). In 1893, Hans Goldschmidt, a German chemist, managed to overcome this difficulty while he was searching for a method of purifying metal ores in his laboratory in Berlin. He discovered that a properly mixed aluminum powder and iron oxide thermite charge could be ignited by a barium peroxide fuse. This innovation led to a patent application for the Thermit® process in 1895. By that time in the late 19th century, aluminum, which is an excellent choice of reducing agent (Belitkus [12]), became widely available at sufficiently low costs to render the metal of commercial value (Samans [13]).

Goldschmidt, who was initially interested in the production of very pure carbon-free metals, soon discovered the remarkable value of Thermit® process in welding of big steel parts (Goldschmidt and Vautin [14]). The thermite reaction generates a large amount of heat to melt the thermite mixture. Then, the molten iron fills the refractory sand mold built around the pieces to be welded, and the slag (aluminum oxide) floats up. In the end,

the slag will be removed from the weld surface. Hence, in contrast to other fusion welding methods, neither electric power nor additional filler material is required for this method of welding.

By the end of the 19th century, thermite welding had been successfully used to make repairs to the large cast and forged steel parts. Later, this welding technology has been adapted for welding large steel components, such as pipes and rails. Today, the primary application of thermite welding is in the railroad industry to join and repair CWR tracks in the field (Steele [15]). Thermite welding is also applicable in the marine industry for underwater welding.

2.3 Development of Rail Welding Technologies

Over the years, the advancement of technologies in the railroad industry has significantly changed the rail connection methods. Traditionally, bolting was the most common way to connect two ends of adjoining rails using steel joint bars (also called fishplates) and four or six metal bolts. However, bolted joints were found to be a large source of failure and high maintenance costs. Most failures were observed in the joint bars, rail ends, or bolts due to high impact dynamic forces (Sih [16] and Mayville [17]). Therefore, new techniques were aimed to improve the dynamic behavior of the joints. The best solution was to eliminate the joints, and thus, continuously welded rails started to appear in stream railroad tracks of Germany in 1924 (Lonsdale [18]). In a few years, CWR became a common practice all around the world. In North America, CWR was first used in the Central of Georgia Railroad for tunnel trackage in 1930. By 1980, continuously

welded rail installations were reported to represent more than 80,000 miles of the main track (Archdeacon [19]). In fact, the rapid development of CWR track was mainly prompted by the versatility of thermite welding technology (Hauser [20]). Compared with the bolted rails, CWR provides a smooth surface for the train to pass, which alternatively reduces undesired train vibrations. Enhanced ride quality and extended service life of the track with lower maintenance costs are among the most important benefits that can be directly attributed to the rail thermite welding (Hauser [20]).

Over the last century, various welding techniques have been used to join rails. This ranges from classical arc-welding to the more advanced methods such as electron beam and laser beam welding (Masubuchi [21]). Basically, rail welding technologies can be categorized into three main groups:

- Pressure welding (electric-flash butt welding, oxyacetylene welding, etc.)
- Enclosed arc welding (covered electrode, submerged, gas shielded, etc.)
- Thermite welding

The weldments fabricated using pressure welding methods usually demonstrate higher quality, since no filler material is used. However, pressure welding often has to be done in fabrication shops using the heavy and expensive equipment. Indeed, the choice of the most appropriate method usually depends on many factors such as location, available workforce, equipment, and consumables. In what follows, a brief description of the most common rail welding technologies is provided.

Electric-flash butt welding (EFB) is a resistance welding process where the heat required to form the weld is generated by the electrical resistance of the material. In this

process, the rail ends to be welded, that are connected to welding transformers, are brought very close to each other to form a short-circuit. As the electrical current passes between the butting surfaces, heavy flashing (sparking) occurs that generates a considerable amount of heat to raise the temperature of rail ends to a fusion limit (1000°C to 1500°C). Then, upsetting starts through which the rail ends are squeezed together while a flashing voltage is applied. At the end of the process, all the extra metal, called upset material, is removed from the periphery of the weldment (Abbott [22], Moin [23]). In general, EFB method is an automated process which produces high quality rail welds with fewer incidence of weld defects such that the average life of the weld is almost equal to the parent rail. In addition, EFB has the highest production rate (1.5-4 mins for each joint) and quite low cost compared to other pressure welding techniques (Masubuchi 1983 [21]). Unlike fusion welds, EFB welds do not require any filler material and the heat affected zone is very small (25-40 mm). Despite all the advantages, the method can be adopted most economically only in stationary welding plants, for which large capital investment is required.

Oxyacetylene pressure welding is a gas-pressure welding process in which the welding gas flames are obtained from the combustion of acetylene (C_2H_2) with oxygen (O_2). Welding takes place in the solid state by grain growth, grain coalescence and diffusion across the joint interface, without the use of filler metal (Oishibashi et al. [24]). In this process, rail ends are clamped together under a constant upsetting pressure of 20.7 MPa (3,000 psi) while oxyacetylene torches are directed at the joint to produce uniform heating. Upsetting occurs at a sufficiently high temperature (~1200°C) when the rail steel

is softened enough for each rail to move about 9.5 mm. At the end of the process, the upset is removed from the weldment and the rail is ground manually. The quality of oxyacetylene pressure welds is close to that of the flash butt welds if abutting surfaces are clean. However, a longer time is required for the welding (lower productivity) and the cost is higher. It also requires heavy welding machines, and thus, it has limited application for on-site welding.

Enclosed arc welding is a procedure to adapt shielded metal arc (SMA) welding technique to butt joints with large cross-sectional areas. In this method, the coalescence of metals is achieved by heating with an arc. For enclosed arc welding, the rail ends are aligned with an 18 mm gap and water-cooled copper shoes are set on sides of the groove to enclose the rail joint. After suitable preheating, the gap is filled with a molten steel from an advancing covered electrode which is consumed under the intensive heat of the arc between the electrode and rail ends. Meanwhile, the decomposition of the electrode coating creates a protective gas shield around the weld pool. Unlike normal SMA welding process, with enclosed arc welding there is no need to remove the slag until the welding is complete (Masubuchi [21]). This method of welding requires simple equipment and shows excellent mobility in the field. The welding time varies with the rail size but it typically takes about 60 minutes. The quality of rail welds produced by this method can be very good, however, the success of the procedure greatly depends on the skill of the welder. For this reason, enclosed arc welding is not very favorable for field applications.

Thermite welding, as described earlier, is an exothermic process to fuse metals using aluminothermic reactions between iron oxides and aluminum powder. The amount

of heat generated during aluminothermic reactions is more than enough for the adequate penetration at rail ends. The welding equipment has a simple structure. Through the casting process, two rail ends act as a part of the mold wall. Furthermore, unlike pressure welding methods, thermite welding does not impose a change in the length of rails. Therefore, despite the development of more advanced rail welding techniques in recent years, the unique role of thermite welding cannot be replaced, and it remains the most popular method to connect rails in the field (Meric and Engez [25]). In fact, the common practice of CWR installation is to weld the individual rail "sticks" together in a manufacturing plant, using EFB, to create 439 meters long rail "strings". Then, rail strings are transported to the rail track location to be joined in the field with thermite welding (Hay [26]). Thus, every 439 meters of a CWR track has at least two thermite welds. It has been reported by a North American railway company that over 27,000 thermite welds were installed over the period of only one year (Lonsdale and Lewandowski [27]). This proves the significance of thermite welding for the railroad industry. Today, there are three major thermite welding manufacturers active in North America:

1.Orgo-Thermit®, by Orgo-Thermit, Inc.

2. Boutet®, distributed by Esco.

3. Calorite®, by Calorite. Inc.

The main drawback of thermite welding is attributed to its cast nature. Plenty of defects and metallurgical discontinuities, such as pores, nonmetallic inclusions, and internal cracks, may form in thermite welds. The weld quality may differ considerably from one weld to another even with highly consistent welding procedures. In some cases, the service

performance of thermite welds can approach the level of electric flash butt welds, while in others failure may occur after only a few train passages. Thus, the fatigue resistance of thermite welds has shown to be lower compared to other types of rail welds. However, mobility, simplicity, and low equipment cost lead to a wide application of thermite welding in the railway industry.

2.4 Rail Thermite Welding Procedure

The Goldschmidt process of reducing metallic oxides by granular aluminum soon found a worldwide application to join and repair continuously welded rails. For the thermite reaction to being suitable for rail welding, two basic requirements are needed. First, the chemical composition of the filler material, produced from the reaction, should well match the composition of the rail steel, and thus, iron oxide has to be one of the major components in the thermite mixture. Second, the heat released from the reaction should be high enough to bring the thermite mixture into the liquid state to ensure the metal-slag separation. There are several elements that can reduce the iron from its oxide, but Al, Mg and Ca are the only ones that can generate sufficient heat to maintain a self-sustaining reaction. In terms of energy generation, Ca and Mg are better candidates but their reaction products (CaO or MgO) have a higher melting point. As a result, Al is the best choice to reduce iron from its oxide. Therefore, finely divided hematite (Fe_2O_3), mill scale (Fe_3O_4), and pure aluminum powder are considered as the major components of the thermite charge. Fe_2O_3 is easier to ignite while Fe_3O_4 creates more heat. Also, the addition of

manganese or copper oxides can significantly improve the ease of ignition. The most common reactions involved in the rail thermite welding are (Steele [15]):

$$Fe_2O_3 + 2Al \rightarrow 2Fe + Al_2O_3 + 181.5\ kcal \quad (2.2)$$

$$3Fe_3O_4 + 8Al \rightarrow 9Fe + 4Al_2O_3 + 719.3\ kcal \quad (2.3)$$

The particle size of thermite charges should be in the range 50-500 μm to achieve an optimum reaction rate (Belitskus [12]). The maximum temperature created by thermite reactions can be extremely high but the heat loss to surroundings brings the melting temperature down to 3500°F (Steele [15]).

Figure 2.1 shows an example of the rail thermite welding fabrication process, performed at TTCI testing facilities for the aim of the present study. In general, the production of a typical modern thermite rail weld includes the following steps (Thermit® Welding Procedures [28]):

(a) *Rail end preparation and alignment:* The ends of the rails to be joined are cut perpendicular to the rail longitudinal axis using an oxygen-propane torch and get cleaned from surface oxide by filing or wire brushing. Then, rail ends should be carefully aligned at the joint with a gap of 25 mm as specified for a standard alumino-thermic weld. Both rail ends should be elevated for about 1.5 mm to allow for a drop when the weld cooling happens.

(b) *Installation of the mold:* The mold should be adjusted and fitted to rail ends. The mold can be sealed to the rail end using the luting sand. It should be assured that the interior surface of the mold is clean and free of sand.

(c) *Preheating of rail ends:* Both rail ends, and the mold should be preheated sufficiently (1.5-5 minutes) using an oxygen-propane torch to ensure that the assembly is dry.

(d) *Placing the thermite charge into the crucible:* The thermite mixture composed of finely divided hematite (Fe_2O_3), mill scale (Fe_3O_4), aluminum powder, and some ferroalloy pellets should be placed into the crucible.

(e) *Ignition and pouring of molten steel:* The reaction crucible should be positioned over the mold opening. Then, the thermite mixture should be ignited with a burning magnesium ribbon. It takes about 20 to 25 seconds to ensure a complete reaction and a good metal-slag separation. After that, the molten steel will pour into the refractory mold while the slag (mostly aluminum oxide) will overflow into external trays.

(f) *Demolding and grinding the running surface:* When the weld is cool and solidified, the mold can be removed. Then, the surplus metal should be ground from the head to obtain the correct railhead profile. The weld collar on the web and base regions of the rail will remain as it is.

Chen et al. [29] suggest a wider weld gap serves to increase the amount of thermal energy available from the molten weld metal, which in turn helps to achieve better melt back of the rail ends. They also explored the influence of various welding parameters on the formation of weld defects in thermite rail welds [30].

(a)

(b)

(c)

(d)

(e)

(f)

Figure 2.1. Rail thermite welding procedure photographed at TTCI testing facilities, Pueblo, Colorado (August 2016)

2.5 Reliability of Thermite Rail Welds

Thermite welding is greatly advantageous for the railroad industry due to its portability, relative ease, the speed of installation, and cost-effectiveness. No external power source is required and the molten metal, produced by aluminothermic reactions, acts as a filler material to join rail sections in the field. However, there are some shortcomings associated with the process.

Field observations show that thermite rail welds are the weakest part of the CWR track. That is mainly because of their casting microstructure which is characterized by large grain size. Therefore, the service performance of thermite rail welds is very lower than parent rails. Recent studies suggest that defective field welds are one of the most challenging issues for CWR railroads (Dick [31]). A class I railroad in North America has reported that each day about 40% of service failures are associated with thermite welds (Dick [31]). Another survey on a heavy-haul main line in North America shows that 31-38% of all broken rails and about 15% of all defective rails are found in thermite welds by nondestructive inspections (Sawley and Reiff [32]). Investigations on the broken rails and major derailments in North America suggest thermite welds are responsible for 85% of all rail welds failing in service (Dick [31]). Hence, this is not surprising that thermite rail welds cost millions of dollars every year for repair and inspection. Although some improvements have been made in thermite weld quality over the years, there still is a strong demand from the railroad industry for more research in this area to ensure the safety and reliability of field-welded rails.

2.6 Properties of Thermite Rail Welds

2.6.1 Macrostructure of Thermite Rail Welds

Commonly, three typical regions can be observed in a thermite weld section: weld metal (WM), heat affected zone (HAZ), and base metal (BM). Figure 2.2 illustrates the macrostructure of a longitudinal section of a rail with a standard thermite weld in the middle, photographed at TTCI testing facilities. The aforementioned regions of the weld are clearly shown in this figure. As seen, the weld width varies along the height of the rail with a characteristic "vase" shape in which the melt-back is minimal at the center of the head and foot regions where rail sections are thickest. Note that the width of weld metal, even at its narrowest part, is always greater than the original weld gap, because the superheated liquid metal melts a certain amount of rail end after pouring (melt-back). In addition, the width of the HAZ is also variable depending on various factors such as the temperature, exposure time, base metal properties, filler metal properties, and welding method. As an example, for a standard gap of 25 mm, the weld size can change between 40 to 50 mm, and the HAZ is usually 15 to 25 mm wide. Laboratory tests show an increased melt-back (penetration) as the preheating time increases (Myers et al. [33]). However, Chen et al. [29] suggest that wider gap welds appear to be less sensitive to preheating conditions.

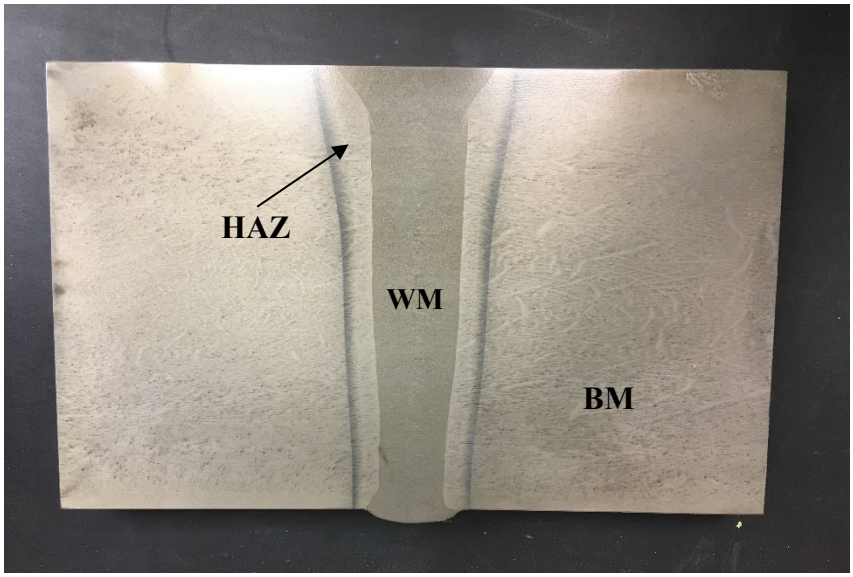

Figure 2.2. Central section of a thermite weld photographed at TTCI testing facilities, Pueblo, Colorado (August 2016)

2.6.2 Microstructure of Thermite Rail Welds

Taken from Myers et al. [33], Figure 2.3 represents the variation in the thermite weld microstructure along a longitudinal section. The microstructure of parent rail steel, shown in Figure 2.3.b, is characterized by pearlitic-ferritic. It usually contains about 1% Mn with about 0.5% C (Pickering [34]).

An experiment on 13 thermite rail welds indicates that the microstructure of the weld metal, shown in Figure 2.3.c, is also predominantly pearlitic, with bantaite in some cases (Schroeder and Poirier [35]). The same study reports 0.24%-0.49% inclusion content in the fusion zone. No martensite is observed in the thermite weld metal.

In the HAZ, however, the heat generated from the molten metal has highly altered the microstructure of the rail steel, and recrystallization happens, see Figure 2.3.a. On the

outside boundary of the HAZ, next to the parent rail, the pearlite structure is partially replaced by spheroidized (Schroeder and Poirier [35]) while on the other boundary, close to the weld metal, the grain size becomes larger.

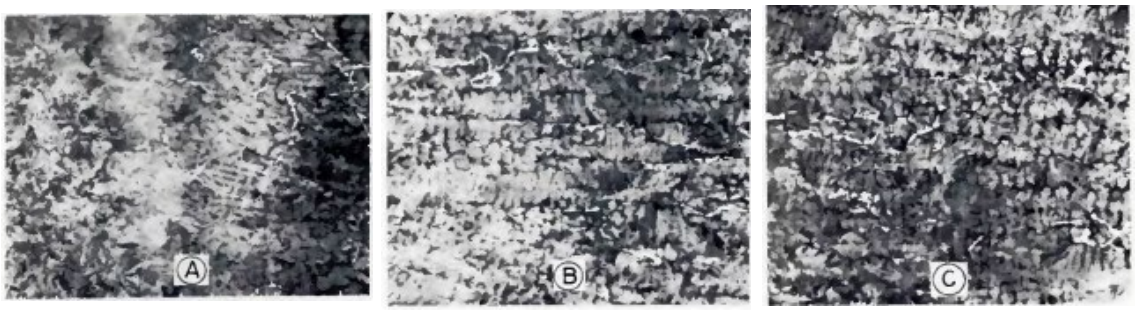

Figure 2.3. Microstructure at (a) HAZ, (b) parent rail, and (c) weld metal centerline (Magnification 48X) (reprinted from Myers et al. [33])

2.6.3 Mechanical Properties of Thermite Rail Welds

Thermite welds usually contain substantial microporosity and inclusions. These imperfections are believed to be the contributing cause of their inferior mechanical properties, such as poor ductility and fracture toughness, as compared to parent rails.

Taken from Key [36] a sample of hardness profile in a standard thermite weld is presented in Figure 2.4. As seen, the hardness of the weld metal is normally higher than the base metal. This figure also shows that the maximum hardness usually happens in the HAZ. As a consequence, thermite rail welds are so brittle and tend to fracture in cleavage mode (Schroeder and Poirier [37]). Many factors, such as alloying composition, preheating conditions, and post-weld heat treatment can affect the hardness profile of weld

metal. However, the hardness in the HAZ only depends on the parent rail properties and post-weld heat treatments.

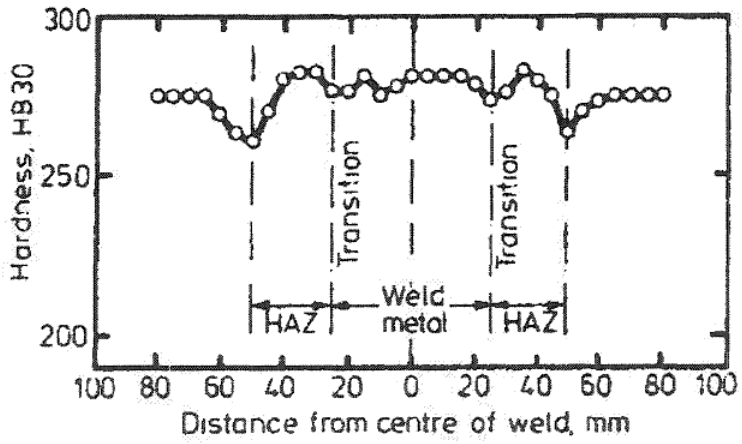

Figure 2.4. Variations of hardness along a thermite rail weld section (reprinted from Key [36])

The yield strength of the weld metal may also differ from the parent rail. In fact, yield strength is linearly correlated to the hardness. Therefore, a higher yield strength is expected in the weld metal, as compared to the base metal, due to the increased hardness. Figure 2.5 shows the linear relationship between the yield strength and hardness for over 150 non-austenitic, hypoeutectoid steels having a wide range of compositions and a variety of microstructures (Pavlina [38]). According to experiments performed by Schroeder and Poirier [35], the yield strength for standard thermite weld varies between 462 and 588 MPa.

On the other hand, the ductility is reversely correlated to the hardness. Thus, due to the enhanced hardness, both the area reduction and elongation are lower in the thermite weld metal and rail HAZ as compared to the base metal. Schroeder and Poirier [35] have reported that thermite weld metals exhibit only 2%-6% reduction in the area for the tensile ductility. Brittleness is one of the main disadvantages of thermite rail welds.

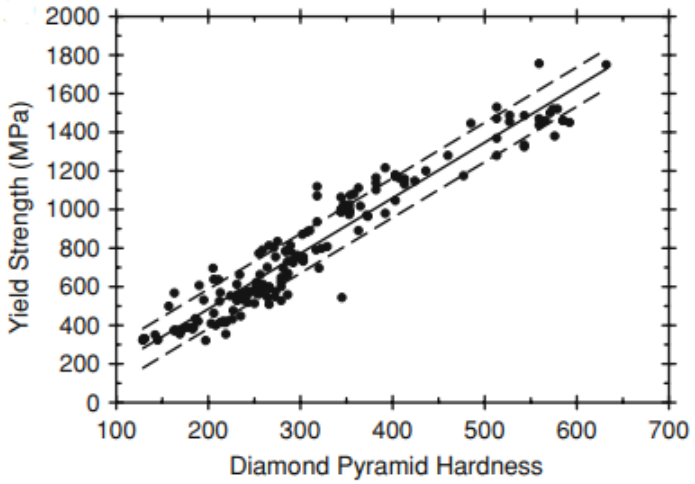

Figure 2.5. Correlation between yield strength and hardness of steel (reprinted from Pavlina and Van Tyne [38])

2.6.4 Residual Stresses in Thermite Rail Welds

As usual for other fusion welding methods, the non-uniform heat flow from molten steel to adjacent metal develops residual welding stresses in thermite rail welds. The longitudinal constraint in CWR tracks which prevents the motion in the longitudinal direction may result in higher residual stresses in the weld region. Different residual stresses can be expected depending on the welding process.

Webster et al. [39] used neutron strain scanning to map the residual stress field that is generated along a standard gap thermite weld. Figure 2.6 shows the variation in the contour of longitudinal residual stresses along the standard weld sample. As seen, near the weld centerline, the longitudinal residual stress is strongly compressive in the head and foot regions while highly tensile in the web. As the distance from the weld center increases, the residual stresses diminish so that 150 mm away from the weld center, the stress field is typical of a long unwelded rail section with some compression in the web and tension in the head and foot (Webster et al. [40]).

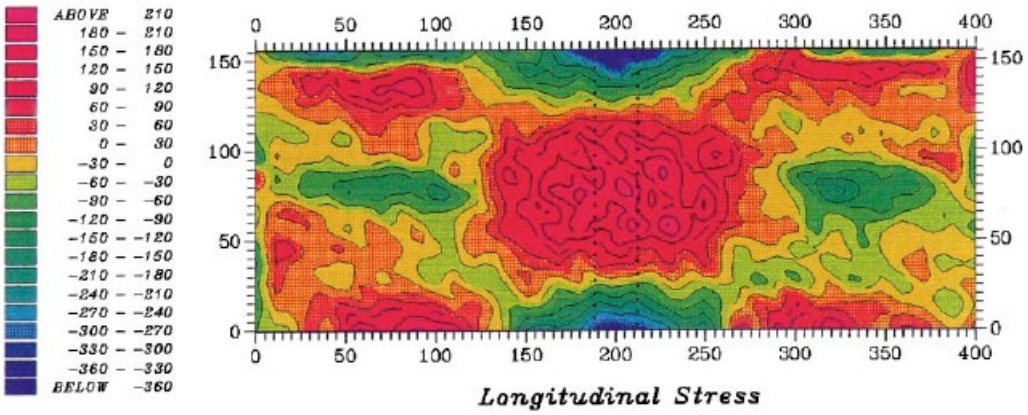

Figure 2.6. Contour of longitudinal residual stresses in a thermite rail weld specimen (reprinted from Webster et al. [39])

The variation of longitudinal residual stresses over the rail cross-section is better shown in Figure 2.7. This figure represents the profile of longitudinal residual stresses at three different locations: weld central section, 50 mm away from the weld central section, and 150 mm away from the weld central section.

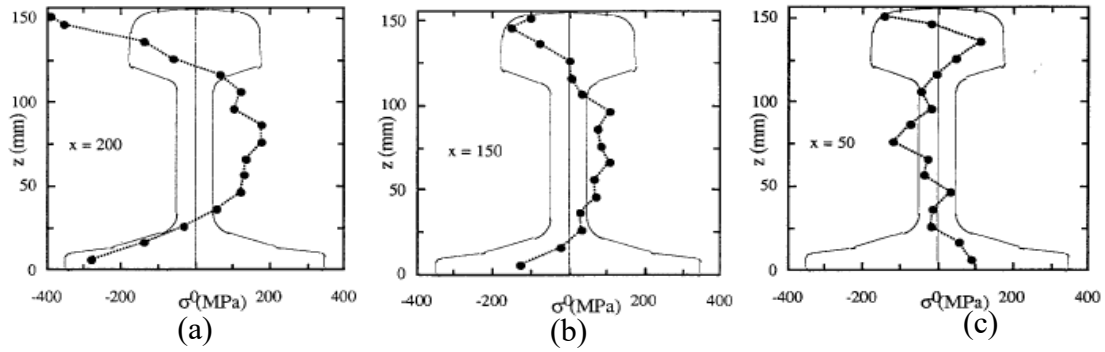

Figure 2.7. Longitudinal residual stress field of a thermite rail weld specimen located at: (a) weld central section, (b) 50 mm away from the weld center, and (c) 150 mm away from the weld center (reprinted from Webster et al. [39])

Several studies suggest similar profile of rail welding residual stresses. For instance, Skyttebol et al. [41] carried out experiments to measure the residual stresses induced by electric-flash butt welding, shown in Figure 2.8. As seen, the overall trend of variations in welding residual stresses is very similar to that of thermite rail welds.

In a more recent study, Khodabakhshi et al. [42] used neutron diffraction technique to quantify the residual stresses in thermite welds. Measurements were performed on a section of the rail right next to the weld collar, where most of the service failures were reported to happen (see Figure 2.9.a). The estimated residual stress field in longitudinal and transverse directions are presented in Figure 2.9.b and Figure 2.9.c, respectively. As seen, peak tensile residual stresses are observed to occur in the web-to-base fillet region of the weld, 50 mm away from the base edge.

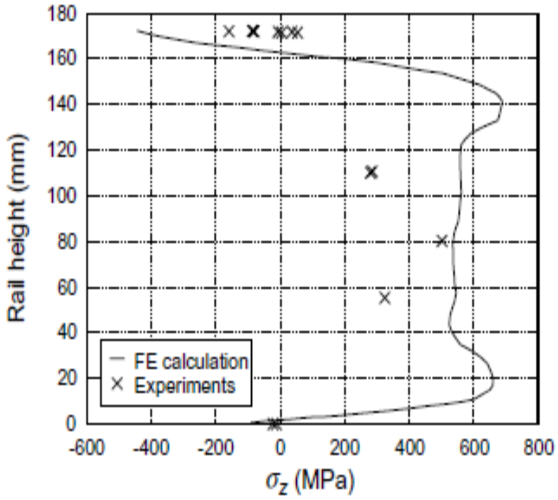

Figure 2.8. Longitudinal residual stress field in flash-but rail welds (reprinted from Skyttebol et al. [41])

Note that compressive residual stresses are beneficial to extend the fatigue life of the weld while tensile residual stresses can accelerate the nucleation of fatigue defects. Welding residual stresses can be reduced by stress relieving treatments. However, the treatment methods commonly require a long time and can only be employed in fabrication shops. Although various studies present the same pattern for the variation of rail welding residual stresses along the rail section, the magnitude of residual stresses highly varies on a case by case basis, and there is no common way to estimate the rail welding residual stresses except by experiment.

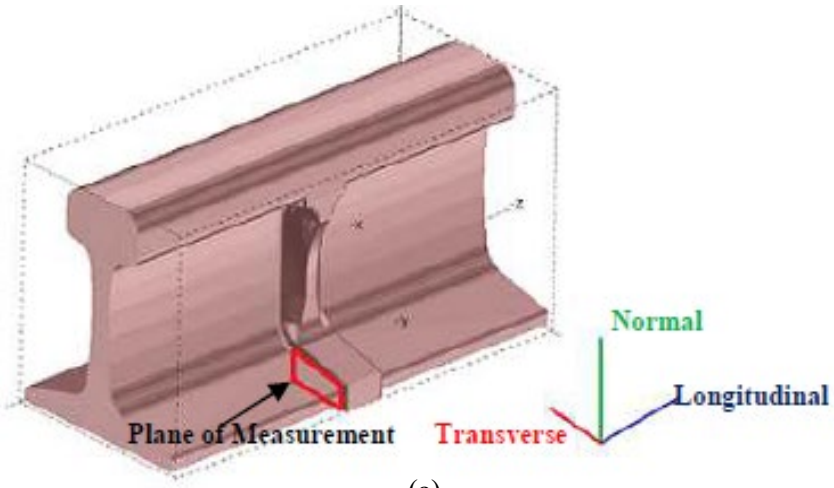

(a)

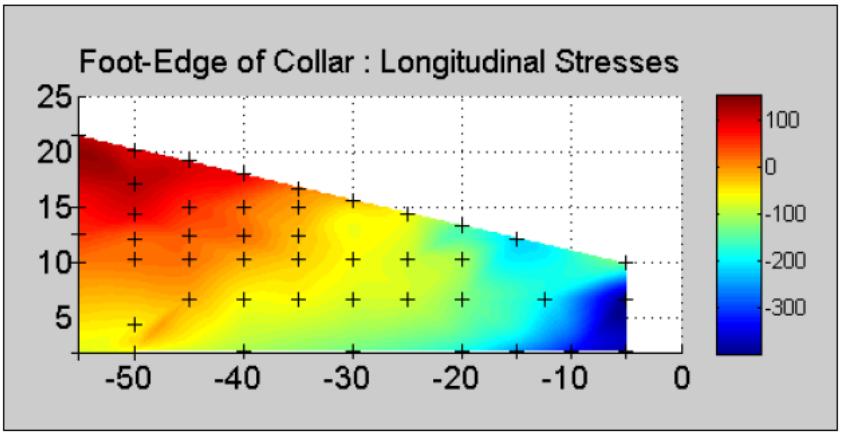

(b)

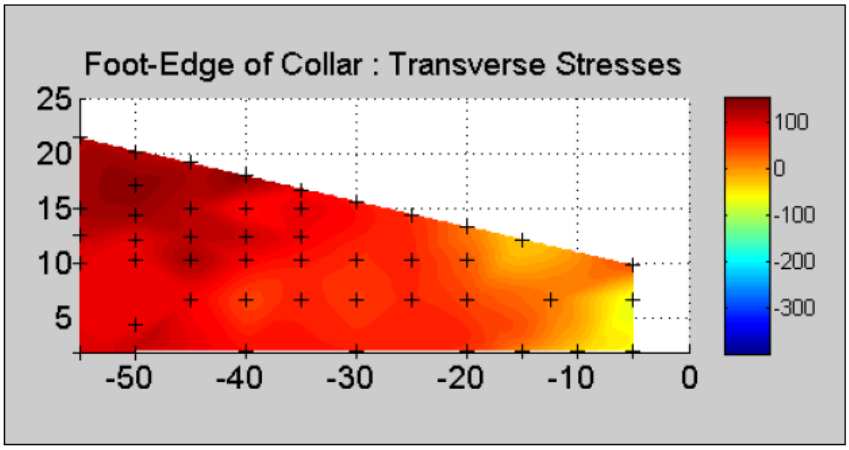

(c)

Figure 2.9. Thermite welding residual stress fields: (a) section of measurement, (b) longitudinal stresses, and (c) transverse stresses (reprinted from Khodabakhshi et al. [42])

2.6.5 Fatigue Crack Nucleation Sites in Thermite Rail Welds

Fatigue process is a progressive and localized structural damage that occurs when a material is subjected to cyclic stress variations. Fatigue fracture resulting from the repeated wheel rolling is known as the primary cause of failure in various components of railway tracks. In general, the service life of thermite welds is far less than that of parent rails and other rail welds. Hauser [20] suggests the expected life of a thermite weld to be only half of an EFB weld. Casting microstructure and weld imperfections are often blamed for the inferior fatigue behavior of thermite welds. Various defects may present in thermite welds such as lack-of-fusion, shrinkage, gas pockets, and nonmetallic inclusions from entrapped slag or mold. These defects act as stress concentrators from which fatigue cracks tend to initiate. Chen [43] performed a research to explore the effect of welding conditions on the formation of fatigue critical defects through thermite rail welds. This study recommends a wider weld gap, increased preheating time, and higher liquid temperature can help to reduce the development of defects in thermite rail welds. The common locations of weld defects from which fatigue cracks develop are schematically presented in Figure 2.10.

In the railhead, two types of fatigue cracks are expected. Near the running surface, where the material experiences severe plastic deformations as a result of heavy contact forces at the rail-wheel interface. The failure mode of material in this region is either low-cycle fatigue (LCF) or ratcheting (Kapoor [44]). At a greater depth from the running surface, localized effects of wheel-rail contact are diminished, and material behaves elastically. The fatigue mechanism in this region is defined as a high-cycle fatigue (HCF) mode. The

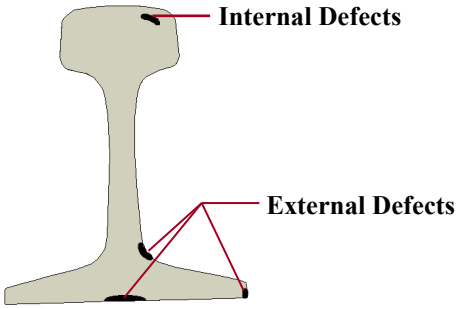

Figure 2.10. Common locations of fatigue crack initiation in thermite rail welds

presence of internal defects and discontinuities in the railhead will act as a stress riser and accelerates the formation of fatigue cracks. Due to large contact forces in the railhead region, fatigue cracks are more frequent in the head compared to the web and base regions. Previous studies on the fatigue performance in the railhead are abundant in the literature (Fry [45], Ekh et al. [46], Jiang [47], Tangtragulwong [48]). However, railhead defects and associated fatigue cracks generally do not cause failure, because they usually can be detected and eliminated by a conventional corrective surface grinding.

Field observations show that most service failures start from either rail web-to-base fillet or rail base locations where HCF fracture is likely to happen. This statement is confirmed by the results of a study on 244 thermite weld service failures which shows that fractures in the majority of broken field-welds were initiated in the web-to-base fillet region (30%), base (30%), and web (28%) (Norfolk Southern Railroad [49]). Since 1997, about 90 percent of thermite weld failures originate at the base or base-to-web fillet region of the weld (Lawrence et al. [8]). Despite its importance, the fatigue behavior in these regions of the thermite rail weld has not received the proper amount of investigation. As

a part of High-Speed Rail IDEA program, a series of studies were conducted by University of Illinois at Urbana Champaign (UIUC) to the improve the reliability of thermite welds (Lawrence et al. [8] and [50]). In that project, the external geometry of the standard thermite mold in stress-critical locations, i.e. the web-to-base fillet and rail base regions, was modified to eliminate the common weld-toe defects found in those weld regions. An improved fatigue resistance was reported for the modified weld specimens using 4-point bending fatigue tests in the laboratory. Following laboratory testing, TTCI installed 10 thermite welds with modified geometry at the Facility for Accelerated Service Testing (FAST) on the High Tonnage Loop. However, no significant improvement was achieved in revenue, during the field testing at FAST.

Therefore, there is an evident knowledge gap for understanding the state of stress and fatigue behavior in stress-critical regions of thermite rail welds where the fatigue failures have been observed to initiate in the field. The non-proportional, multi-axial state of stresses caused by wheel rolling, harsh environmental conditions, and residual stresses that are generated through the welding process made the problem more complicated. Therefore, an advanced multi-axial fatigue model is aimed to properly assess the fatigue behavior of thermite rail welds. Upon validation, the model can be used for improving the thermite weld performance under the increasing traffic of train heavy axle loads.

2.7 Summary

- Thermite welding technology has an essential value for the railway industry to join and repair CWR tracks in the field.
- Portability, relative ease, the speed of installation, and cost-effectiveness are considered as main advantages of rail thermite welding. Neither electric power nor additional filler material is required for this method of welding.
- In the HAZ of thermite rail welds, the hardness and yield strength are comparable to parent rail while the ductility and fracture toughness are substantially lower. As a result, brittle fracture failure is expected in those regions next to the weld metal.
- The quality of thermite welds is not as good as neither parent rails nor other rail plant-welds, due to the casting nature of the process. Weld defects are mainly responsible for the inferior fatigue performance of thermite rail welds.
- Field observations show that most of rail service failures initiate in thermite welds from either rail web-to-base fillet or rail base location. Despite its importance, the fatigue behavior in these critical regions of the weld is not well understood.

3. SIMULATION OF WHEEL-RAIL INTERACTION

3.1 Introduction

Stress analysis is the key to predict the fatigue behavior of any structure. Therefore, a detailed, full-scale, 3-D replica of a wheel-track system is simulated and analyzed using the finite element method. This advanced model features the ability to capture stress/strain fields that are developed at different locations of the wheel-track system with high level of accuracy. The results of the finite element analysis later will be used as an input for the multi-axial critical-plane fatigue model to predict the location and orientation of nucleating fatigue cracks in thermite rail welds. In this section, the mechanical-thermal stress fields caused by the time-dependent rolling of a train wheel and rail temperature change are presented. In addition, the influence of different track parameters, such as the external shape of the thermite weld and foundation stiffness, are explored.

3.2 Wheel Rolling Contact

Large rolling contact forces caused by heavy train wheel loads are the major cause of failure in various track components, including the rail welds. In general, the simulation of wheel-rail interaction can be performed by two approaches. In the first approach, a predefined 2-D Hertzian pressure distribution (Johnson [51]) is applied onto the running surface of a rail, assuming contact stresses are localized and limited to some distance from the contact area. Other assumptions behind the Hertzian theory are that the material behaves elastically and the contact area is much smaller than the characteristic radius of

bodies in contact (wheel and rail). Simplicity and low computational cost are the main advantages of this approach. However, large wheel loads used in heavy-hauled locomotives can cause plastic deformations near the running surface of the rail, and the size of the contact region between the wheel and rail is not negligible. In the second approach, rail and wheel models are made into a contact to simulate the actual operational configuration. The wheel is driven over the rail surface as a result of friction forces resisting the forward translation of the wheel, making the simulation of contact closer to reality but with higher computational cost. Note that the forward motion of a driven wheel is caused by the translation along the running direction resisted by friction forces acting at the contact interface in the backward direction, while the driving wheel is displaced by a torque that is applied to the wheel axle (see Figure 3.1).

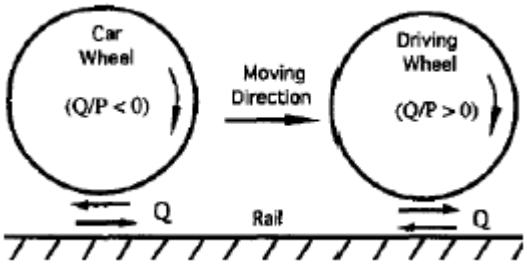

Figure 3.1. Schematic representation of driven wheel versus driving wheel (reprinted from Jiang and Sehitoglu [52])

In this study, the wheel rolling is simulated using the second approach. The wheel-rail interaction is defined within the finite element analysis as a surface-to-surface contact

with “hard” pressure-overclosure relationship to minimize the penetration between interacting surfaces.

3.3 Rail Thermal Variations

The elimination of joints from rail tracks followed by the development of CWR has made railroads susceptible to seasonal temperature changes. Since long spans of CWR track are constrained against the motion in the longitudinal direction, the excessive temperature deviation from the rail neutral temperature can create large axial stresses along the rail section. Rail neutral temperature (RNT) refers to the temperature at which the rail is considered to be “stress-free”. Hypothetically, this temperature is equal to the temperature at which the track was installed (27 ℃). However, in practice, the rail neutral temperature can be affected by train operations, maintenance activities, and environmental conditions (Sluz et al. [53]). Therefore, RNT must be controlled during the rail installation and maintenance to minimize the longitudinal stresses that can form as a result of temperature changes. For a continuously welded straight track, the thermally induced axial stress, σ_T, is defined by

$$\sigma_T = -E.\alpha.(T - T_{RNT}) \tag{3.1}$$

where α is the coefficient of the thermal expansion for rail steels, E is the rail modulus of elasticity, T_{RNT} is the rail neutral temperature, and T is the rail temperature at service. Thus, when the rail temperature rises above the neutral temperature, CWR tends to expand and therefore compressive stresses develop in the rail which can cause the fixed track to buckle. Conversely, as the rail temperature falls below the RNT, tensile stresses develop

that can initiate the rail breaking. If the temperature is too low, the axial tension becomes large enough to accelerate the crack growth and pull the rail apart at welds or flaws. Hence, it is not surprising that the possibility of the rail fracture escalates through the cold winter time when tensile stresses are higher. This is clearly shown in Figure 3.2 which represents the frequency of broken rails along with the average temperature during a six-month period for a CWR track installed in Germany (Zerbst et al. [54]). As seen, the rate of failure reaches its peak in the late December when the temperature is the lowest (-10 ℃).

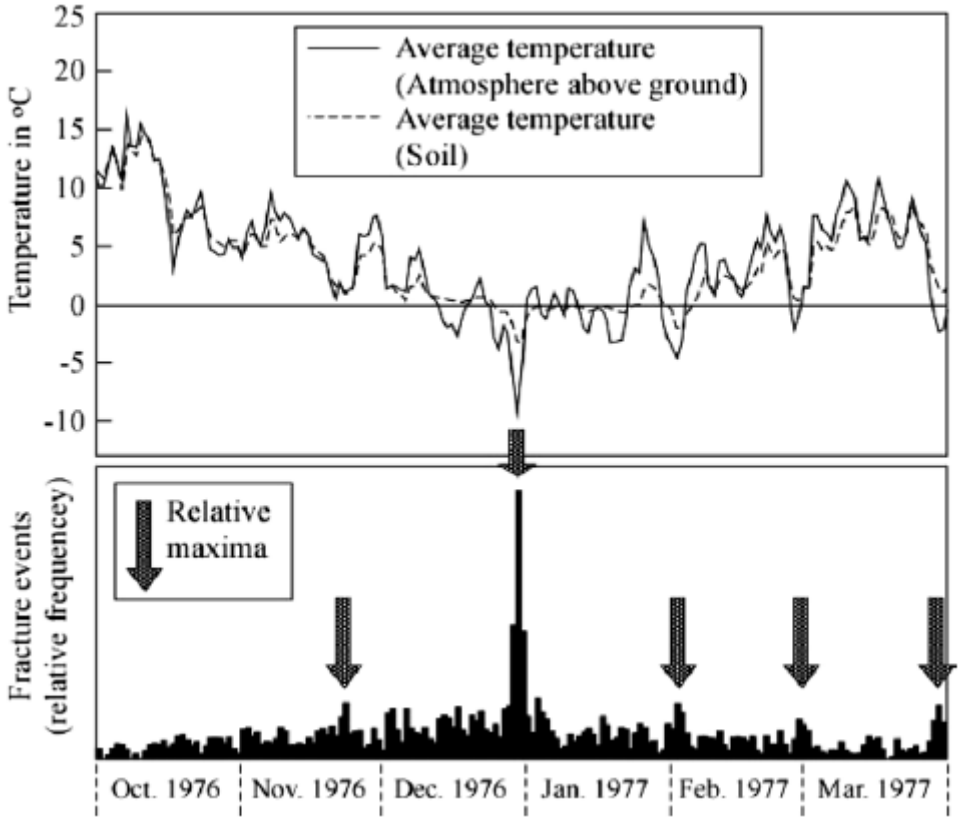

Figure 3.2. Influence of ambient temperature on the relative frequency of fracture events in a CWR track installed in Germany (reprinted from Zerbst et al. [54])

Therefore, severe temperature variations may have a considerable influence on the service life of railroad rails. The effect of thermal stresses can be added to stress fields caused by wheel loads and residual stresses, using the principle of superposition, if the material behavior is linear elastic.

3.4 Finite Element Analysis of Wheel-Rail Interaction

Finite Elements Analysis (FEA) is a powerful tool to examine the structural response (stress/strain) of a welded rail under rolling wheel loads of freight train cars. The commercial program ABAQUS/CAE® [55] is used in this study as a pre/post processing software and FE solver to simulate a full-scale replica of a wheel-track system in 3-D. This computational model, shown in Figure 3.3, comprises seven main parts: axle, wheel, rail with extending beam elements, thermite weld, tie-plates, wood cross-ties, and vertical spring elements representing the ballast and subgrade material. 136 RE rail section is used which is common in HAL tracks. The depth of the rail section is 185.7 mm. The extending beam elements are possessing the same cross-sectional properties as the actual rail section. The wheel section corresponds to M-208 (HAL wheel) with a radius of 482.6 mm. As seen, the z-axis coincides with the longitudinal direction of the rail while the y-axis and x-axis are aligned with vertical and transverse directions, respectively. The cross-section of the wheel-rail assembly is illustrated in Figure 3.4. Only a single wheel and one side of the track are included in the simulation because of the symmetry along the running direction of the train. The axle is defined to represent the un-symmetric vertical load from the train truck. TIE constraint within ABAQUS/CAE® is used to connect the axle to the

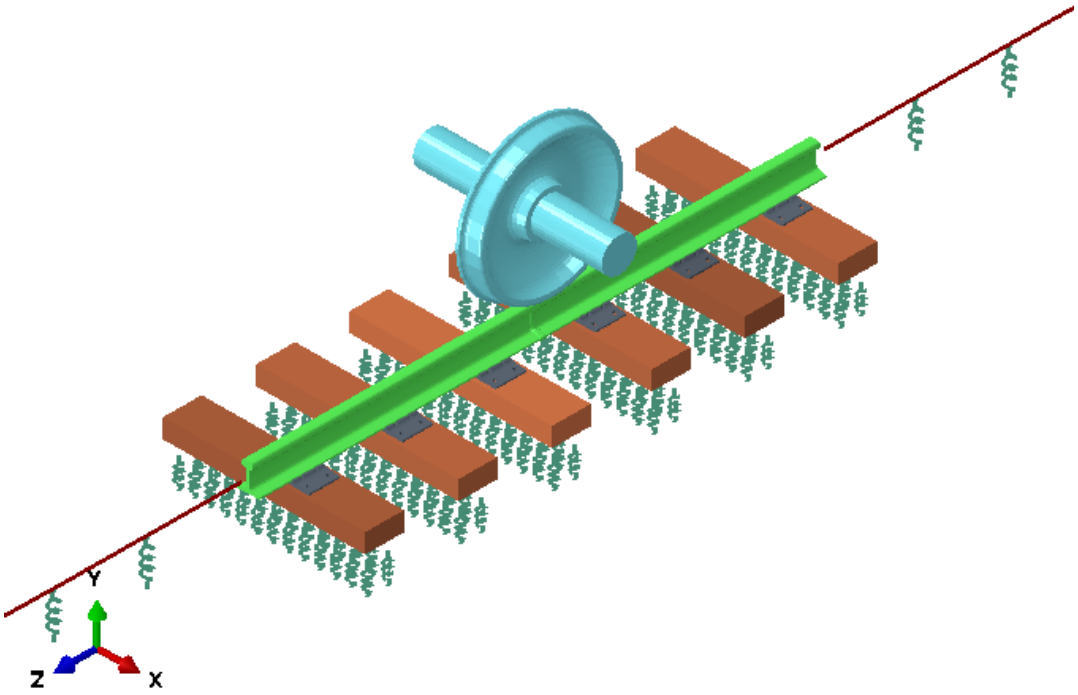

Figure 3.3. Full-scale simulation of wheel-track system constructed in ABAQUS/CAE®

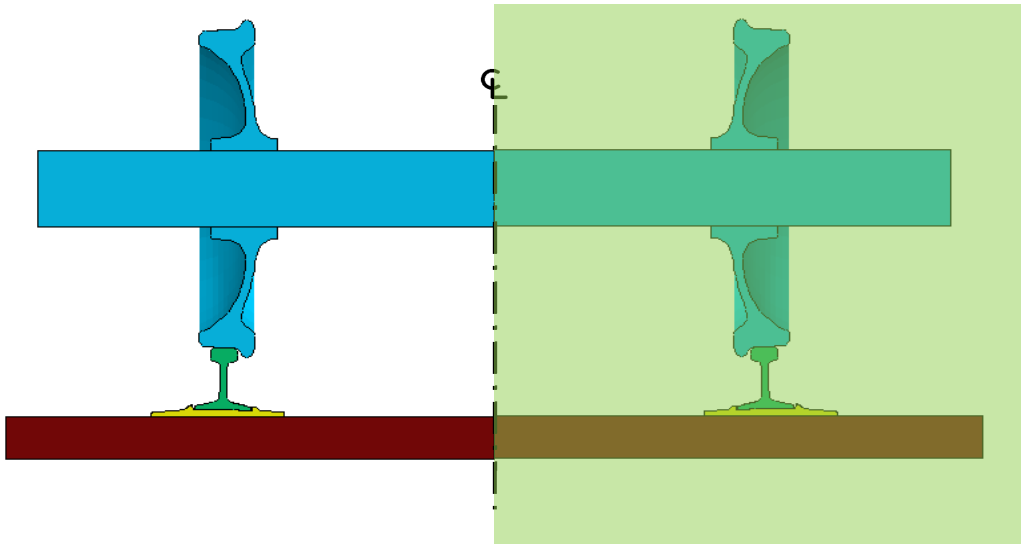

Figure 3.4. Cross-section of the wheel-track system

wheel hub, making them act as a unit. To resemble the heavy axle load environment of the modern North America railroad, a mass representing 160 kN wheel load is imposed on a node on the longitudinal axis of the axle, on the gage side, to simulate the eccentrically applied vertical load carried by each wheel. This mass corresponds to one wheel of a full 286 kips freight car.

Two pieces of 1,800 mm long rail sections are joined together with a standard, 25 mm gap, Orgo-Thermit® weld. However, as explained before, the weld width is always greater than the initial gap because of the melt-back at rail ends. For this study, it is assumed that the weld width is equal to the weld collar width, i.e. 40 mm. The cross-tie spacing is 600 mm, and thereby, each rail piece is installed on three cross-ties. Each rail's end is attached to a 5,700 mm long beam element, having the same cross-sectional properties as the actual rail section. The kinematic coupling function within ABAQUS/CAE® is used to match the displacements at beam-rail connections. This provides an overall 15,000 mm length of a continuously welded rail.

The external geometry of the Orgo-Thermit® weld is directly measured from a test specimen at TTCI testing laboratories. The 3-D scanned mesh of the weld was then imported as a solid part into ABAQUS/CAE® to replicate the thermite rail weld. The rail weld specimen is shown in Figure 3.5.

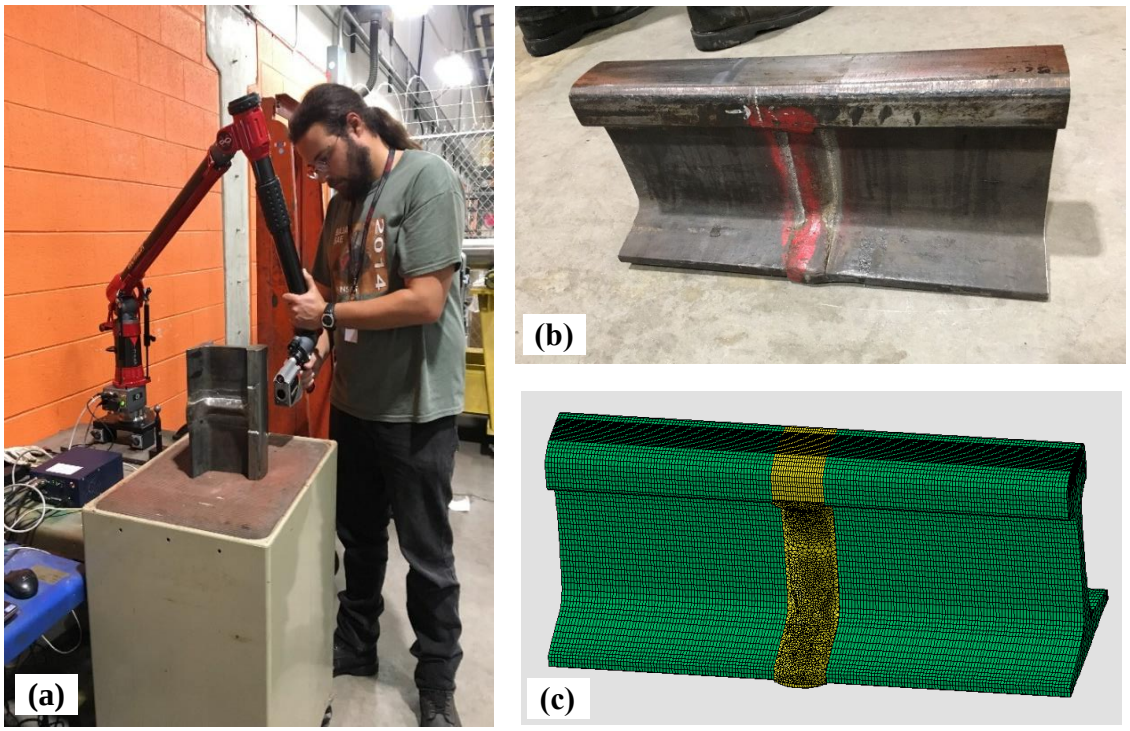

Figure 3.5. Standard Orgo-Thermit rail weld: (a) 3-D geometry measurement, (b) test specimen, and (c) computational model in ABAQUS/CAE®

The track foundation is another important parameter that requires a special attention. The quality of the ballast can impose a major influence on the deformation and stress field at the rail base. In this study, the ballast and sub-grade material are replaced by vertical spring elements attached to the cross-ties, and to the beam's nodes. The spring constant for 600 mm tie pitch and 208 MPa ballast modulus is 62.4 kN/mm. Note that the ballast equivalent modulus usually ranges between 100-350 MPa (Desai and Siriwardane [56]) and the selected value of 208 MPa is a representative of a well-maintained track in revenue service. This simplified model can effectively define the catachrestic behavior of

the track foundation without excessive computational cost. Figure 3.6 shows the configuration of vertical spring elements with respect to extending beams and cross-ties. As seen, only one spring is used under each of the beam's nodes while a set of 26 parallel springs, with the equivalent stiffness of 2.4 kN/mm, are uniformly placed in two rows under each of the cross ties.

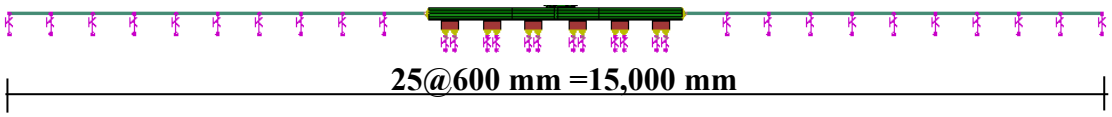

Figure 3.6. Representation of ballast material using vertical spring elements

Contact capabilities within ABAQUS/CAE® are used to define interactions between the wheel-rail and rail-tie plates. All the contact pairs are of the surface-to-surface type with a strict master-slave relationship and finite sliding algorithm. The contact pressure over-closure relationship is of the "hard" type. This definition minimizes the penetrations between contact surfaces and prevents the transmission of tensile stresses across the contact interface. To trigger the wheel rotation, a friction factor of 0.3 has been applied at the wheel-rail contact as commonly proposed in steel-to-steel rolling contact studies (Kiani [57], Ekberg and Kabo [58])

A variable mesh size is used in the model as very fine elements are located at contact regions. A 10-node quadratic tetrahedron element (C3D10) is employed to mesh the thermite weld collar due to its complex geometry. For the rest of solid parts, an 8-node

brick element (C3D8R) with reduced integration is used throughout the model, as it provides more accurate pressure distribution in the contact problem with relatively short run time. Overall, the model has total of 1,296,686 nodes and 1,131,431 elements.

As explained before, this study is mainly focused on the web and base region of the rail, shown in Figure 3.7.a, through which most of the service failures caused by thermite weld fracture are observed to originate. This critical section, highlighted in yellow in Figure 3.7.b, is called the "cross-section of interest" through this study. Later, the fatigue parameters will be calculated at each node of this section as a tool to investigate the fatigue behavior of thermite rail welds.

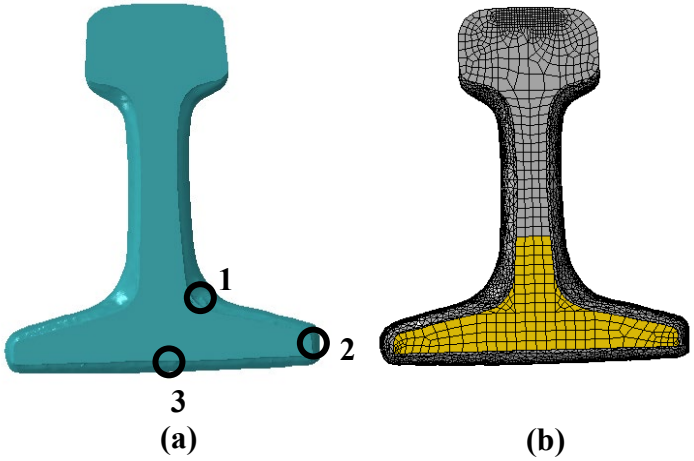

Figure 3.7. (a) Fatigue crack nucleation sites based on field observations and (b) cross-section of interest for fatigue analyses (highlighted in yellow)

3.5 Material Model

In general, the main components of the wheel-track system, including the rail and wheel, are made of pearlitic steel with elastic-plastic behavior. The response of an elastic-plastic material to a cyclic loading with non-zero mean load evolves with the increasing load level. First, the system deforms perfectly elastically when loaded below its elastic limit. As the load level increases, a plastic flow happens that expands the yield surface (strain-hardening). The hardening process will help the system to shake down to its elastic behavior to resist the plastic flow that occurs in subsequent loading cycles. Further loading beyond the elastic shakedown limit may result in either plastic shakedown with a stabilized closed loop stress-strain path or ratcheting with a progressive accumulation of plastic strains. Figure 3.8 schematically illustrates the four types of material behavior as explained above.

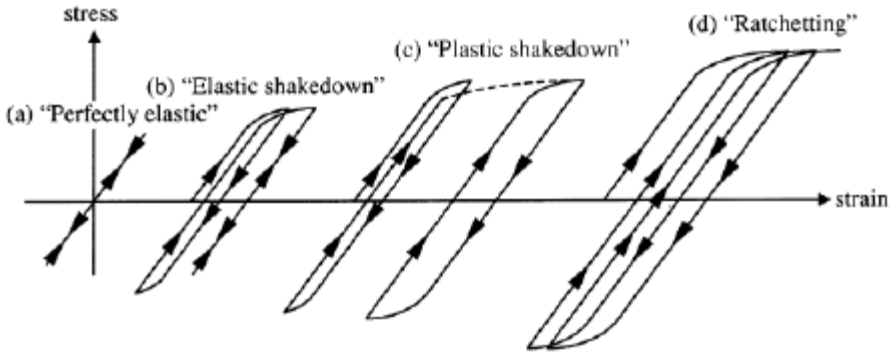

Figure 3.8. Material behavior under cyclic loading with a non-zero mean load (reprinted from Ringsberg et al. [59])

When the rail is loaded by heavy train wheels, localized plastic deformation occurs in the railhead, close to the wheel-rail contact interface (Bower and Johnson [60]). However, elastic behavior dominates at some distance remote from the running surface. Since the main focus of this study is placed on the fatigue crack nucleation in the web and base region of thermite rail welds, no plastic behavior is expected. Therefore, pearlitic steel with an elastic modulus of 209 GPa and Poisson's ratio of 0.29 is used for the rail, wheel-axle, and tie-plates. Although the material behavior in the weld region is variable and depends on the welding procedure, elastic properties of the thermite weld are assumed to be similar to that of the parent rail. In fact, most of the fatigue cracks are observed to initiate in the HAZ of the rail, next to the thermite weld, and thus, this assumption is supposed to have a minimal influence on the results of the analysis. The yield strength in the thermite weld (σ_y) is set to 568 MPa based on the monotonic proportional limit value given by Fry [61]. The cross-ties are made of wood with an elastic modulus of 12 GPa and Poisson's ratio of 0.3.

Additionally, thermal-mechanical coupling due to rail temperature changes is incorporated into the analysis. The temperature is uniform over the cross-section, and the coefficient of thermal expansion for the rail steel is equal to $1.05 \times 10^{-5}/℃$.

3.6 Loading Steps

The distribution of the vertical force generated by a train wheel on the railhead surface is stochastic due to dynamic vehicle-track interactions. Figure 3.9 shows an example of a vertical wheel load distribution under HAL operation conditions (39 tonnes axle) based on the instrumented data collected from the FAST track at TTCI testing facilities in Pueblo, Colorado (Li et al. [62]). As seen, the vertical wheel load ranges between 26 and 60 kips as compared to the nominal static load of 39 kips.

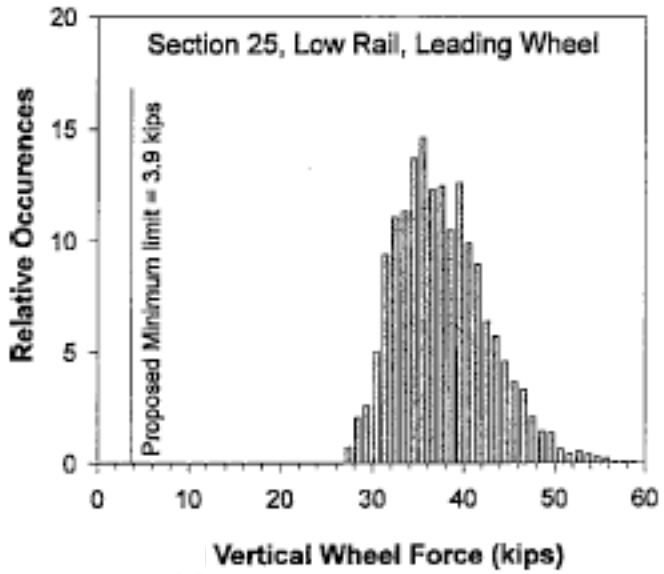

Figure 3.9. Histogram of vertical wheel load under HAL (reprinted from Li et al. [62])

Since the region of interest for the present study is remote from the wheel-rail contact interface, the effects of dynamic vehicle-track interaction are negligible. Therefore, the mean vertical load of 160 kN (35.75 kips), which corresponds to one wheel

of a 286 kips freight car with four axles, is quasi-statically applied to the rail. Rolling of the wheel is simulated in three steps:

- **Step 1:** The wheel-axel assembly is slowly displaced in the vertical direction for 0.5 mm to establish a firm wheel-rail contact.
- **Step 2:** A mass of 16,000 kg is gradually applied to a node on the axle centerline to simulate the mean vertical load of 160 kN. Uniform gravity is applied to the whole system.
- **Step 3:** The wheel-axle assembly is translated in the longitudinal direction of the rail (z-axis) for 1,000 mm to simulate one cycle of wheel loading in the foot region of the thermite rail weld. This translational motion will also induce the wheel rolling due to the presence of friction at the wheel-rail contact interface.

As mentioned before, the stress field in the thermite weld is caused by three major sources: vertical wheel loads, seasonal temperature variations, and residual welding stresses. The effects of rail temperature change are included in the simulation as a predefined stress field that can be added to the wheel load stress field by linear superposition (elastic material). However, the effects of welding residual stresses are not considered in this preliminary study due to high uncertainties that are present in the magnitude of measured welding residual stresses available in the literature.

3.7 Results and Discussion

ABAQUS/CAE® is employed as the FE solver to analyze the computational model of the wheel-track system, represented in Figure 3.3, under the given loading and boundary conditions as described before. Time histories of six components of the stress tensor are recorded for all the point within the cross-section of interest, shown in Figure 3.10. Later, the stress fields will be further analyzed to investigate the fatigue behavior of the thermite rail weld. In this section, the results of the stress analysis are presented and discussed. Also, the influence of different track parameters on the stress field in the rail foot is investigated. Normal stress directions are defined according to the three principal directions shown in Figure 3.11.

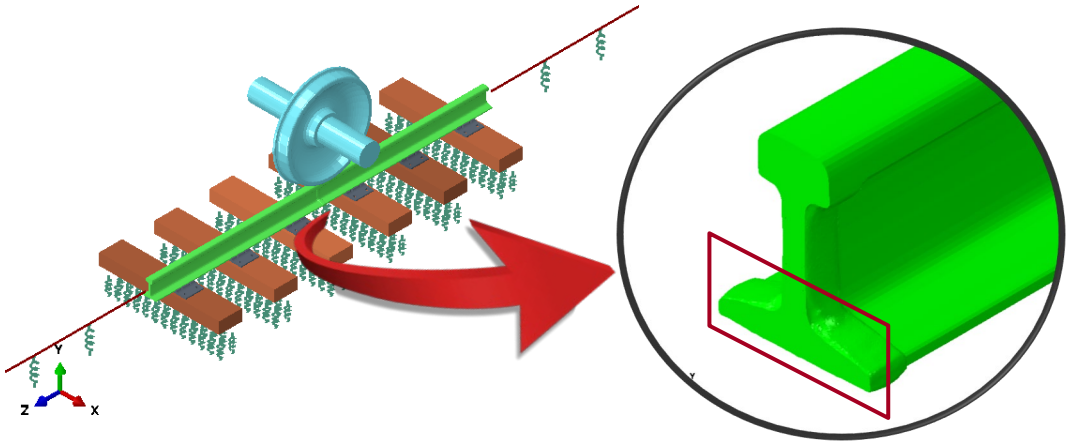

Figure 3.10. Representation of the cross-section of interest through which fatigue cracks are most likely to initiate

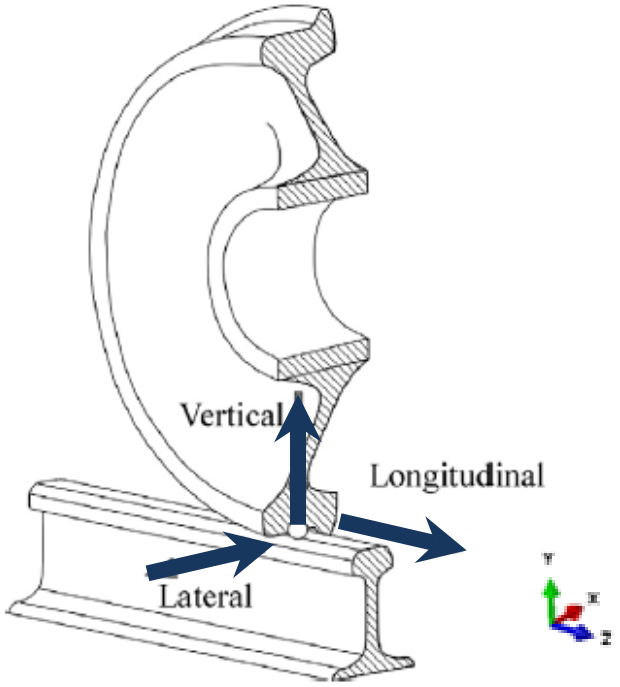

Figure 3.11. Three principal directions of the wheel-track system (reprinted from Zerbst et al. [54])

3.7.1 Rail Stresses under a Rolling Wheel

The loading that a passing train imparts on the rail generates a complex non-proportional, multi-axial state of stress. To investigate the variation of the stresses throughout the model, the effective von-Mises stresses are studied as a uniaxial equivalent of a multi-axial stress state. In fact, the equivalent von-Mises stress converts any 3-D stress state to a single positive stress value, proportional to the deviatoric part of the stress tensor, $\boldsymbol{S}$, defined by

$$\sigma_{von-Mises} = \sqrt{\frac{3}{2}\boldsymbol{S}:\boldsymbol{S}} \qquad (3.2)$$

In general, if the equivalent von-Mises stress is less than the yield strength limit, the material is assumed to behave elastically.

Figure 3.12 shows the variation of von-Misses stress in the wheel-rail contact region. As seen, high localized stresses occur near the running surface where plastic deformations are expected to take place. As moving down further from the contact interface, the stress field gradually diminishes to below 150 MPa. Compared to the high yield strength of the thermite weld (568 MPa), this figure validates the assumption of elastic behavior in web and base regions of the rail.

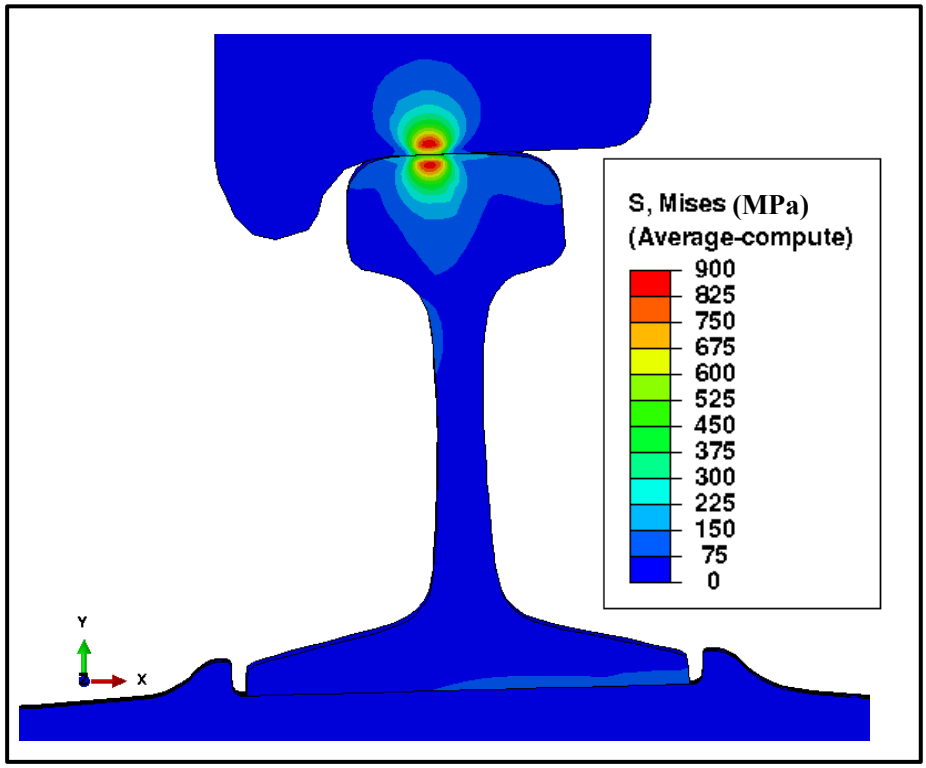

Figure 3.12. von-Mises stress contour in the wheel-rail contact region

In particular, the variation of von-Mises stresses in the weld zone is illustrated in Figure 3.13. On the top, we are looking at the projection of stress values into the y-z plane along the negative x-direction, and on the bottom, we are looking at the projection of stress values into the x-z plane along the positive y-direction. This figure corresponds to the time when the wheel-rail contact is located in the center of the weld. As seen, high-stress concentration spots can be identified in the rail, next to the thermite weld, on the center and corners of the rail base where tensile flexural stresses reach their peak. Therefore, the presence of external defects in hot spot regions of the rail base is expected to result in a

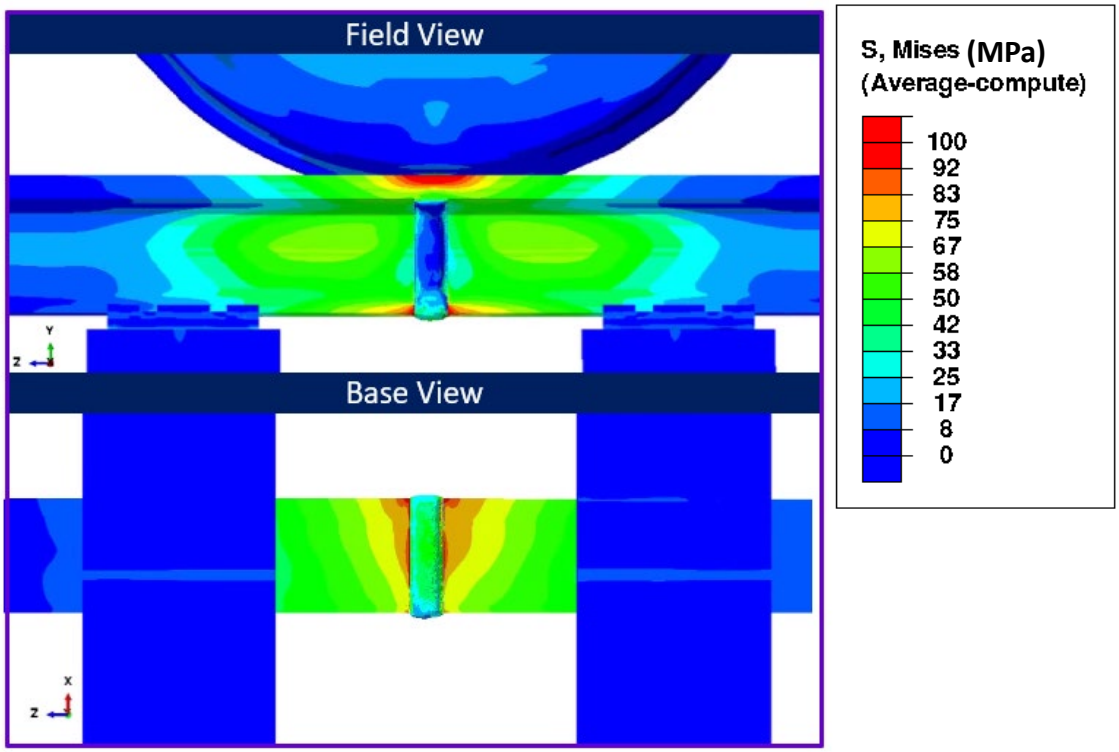

Figure 3.13. von-Misses stress contour in the thermite rail weld region

premature failure of the thermite weld. Note that the magnitude of the stress in the web-to-base fillet region, induced by the vertical wheel load, is relatively small.

3.7.1.1. Weld Geometry Effects

For a thermite weld, both external weld geometry and formation of weld defects can act as a stress-raiser to create stress concentrations. In the past, it was common to remove the weld collar from the whole rail section by grinding, but due to metallurgical issues, it is not the case anymore. Figure 3.14 compares the equivalent stress field at the weld-toe of a thermite rail weld with and without the collar. In both cases, the contact

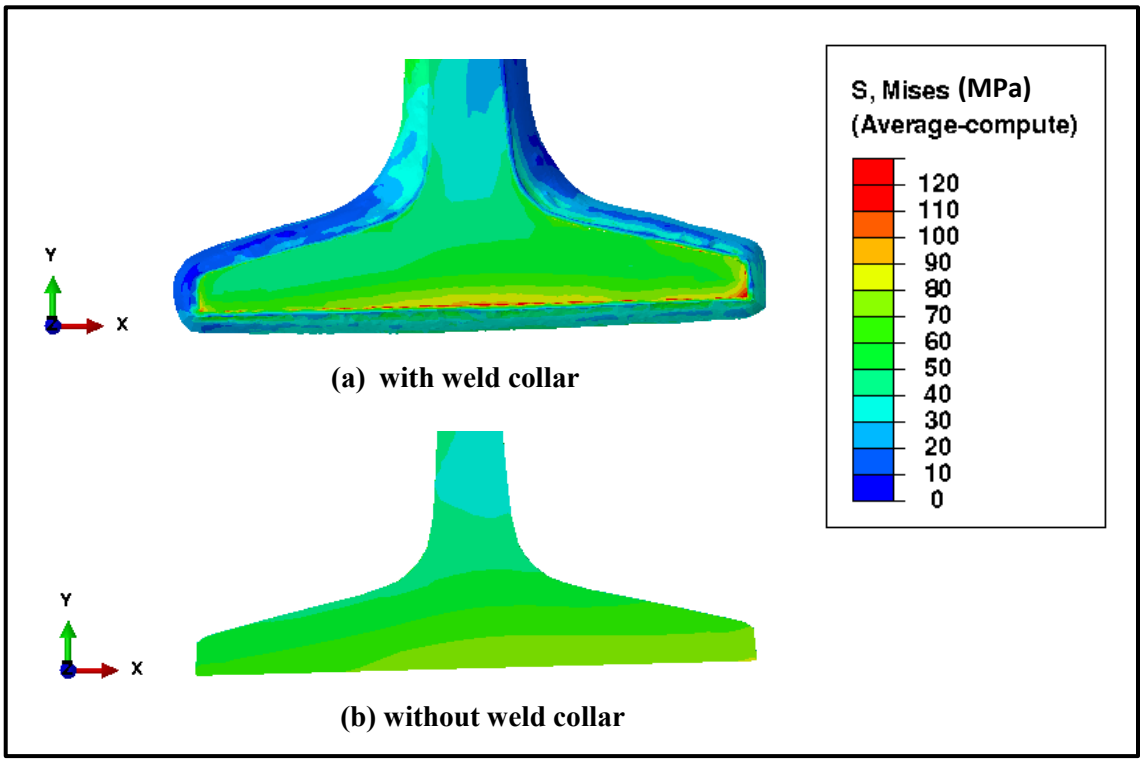

Figure 3.14. Effect of the weld collar on the stress field in the thermite weld region

is right above the cross-section of interest. As seen, the presence of the weld collar creates a region of localized stress concentration on the rail base surface, next to the weld, where the peak value of effective stress goes beyond 100 MPa. This is almost two times greater than the maximum stress in a rail base of a weld without a collar. Note that different shapes of the weld collar may induce different stress fields in the weld region.

3.7.1.2. Boundary Conditions Effects

The quality of the support condition is another important parameter that can influence the integrity of the weld joint. In the computational simulation of this study, ballast and sub-grade materials are replaced by discrete vertical spring elements that are placed uniformly under the ties. Figure 3.15 shows the effect of support stiffness on the stress field in the rail base. A comparison has been made between two cases with a ballast elastic modulus of 208 MPa and 70 MPa as a representative of well-maintained ballast and degraded ballast support, respectively. The wheel-rail contact is right above the section of interest for both cases. The considerable influence of the support stiffness on the vertical deformation, and consequently, the stress field in the rail base can be observed. Results show that von-Mises stresses in the base region of the weld are significantly magnified when the support condition is degraded. Therefore, proper simulation of the track foundation support has an essential impact on the reliability of the model.

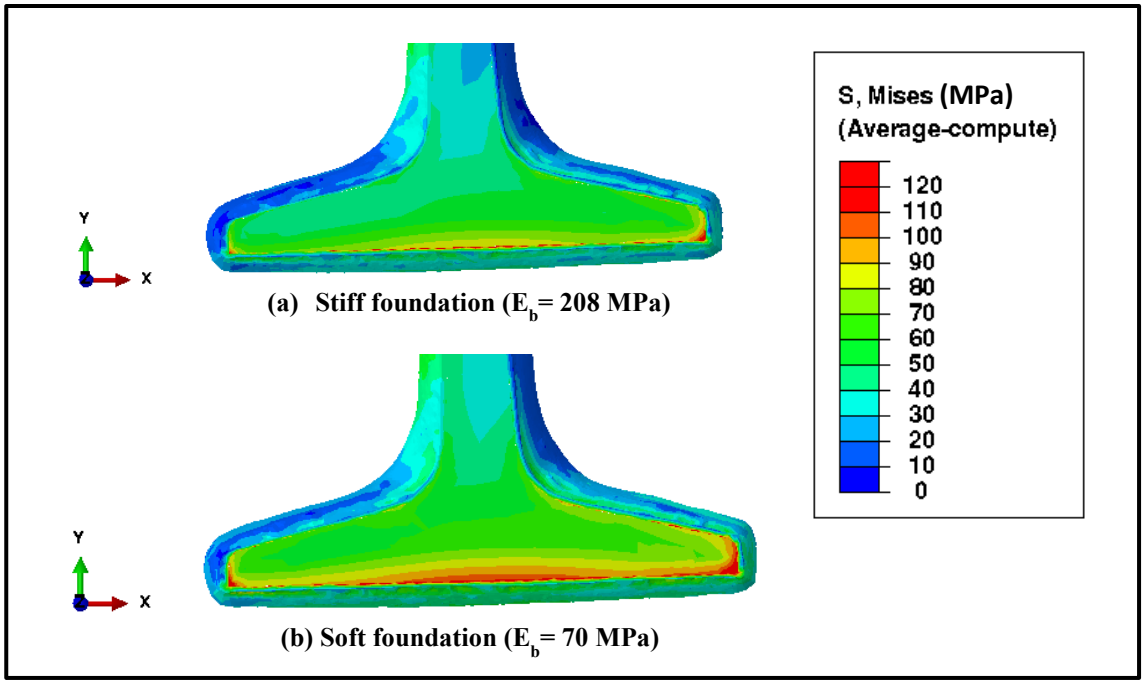

Figure 3.15. Effects of support conditions on the state of stresses in the thermite rail weld region

3.7.2 Rail Thermal Stresses

As mentioned earlier, the temperature deviation from the rail neutral temperature can create large axial stresses over the rail section of CWR tracks. When the temperature falls too low during the winter, large tensile stresses are expected which can break the rail apart. The stress field caused by a temperature change is more complex in the thermite weld region due to the weld external geometry. Also, the presence of weld flaws and imperfections makes the weld zone more susceptible to fracture when the rail temperature significantly decreases. As an example, Figure 3.16 shows the thermally induced stress field in the rail, next to the thermite weld, for an extreme scenario through which the rail temperature uniformly drops 100 ℃ below the RNT. As seen, hot spot regions can be

identified at the web-to-base fillet and base corners where the von-Mises stress is over 300 MPa. At some distance further away from the thermite weld, the thermal stress is practically constant over the rail cross-section with an average value of 220 MPa.

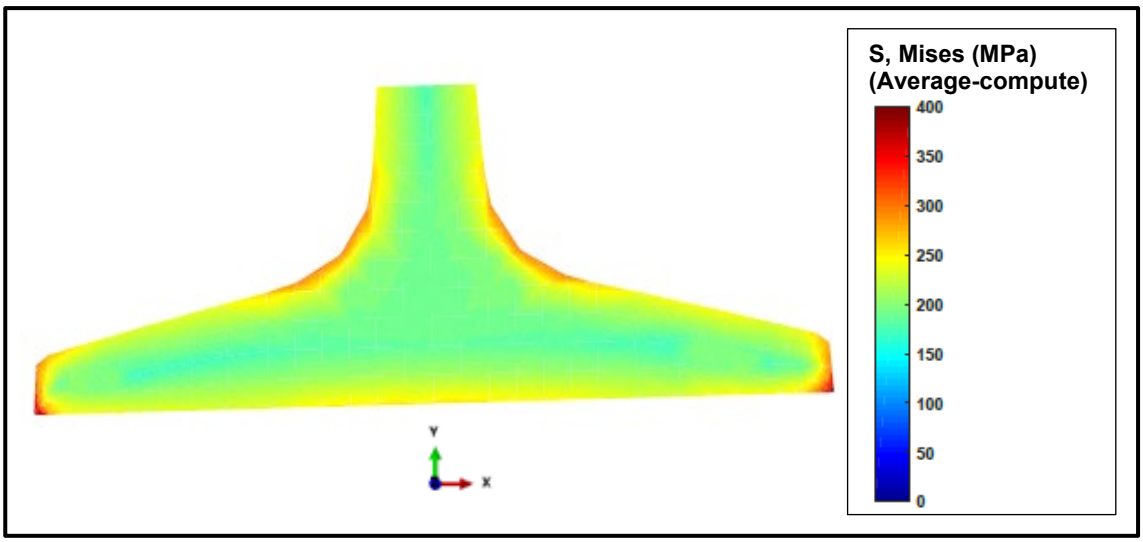

Figure 3.16. Stress field caused by -100 ℃ temperature variation from RNT at a rail section next to the thermite weld

3.7.3 Simplified Model

The wheel-track model that was used for simulations so far requires a great amount of computational resources. Each simulation can take several hours to run on supercomputers. Furthermore, adding more details to the model, such as increasing the number of train axles, may impede the analysis due to computational limitations.

Therefore, it is appealing to improve the simulation performance by simplifying the computational model without sacrificing much accuracy.

In this regard, the train wheel is replaced by a static vertical load of 160 kN which is applied to the wheel-rail contact area. In fact, the effect of rolling contact is shown to be negligible in web and base regions of the rail, remote from the contact interface. A comparison is made in Figure 3.17 between the stress field caused by a rolling wheel and the one corresponding to a vertical load. As seen, differences between the two models are not noticeable in the lower portion of the rail. This is confirmed by the Saint-Venant's principle which states that the difference between the effects of two different, but statically equivalent loads becomes very small at sufficiently large distances from the load (Love [63]).

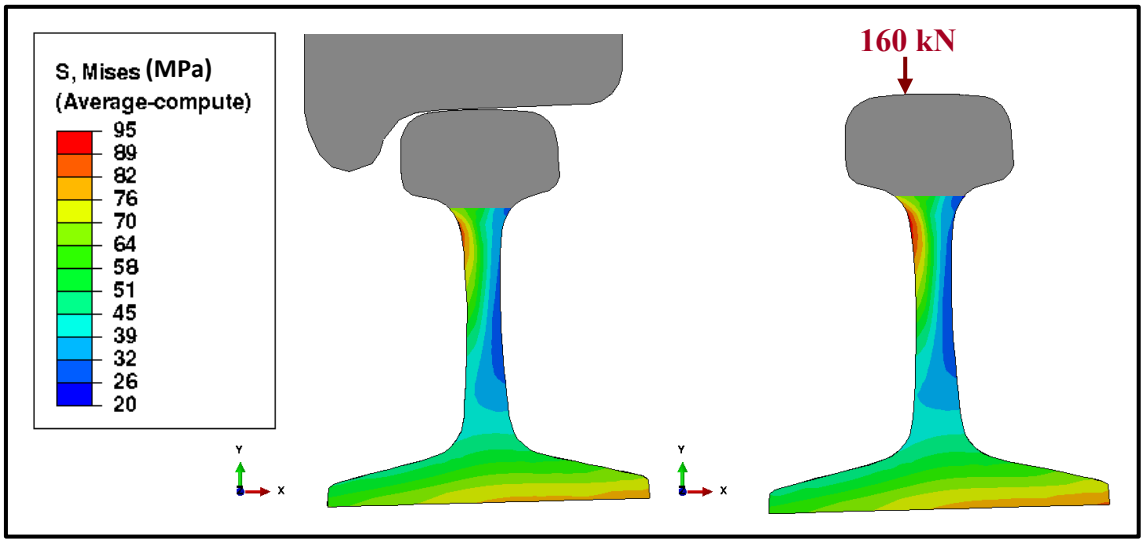

Figure 3.17. Rolling contact stress field (left) and simplified model (right)

Note that although the simplified model of the wheel-track system can significantly reduce the cost of calculations, the application of the advanced model is still valuable for more accurate fatigue studies due to the complexity of stress fields in the weld region.

3.8 Summary

- A detailed finite element analysis was performed as a means to study the state of stresses in a thermite rail weld caused by the time-dependent wheel rolling and the seasonal rail temperature change.
- In the web and base region of the rail, remote from the wheel-rail contact area, plastic deformations are not likely to happen.
- High stress concentration occurs in the rail HAZ, next to the weld, on the center and corners of the rail base where tensile flexural stresses reach their peak.
- The external shape of the thermite weld collar acts as a stress-riser and magnifies the stress field in the weld region.
- The quality of the track foundation has a significant influence on the state of stresses in the rail base.
- Seasonal temperature changes create axial stresses in CWR tracks. When the rail temperature falls too low, the tensile stress may become large enough to pull the rail apart. This study shows the effect of rail temperature change is more crucial in the thermite weld region, especially in web-to-base fillet and base center areas.

Thermal stresses can be superimposed to wheel load stresses because of the elastic material behavior.

- A simplified model of wheel-rail interaction was proposed to study stress fields in regions remote from the wheel-rail contact interface. The simplified model can be used to predict the overall behavior of the system. However, the advanced computational model is helpful to estimate the service life of welds more accurately due to the complexity of stress fields in the thermite weld region.

4. FATIGUE MODEL

4.1 Introduction

Fatigue process is a progressive and localized structural damage that occurs when a material is subjected to cyclic stress variations. Fatigue damage is a common source of failure in various railroad components due to the cyclic nature of wheel loads. Since railroads usually behave in a brittle manner, as soon as cracks nucleate it may take only a short period of time for cracks to grow and eventually break the rail.

In general, the total fatigue life of a component can be expressed as the combination of two parts: the number of cycles required for crack nucleation and early crack growth, and the number of cycles required for the crack propagation (Bannantine et al. [64]). For high strength pearlitic rails, the crack nucleation and early growth consume most of the service life, and the life in crack propagation stage, which can be analyzed by fracture mechanics, is assumed to be minimal (Fry [45]).

Rolling contact fatigue (RCF) is considered as one of the major roots of fracture in railroad rails (Smith [65]). A differentiation has to be made between the rolling-contact fatigue (RCF) and "classical" fatigue analysis because of following reasons: 1) rolling causes non-proportional, multi-axial stress fields and principal stress directions change as rolling progress, and 2) cracks propagate in mixed modes and the friction between the crack faces plays an important role in crack growth (Ekberg [66]).

As discussed before, the effects of rolling contact fatigue (RCF) is more considerable near the wheel-rail contact interface. Two types of fatigue cracks may form

in the railhead due to RCF: surface cracks and subsurface cracks. Surface cracks commonly form as a result of large plastic deformations near the running surface, whereas subsurface cracks nucleate from internal metallurgical imperfections that are present at some distance (more than 10 mm) below the running surface where material deforms elastically (Ekberg and Marais [67]). On the other hand, in the web and base regions of the rail where the stress level is relatively low, fatigue cracks typically initiate from pre-existing external defects next to the thermite welds (Lawrence et. al [8])

Over the past three decades, many researchers have studied RCF in railheads and train wheels with an intent to extend the service life of the system, increase the track safety, and reduce the cost of failures. Fry [45] used a simplified 2-D railhead local stress fatigue model (RAHELS) to predict the type of railhead defects that form in thermite welds under a given set of operating conditions and to predict the fatigue nucleation life of defects. Later, Ekberg [66] used a semi-analytical procedure, assuming elastic material behavior and Hertzian contact theory, to predict the fatigue crack-initiation time in "defect-free" materials. However, his results were not in agreement with the field data. In recent years, the revolutionary advancements in supercomputing facilities and commercial finite elements analysis programs made the simulation of full-scale models possible. Tangtragulwong [48] performed a multi-axial fatigue analysis on the full-scale model of a wheel-rail interaction with a nonlinear isotropic-kinematic hardening material model to study the fatigue crack nucleation in the railhead. Similarly, Kiani [68] developed a multi-axial strain-based fatigue model to study the development of subsurface fatigue cracks in railway wheels under RCF.

Despite its significance, there is much less literature available on the fatigue behavior in the web and base region of rail welds. Skyttebol et al. [41] studied the fatigue crack growth of pre-existing flaws located in flash-butt welds, right above the rail web. He showed that surface cracks are more dangerous in the web-railhead area compared to embedded cracks. Lawrence et al. [8, 50] carried a set of experiments to eliminate the initiation of fatigue cracks that form in the web and base region of thermite rail welds. They suggested a new configuration for the thermite welding mold with an intent to improve the thermite weld geometry. Taken from [69], Figure 4.1, shows the changes that were made to the weld geometry. As seen, the weld collar flank angle (the angle that the collar intersects the rail) was reduced to 33° and a toe radius of approximately 3 mm was

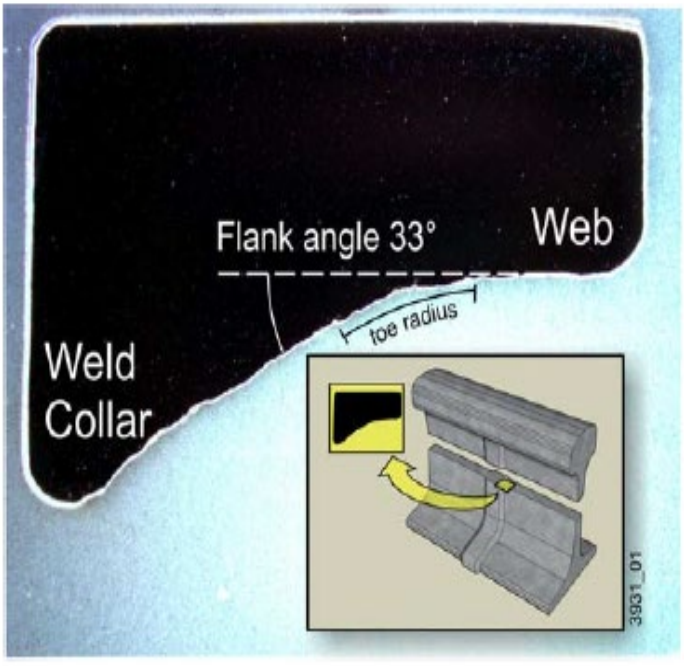

Figure 4.1. Modification of thermite rail weld geometry (reprinted from Gutscher [69])

added at the intersection to reduce stress risers. Although the welds with modified geometry resulted in a 34% increase in fatigue life under 4-point bending laboratory tests, installation of the proposed weld model on High Tonnage Loop of the FAST track did not produce useful data for determining any benefit that geometry modification may have provided. Therefore, more research is demanded to understand the fatigue behavior of thermite rail welds under HAL operating conditions.

In this section, an advanced algorithm is developed in Matlab® to study the fatigue cracking in rail welds. The results of the finite element analysis are utilized to estimate the fatigue crack nucleation life of thermite rail welds based on a multi-axial critical-plane fatigue criterion. Findley fatigue index is employed through the fatigue analysis to predict the location and orientation of nucleating fatigue cracks.

4.2 Multi-axial Fatigue Criteria

Over the years, various methods have been developed to quantify the fatigue damage in structures that experience a multi-axial stress field. The most fundamental part of any fatigue model is the method used for computing fatigue damage. Multi-axial fatigue parameters are functions constructed to isolate tensor field characteristics that contribute most to fatigue damage in a material. Often the parameters are empirically based.

Basically, multi-axial fatigue models can be categorized according to the physical quantity used in the model. Thus, multi-axial fatigue models can be identified as stress-based, strain-based, energy-based, and fracture mechanics-based. The stress-based approaches are applicable to the high-cycle fatigue (HCF) regimes where the stress-strain

relationship is linear. Strain-based approaches, on the other hand, are more general to cover both LCF and HCF regimes. Garud [70] provides an extensive survey on the history and early development of all the aforementioned methods.

Another way to classify multi-axial fatigue criteria is based on the format by which the fatigue index is presented: as a scalar or in a critical plane format (Jiang et al. [71]). In the scalar format, the fatigue model takes as input components of a tensor history to generate a single number that represents a reference damage value averaged over all material planes. Therefore, these models do not provide any information about the plane of crack nucleation. The energy-based and equivalent stress criteria are two examples in the scalar format. On the other hand, critical plane fatigue criteria are formulated based on experimental observations showing that fatigue cracks tend to initiate on preferred planes within the material. Critical plane criteria can be either stress-based or strain-based, depending on the material behavior. Fatigue index is determined by transforming the time history of stress and/or strain tensors into normal and shear components for all possible planes passing through the evaluation point. The plane corresponding to the largest fatigue index is considered as the critical plane, which indicates the direction of crack propagation. Therefore, critical plane approaches have added the benefit of being able to predict the failure plane orientation, which is useful if a subsequent fatigue crack growth analysis is to be performed. The use of critical plane fatigue analysis requires a detailed finite element analysis to capture the time history of stress/strain tensors within the material. A comprehensive review on critical plane criteria is presented by Karolczuk and Macha [72]. In both formats, the fatigue criterion is regarded as a numerical index of

fatigue damage. These values are often correlated with experimental data so that fatigue life estimates can be made.

Critical plane models should incorporate accurate constitutive parameters governing the crack nucleation and fracture mechanism in a given material. Failure modes usually depend on the material type. For instance, fatigue crack nucleation in a brittle material is more sensitive to the normal stress compared to a ductile material. As a result, a fatigue criterion can be more suitable for one material than the other, and thus, the selection of the appropriate fatigue criterion has to be done with caution. In addition, the proposed multi-axial fatigue model must be able to correlate the fatigue damage to the fatigue life according to a set of experiments that are performed with different loading configurations (uni-axial, biaxial, torsional, or bending) and different loading histories (proportional and nonproportional). Jiang et al. [71] has studied the capability of some critical plane approaches to predict the fatigue life and planes of failure in a structural steel (S460N). In what follows, some of the most popular critical plane fatigue approaches are discussed with further details.

4.2.1 Findley Fatigue Criterion

Based on observations from experimental results, fatigue cracks tend to nucleate on or around either the maximum principal plane or the plane of maximum alternating shear stress. Findley [73] suggested that the tensile normal stress acting on the maximum shear plane can also affect the fatigue crack nucleation process as it leads to the separation of crack surfaces under alternating shear stresses and promotes the movement of

dislocations on that plane. He proposed a stress-based critical plane criterion, in which the damage will occur on a plane where the linear combination of the shear stress amplitude and the factorized normal stress is the largest. Findley fatigue criterion, f_{FIN}, can be expressed by the following equation

$$f_{FIN} = \frac{\Delta\tau_{max}}{2} + \kappa\sigma_n \tag{4.1}$$

where $\Delta\tau_{max}$ and σ_n are the maximum shear stress range and the maximum normal stress experienced on a plane with the largest Findley fatigue index during one cycle of loading, respectively. The coefficient κ is an empirical material constant that changes from 0.3 for ductile steel to 0.7 for brittle steel. As this equation shows, positive normal stresses (tensile) will assist the crack nucleation process, while negative normal stresses (compressive) will do the opposite (Socie [74]). The Findley fatigue parameter has the unit of a stress, i.e. MPa in this study.

The coefficient used to include the influence of normal stresses, κ, is called the normal coefficient in this study. The normal coefficient is a material dependent parameter which must be determined by regression analysis of fatigue-life data from multi-axial and torsional fatigue experiments. This parameter is a representative of the material sensitivity to the tensile-based damage mechanisms. For instance, a ductile failure mode will be expected for κ equals to 0, where the shear stress amplitude term is dominant. Conversely, as κ increases, the contribution of normal stresses in crack nucleation and early growth will increase and the failure happens in a more brittle manner. Therefore, brittle materials are more sensitive to the normal stress term. For pearlitic rail steel, κ equals to 0.3 presented the best fit based on the regression analysis of a set of experimental fatigue life

data from previous studies (Tangtragulwong [48]). Kaufman and Topper [75] suggest imposing an upper-bound on the influence of the tensile normal stress in a way that when a limit is reached, indicating the full separation of crack surfaces under alternating shear stress amplitude, the further increase of tensile stresses will have no effect on the fatigue life.

Findley fatigue parameter has shown satisfactory predictions of the damage in high-cycle fatigue problems where the stress level is less than material yield limit (Tangtragulwong [48], Fry [45]).

4.2.2 Dang Van Fatigue Criterion

Dang Van proposed an endurance limit criterion based on the principle of elastic shakedown, which defines the fatigue damage parameter as the onset of accumulated mesoscopic plastic strains (Dang Van et al. [76]). A fatigue crack is thus assumed as a local process that begins in grains once the elastic shakedown limit is exceeded, meaning that the mesoscopic stresses exceed the elastic yield limit of the crystal, forming characteristic slip bands.

The nucleation of fatigue cracks in intragranular slip bands justifies the hypothesis that the microscopic shear stress on a grain must be an important parameter. Similarly, the microscopic hydrostatic stress is also significant due to its influence on the opening of the crack faces. The simplest approach to correlate these two variables is a linear combination, given by (Socie and Marquis [77])

$$\tau(t) + a\,\sigma_h(t) = b \tag{4.2}$$

where $\tau(t)$ and $\sigma_h(t)$ are the instantaneous microscopic shear stress and hydrostatic stress, respectively. a is and an empirical material constant and b is directly related to the fatigue resistance of the material. The microscopic shear stress and hydrostatic stress are computed from the microscopic principal stresses at every instant of the loading by

$$\tau(t) = \frac{1}{2}[\sigma_1(t) - \sigma_3(t)] \tag{4.3}$$

$$\sigma_h(t) = \frac{\sigma_1(t) + \sigma_2(t) + \sigma_3(t)}{3} \tag{4.4}$$

The failure criterion then can be interpreted as an inclined line in $\tau - \sigma_h$ plane. As shown in Figure 4.2, if a loading path remains within the two bounding failure lines an infinite life is expected. Conversely, any path that passes damage boundaries is subjected to the fatigue failure. Unlike to other stress-based methods, the output from the Dang Van criterion is always expressed as a safety factor, without any estimation on the fatigue life.

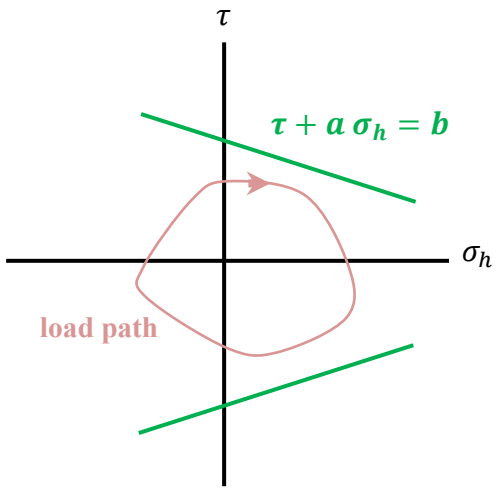

Figure 4.2. Schematic of Dang Van fatigue failure criterion

The Dang Van criterion formulates the microscopic stress, $\sigma_{ij}(t)$, as a function of the macroscopic bulk stress, $\Sigma_{ij}(t)$, and microscopic residual stress (Socie and Marquis [77])

$$\sigma_{ij}(t) = \Sigma_{ij}(t) + dev\ \rho^* \tag{4.5}$$

where $dev\ \rho^*$ is the deviatoric part of the stabilized residual stress tensor. For engineering purposes, the Dang Van criterion can be reformulated to solely use macroscopic stresses, assuming that elastic shakedown occurs both at mesoscopic and macroscopic levels.

4.2.3 Brown-Miller Fatigue Criterion

Analogues to the Findley fatigue criterion, Brown and Miller [78] formulated a strain-based criterion for the shear failure mode as a linear combination of the cyclic shear strain amplitude and factorized normal strain on the plane of maximum shear strain amplitude. They suggest that cyclic shear strains cause the crack nucleation, while normal strains assist in the crack growth. Brown-Miller fatigue criterion is defined as

$$\frac{\Delta\hat{\gamma}}{2} = \frac{\Delta\gamma_{max}}{2} + S\Delta\varepsilon_n \tag{4.6}$$

where $\Delta\hat{\gamma}$ is the equivalent shear strain range, $\Delta\gamma_{max}$ is the maximum shear strain range, S is an empirical material dependent constant, and $\Delta\varepsilon_n$ is the normal strain range on the plane experiencing the maximum shear strain range. As seen, the Brown-Miller fatigue model is a pure strain-based approach with no stress component. Hence, this model is not able to incorporate the effect of tensile stresses into fatigue damage predictions.

4.2.4 Fatemi-Socie Fatigue Criterion

To account for the friction between crack faces, Fatemi and Socie [79] suggested replacing the normal strain component in the Brown-Miller fatigue criterion with a normal stress component. This fatigue parameter was formulated based on the idea that while alternating shear strain is the main driving force behind the fatigue crack initiation, the maximum normal stress acting on the crack plane will also influence the nucleation and growth of small cracks by changing the friction between crack faces. The conceptual basis for this damage model is shown in Figure 4.3. When a pure shear loading is applied, the irregular shape of crack surfaces creates frictional forces that oppose shear deformations. This mechanism can impede the crack growth, and thus, extend the fatigue life of the material. Tensile stresses, on the other hand, will separate crack faces and reduce frictional forces between them, which is expected to favor the crack growth.

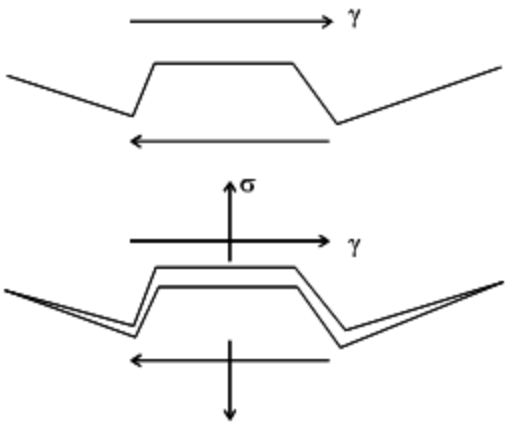

Figure 4.3. Physical basis of Fatemi-Socie fatigue model
(reprinted from Marquis and Socie [80])

They also modified the Brown-Miller fatigue criterion in a way that no pure axial static load will result in fatigue damages meaning that the alternating shear strain is required for the fatigue damage to occur. The Fatemi-Socie damage index is a strain-based fatigue criterion which is valid for both HCF and LCF regimes. The fatigue parameter is defined as

$$f_{FS} = \frac{\Delta\gamma_{max}}{2}(1 + \eta\frac{\sigma_n}{\sigma_y}) \tag{4.7}$$

where $\Delta\gamma$ is the maximum shear strain range on any plane during the loading cycle, σ_n is the maximum normal stress occurring on the plane of maximum shear strain range for the cycle of interest, σ_y is the material yield strength (568 MPa for thermite rail weld), and η is an empirical material constant ranging from 0.5 for ductile steels to 3 for brittle steels. The normal stress component is normalized by the monotonic tensile yield stress to maintain the unitless feature of the strain. The Fatemi-Socie fatigue criterion has shown satisfactory results in fatigue life predictions for various types of metals exhibiting shear failure mechanisms (Jiang et al. [71], Tangtragulwong [48], and Kiani [68]). However, since the normal stress term is multiplied by the shear strain range, the cyclic shear strain must be present in order for the fatigue damage to occur. This may prevent an accurate prediction of fatigue damage in situations where the normal stress term dominates on a plane and the shear strain range is too small.

4.3 Fatigue Index Calculation

In order to study the fatigue damage caused by a rolling wheel, it is preferable to describe the phenomena with multi-axial fatigue criteria in a manner that holds physical significance. Among all multi-axial fatigue criteria available in the literature, the Findley fatigue model is found as a convenient method to quantify the fatigue damage in various types of steel if HCF dominates and the material is elastic. In fact, both strain-based and stress-based approaches are theoretically the same for HCF applications. In this section, the implementation of the Findley fatigue index is discussed as a means to predict the location and orientation of nucleating fatigue cracks in the web and base region of thermite rail welds, remote from the wheel-rail contact. For this purpose, a computer algorithm is developed in Matlab® that takes time histories of the stress tensor, derived from wheel-track FE simulation, as an input to compute the fatigue damage.

To understand the fatigue behavior of thermite rail welds, the Findley fatigue index, given by equation (4.1), needs to be calculated for every single node on the cross-section of interest through all passing planes. A site of crack nucleation is where the Findley damage index is the largest. Crack initiation is expected at this location if the same loading configuration is applied repeatedly. However, if loading configuration is a function of time, the summation of the fatigue index on each plane over different loading configurations will instead determine the location of crack nucleation and early growth. According to Socie [74], no interaction is expected between different damaged planes, based on experimental results by McDowell et al. [81] and Hayhurst et al. [82]. Therefore,

he suggests that the fatigue index should be tracked independently for each plane when the fatigue damage accumulation happens.

For each evaluation point, the critical plane, representing the plane upon which a fatigue defect is predicted to nucleate, is the one that results in the most damaging fatigue parameter value through the time. In order to find the critical plane, an exhaustive plane search is required to examine all possible planes passing from evaluation points. To optimize the calculation time, the plane search is performed in the spherical coordinate system, as shown in Figure 4.4, with 10-degree increments of theta (θ) and phi (ϕ). The normal vector that defines a plane can be written as

$$\bar{n} = \begin{Bmatrix} n_1 \\ n_2 \\ n_3 \end{Bmatrix} = \begin{Bmatrix} sin\,\theta\, cos\phi \\ sin\,\theta\, sin\,\phi \\ cos\,\theta \end{Bmatrix} \tag{4.8}$$

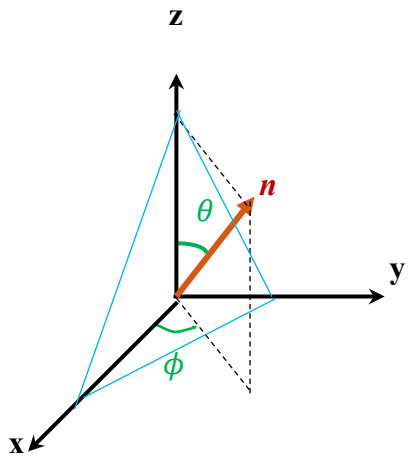

Figure 4.4. Spherical coordinate system

As a wheel rolls over the running surface of the rail, the state of stress gradually changes through many successive time increments. Therefore, the time history of stress tensors at each node of interest should be tracked through the loading cycle. This has been done using the finite element analysis, as described in the previous section. The stress tensors are then transformed into vectors, acting on any plane defined by a normal vector $\bar{n}$, as given by the following relation.

$$\bar{T} = \bar{\bar{\sigma}}.\bar{n} \tag{4.9}$$

where $\bar{T}$ is the stress vector and the dot symbol denotes the inner product of the stress tensor and normal vector. The stress vector should also be resolved into normal stress and shear stress components as required by equation (4.1).

$$\bar{\sigma}_n = (\bar{n}.\bar{t})\bar{n} = \sigma_n\bar{n} \tag{4.10}$$

$$\bar{\tau} = \bar{T} - \bar{\sigma}_n = \bar{T} - \sigma_n\bar{n} \tag{4.11}$$

For each point of interest, stress transformations are done for all time instants, over all the possible planes that are passing through that point. For each candidate plane, the maximum range of shear stress as well the maximum normal stress has to be determined. In this study, a Matlab® computer program is used to perform the critical plane search and calculate the Findley fatigue index at each location. The same procedure is also applicable to the transformation of strain tensors when a strain-based critical plane fatigue criterion is to be used.

4.4 Fatigue Life Predictions

One of the important aspects of the fatigue analysis is to estimate the service life of structures. A multi-axial fatigue model must be able to properly correlate the fatigue damage parameter to the fatigue life, based on the material behavior. As mentioned earlier, the accuracy of fatigue models may vary for different materials. Therefore, for a given material, a large set of data from various experiments with different loading configurations and different loading histories is required to assure successful fatigue life predictions.

The logarithm of fatigue life is commonly regarded as being inversely proportional to the logarithm of the Findley fatigue index. For pearlitic rail steel, Tangtragulwong [48] performed a regression analysis to correlate the Findley fatigue index and fatigue life (Figure 4.5). He utilized a comprehensive set of fatigue test results from: 1) uni-axial tests (Iwafuchi et al [83], Scutti et al. [84], and Ahlstrom and Karlsson [85]), 2) axial-torsion tests (Stadlbauer and Werner. [86]), and 3) bending tests.

Tangtragulwong suggests that $\kappa = 0.3$ gives the best linear fit between the Findley fatigue parameter and fatigue life on the log-log plot, meaning that the calculated least square error is minimized. Based on the regression analysis results for $\kappa = 0.3$, the fatigue-life equation of the rail steel is proposed to be expressed as

$$N = [10^{-3.047} \times f_{FIN}]^{(-1/0.1319)} \tag{4.12}$$

where N is the number of cycles to fatigue failure, and f_{FIN} is the Findley fatigue index. Special attention needs to be given to the definition of the "failure", which is a major source of discrepancy in correlating fatigue life data. In this model, failure happens when the first mirco-crack nucleates. Therefore, the fatigue life refers to the number of cycles

for crack nucleation and early growth and the life in crack propagation stage is considered to be minimal. Tangtragulwong fatigue-life equation has been employed in this study to estimate the service life of thermite rail welds.

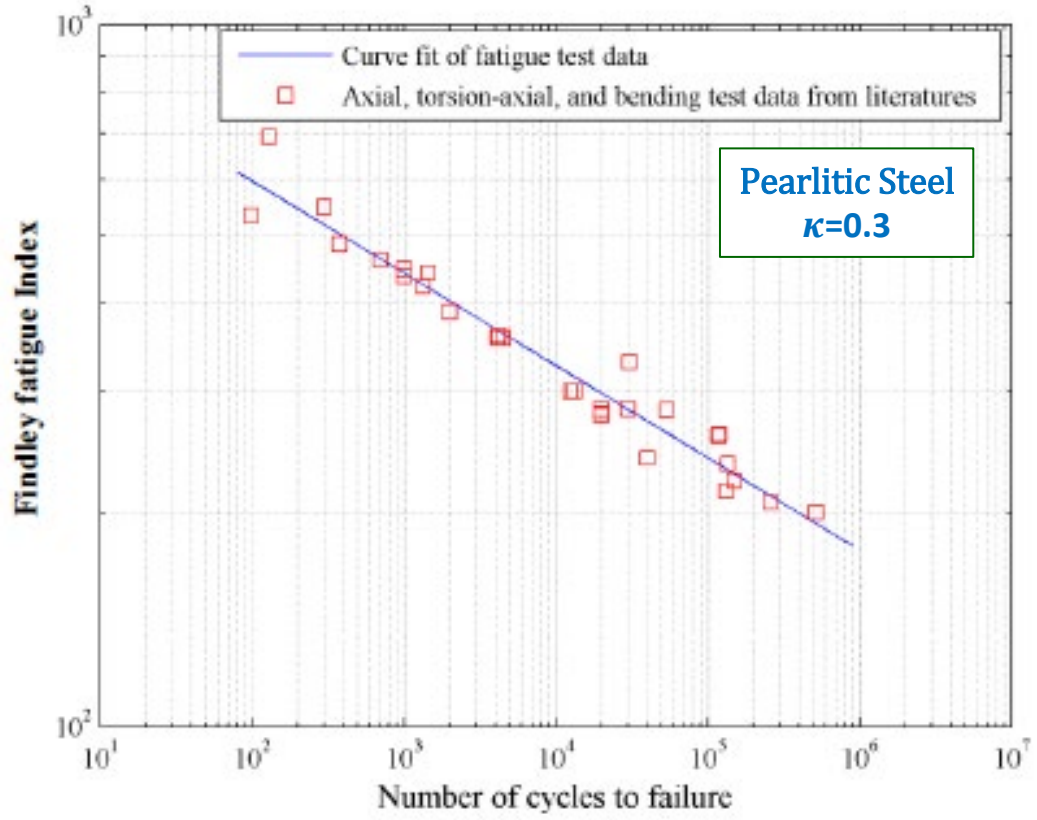

Figure 4.5. Correlation between the Findley fatigue index and the number of cycles to failure for $\boldsymbol{\kappa = 0.3}$ (reprinted from Tangtragulwong [48])

4.5 Results and Discussion

A multi-axial critical plane fatigue algorithm is developed in Matlab® with two major goals: 1) to predict the location and the plane of fatigue crack-initiation and 2) to predict the fatigue life of thermite rail welds. The Findley fatigue criterion is used to estimate the fatigue damage in the web and base region of the rail, next to the thermite weld. As presented in Section 3, the stress level in this region of the weld, remote from the wheel-rail contact area, is relatively small, and thus, HCF is expected to happen. This validates the assumption of elastic behavior behind the Findley parameter. Tangtragulwong fatigue-life equation is used to correlate the Findley damage index and fatigue life. Time histories of the stress tensor that are captured using the finite element analysis are utilized as an input to the fatigue model. The material is nominally assumed to be "defect-free". The results of the fatigue analysis are presented and will be discussed in the following subsections.

4.5.1. Study of Fatigue Cycles

The simplified model of wheel-rail interaction that was proposed in Section 3 is used here to scrutinize fatigue cycles in the rail weld base. A freight train with two full 286 kips cars is moved over the running surface of the rail and the variations of the axial stress and Findley fatigue parameter are tracked at a point located in the center of the rail base, next to the thermite weld. Figure 4.6 shows the configuration of train axle loads. In this model, each of the eight wheels is replaced by a 160 kN static vertical load.

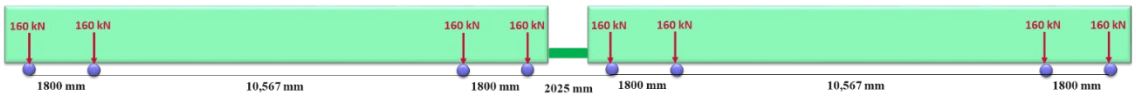

Figure 4.6. Configuration of train axle loads

To study the fatigue behavior, it is very important to find the loading configuration that creates fatigue cycles in thermite rail welds. Typically, fatigue cycles may be generated by each wheel, truck, car, or train passage. Figure 4.7 illustrates the time history of the axial stress and Findley fatigue damage parameter in the base center of the rail. As seen, the axial tensile stress reaches a peak value at every instant of time when a wheel passes over the observation point. At the same time, Findley fatigue index rises to its maximum value when a wheel is right above the observation point. Therefore, it can be concluded that every wheel passage will cause a fatigue cycle. This validates the finite element model of this study where only one wheel of the train has been simulated.

Furthermore, Figure 4.6.a shows that the maximum tensile stress in the rail base center is about 15% of the material yield strength. Since shear stress range in the rail foot is also relatively small, theoretically, a long service life would be expected for this region if the material is “defect-free” and there is no contribution of thermal stress fields and/or welding residual stresses.

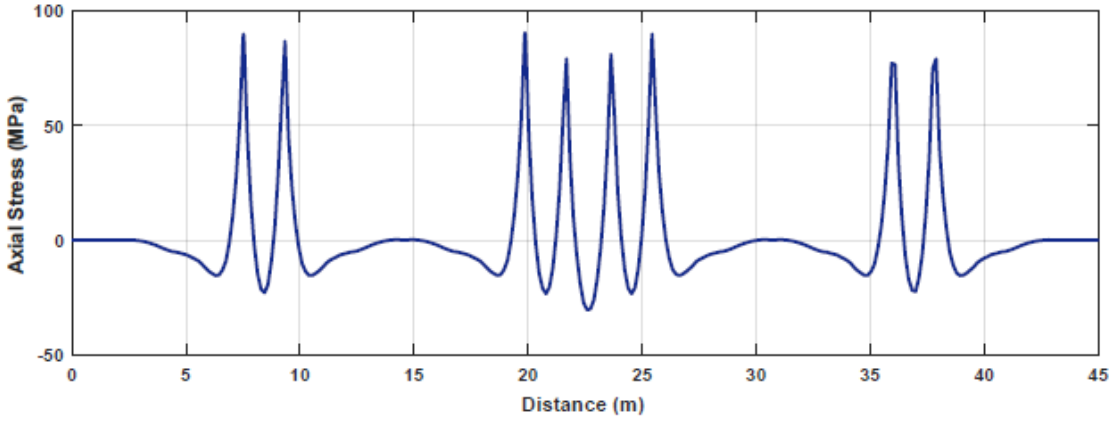

(a)

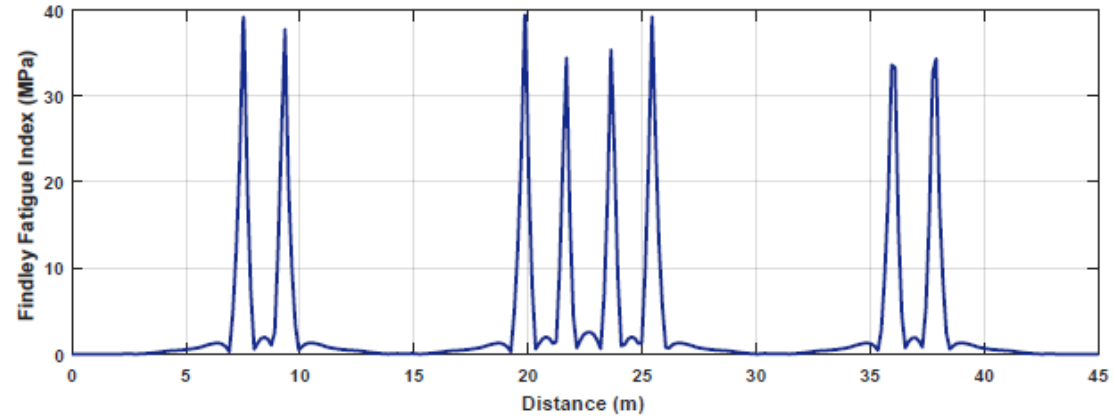

(b)

Figure 4.7. Time history of: (a) axial stress and (b) Findley parameter, in the center of the rail base, right next to the thermite weld

4.5.2. Fatigue Damage under a Rolling Wheel

For each evaluation point along the cross-section of interest, shown in Figure 4.8, the Findley fatigue index is calculated from the stress tensor history for one wheel rolling cycle, through all possible planes. Among those planes, the largest damage index at each point is presented in Figure 4.9, to construct the fatigue index contour.

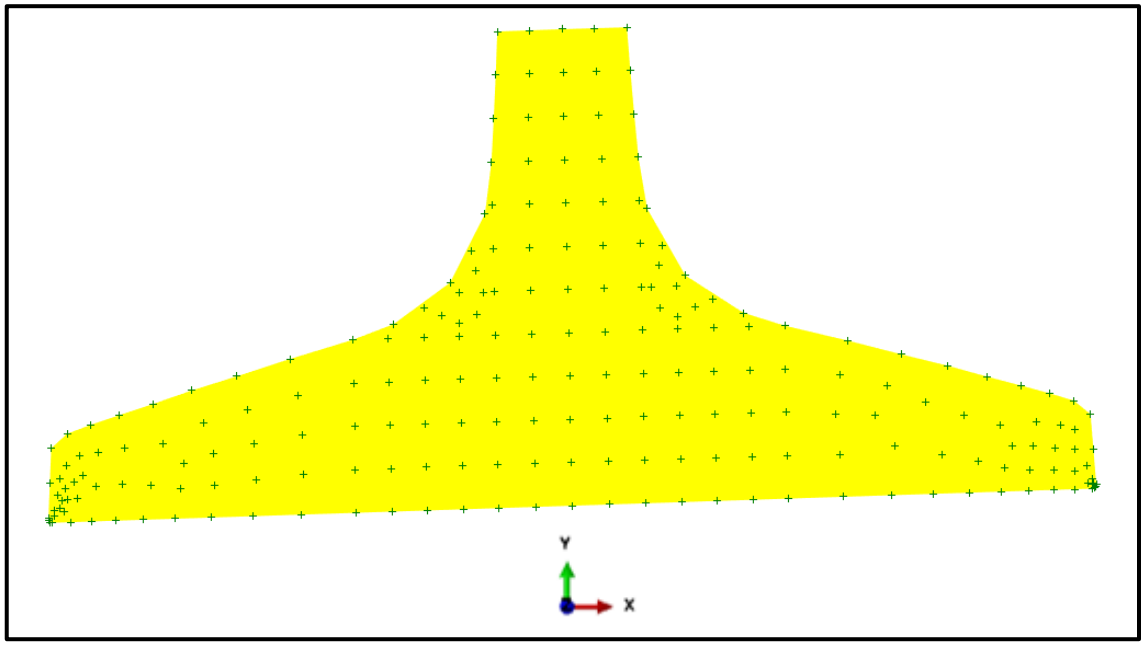

Figure 4.8. Cross-section of interest for the fatigue study

Fatigue cracks are expected to nucleate at sites where the Findley fatigue index is the largest. As seen in Figure 4.9, the contour of fatigue index is highly localized on rail base corners with the largest fatigue index of 70 MPa. A lower peak value of about 44 MPa can also be observed in the center of the rail base. In the web-to-base fillet region, the maximum value of fatigue index is comparable to that of the rail base center but less localized.

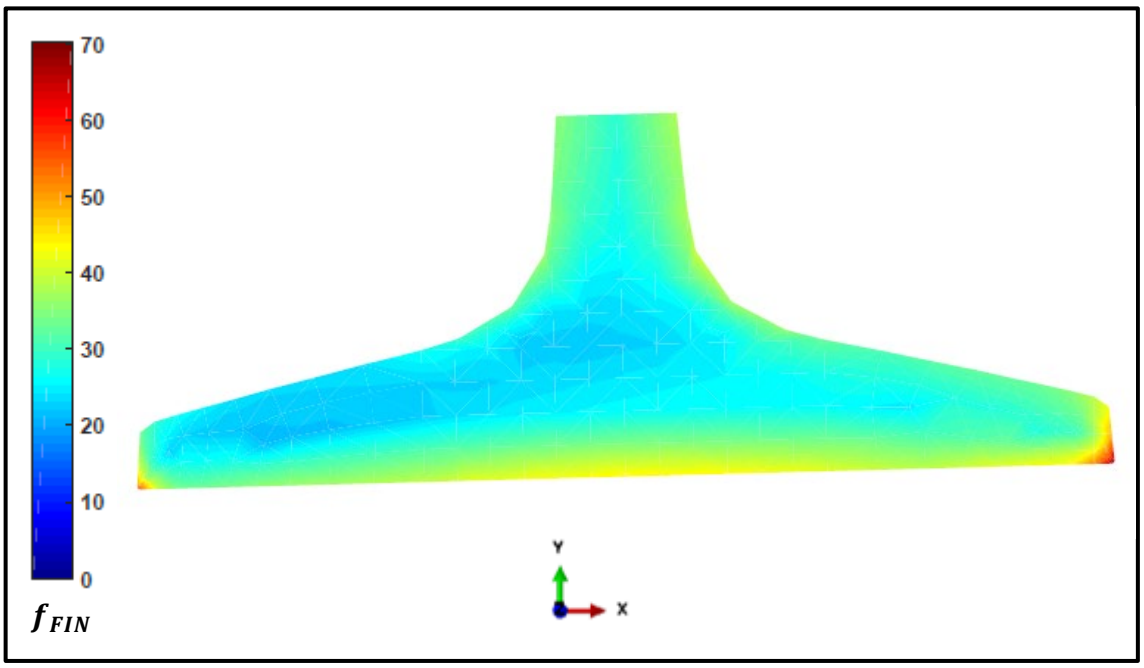

Figure 4.9. Maximum Findley fatigue index contour caused by a rolling wheel (MPa)

In order to assess the service failure of thermite rail welds, the fatigue crack nucleation is studied at three critical locations where most reported weld service failures occur. This includes rail base corners, rail base center, and web-to base fillet, as shown in Figure 4.10. The direction cosine of critical planes, as an approximation to cracking planes, along with the corresponding fatigue damages for all cases are summarized in Table 4.1. As seen, the critical plane for all three locations approximately coincides with the transverse plane. Thus, it can be inferred that mode I cracking dominates where tensile stresses are acting normal to crack faces. Note though critical planes are not always necessarily the same.

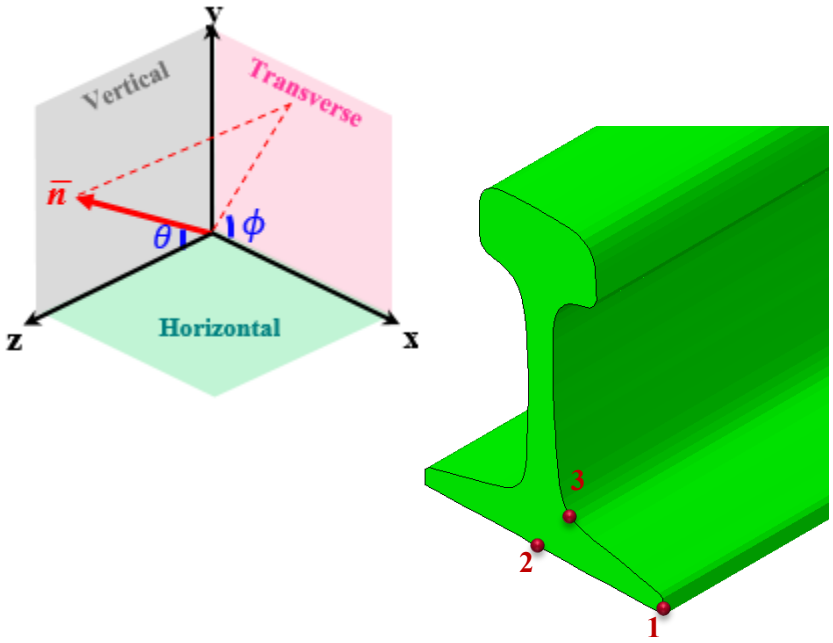

Figure 4.10. Critical locations from which service failures are observed to initiate (right next to the thermite weld)

Table 4.1. Summary of possible fatigue crack nucleation sites and cracking planes caused by a rolling wheel

	Location	f_{FIN} (MPa)	$\theta°$	$\phi°$	n_1	n_2	n_3
1	Base Corner	70	145	345	0.55	-0.15	-0.82
2	Base center	44	30	15	0.48	0.13	0.87
3	Web-base fillet	40	170	60	0.09	0.15	-0.98

The Findley fatigue index values are then utilized to estimate the fatigue life of the thermite rail weld at those three critical locations and Table 4.2 summarizes the results. According to this fatigue model, the failure is most likely to originate from the rail base corners where the service life is the lowest. The center of the rail base is the next possible location of the failure, and the fatigue life in the web-to-base fillet is very large compared to the base. In fact, the results of this analysis predict a high fatigue resistance in the web and base region of the thermite rail weld if the material is "defect-free". The estimated long-life fatigue behavior can be attributed to practically small stresses that are formed in this region resulting from the wheel load. Statistics, on the other hand, have reported that plenty of service failures started in either base-center or web-to-base fillet areas. Taken from Lawrence et al. [8], Figure 4.11 shows that about 90% of broken thermite welds started to fracture in the base, web, and web-to-base fillet regions. In addition, Laboratory fatigue tests on field-welded rails suggest similar outcomes. For example, 4-points fatigue

Table 4.2. Summary of fatigue crack nucleation sites and estimated service life associated with wheel loading

	Location	f_{FIN} (MPa)	N	Estimate Life (MGT)
1	Base Corner	70	1.26E+09	44,992
2	Base center	44	4.25E+10	1,518,978
3	Web-base fillet	40	9.14E+10	3,265,832

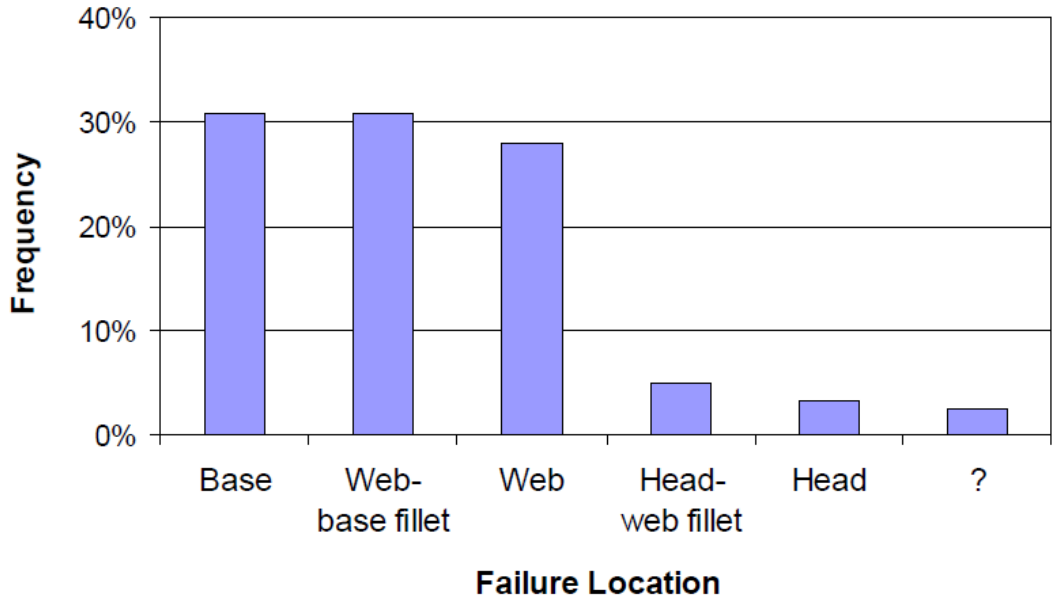

Figure 4.11. Analysis of 244 thermite service failures reported by a class I railroad (reprinted from Lawrence et al. [8])

experiments performed by Fry [87] present a premature fracture in the web-to base fillet. The fracture surface for some of the test specimens is shown in Figure 4.12 toFigure 4.14. Therefore, the presence of defects through the web and base region of thermite rail welds, and/or thermal/residual stresses can be considered as potential roots for accelerating the fatigue fracture in thermite welds. The influence of "pre-existing" imperfections will be discussed in more depth through the next section.

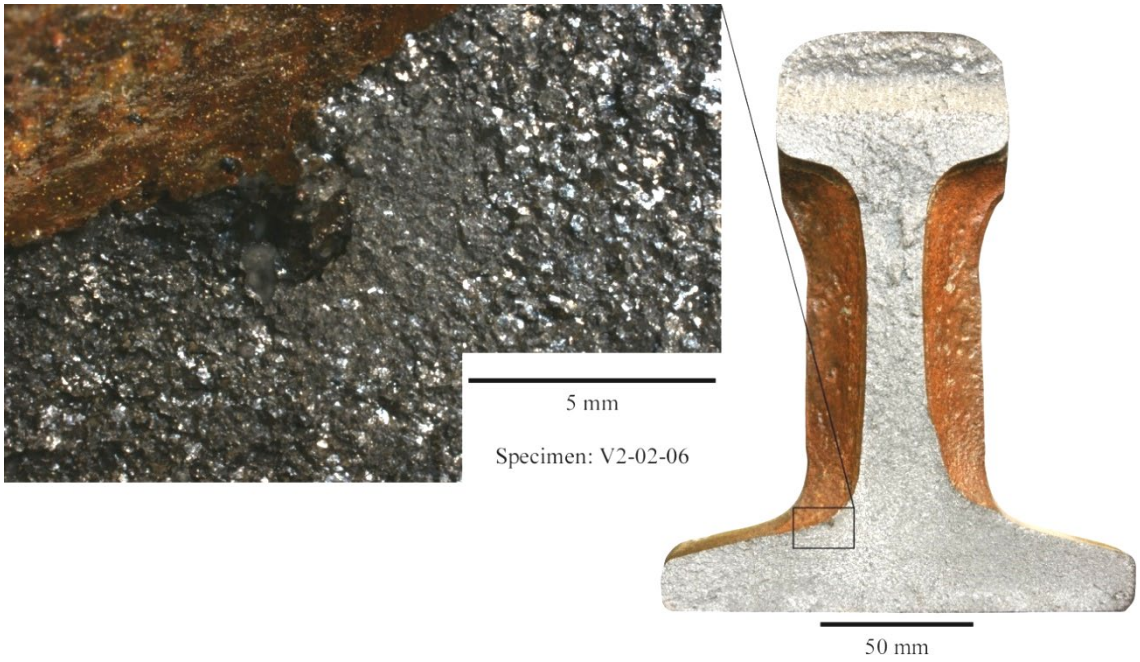

Figure 4.12. Fatigue crack nucleation from a pore defect located in the web-to-base fillet of a thermite rail weld specimen

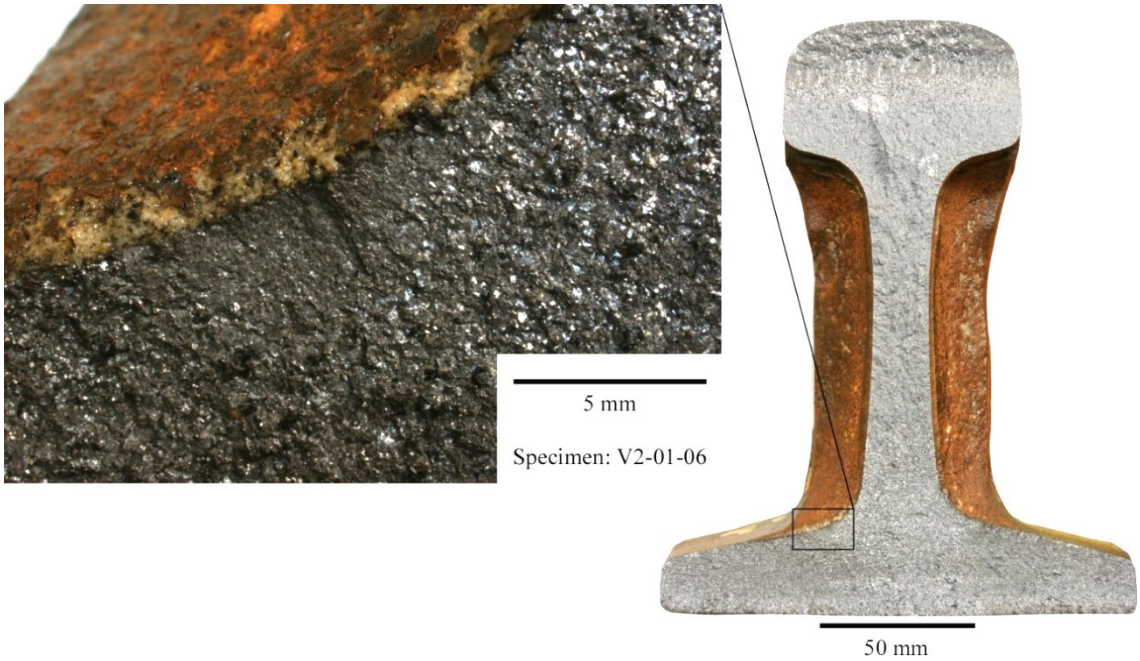

Figure 4.13. Fatigue crack nucleation from a metallurgical imperfection (a layer of glass-type material) located in the web-to-base fillet of a thermite rail weld specimen

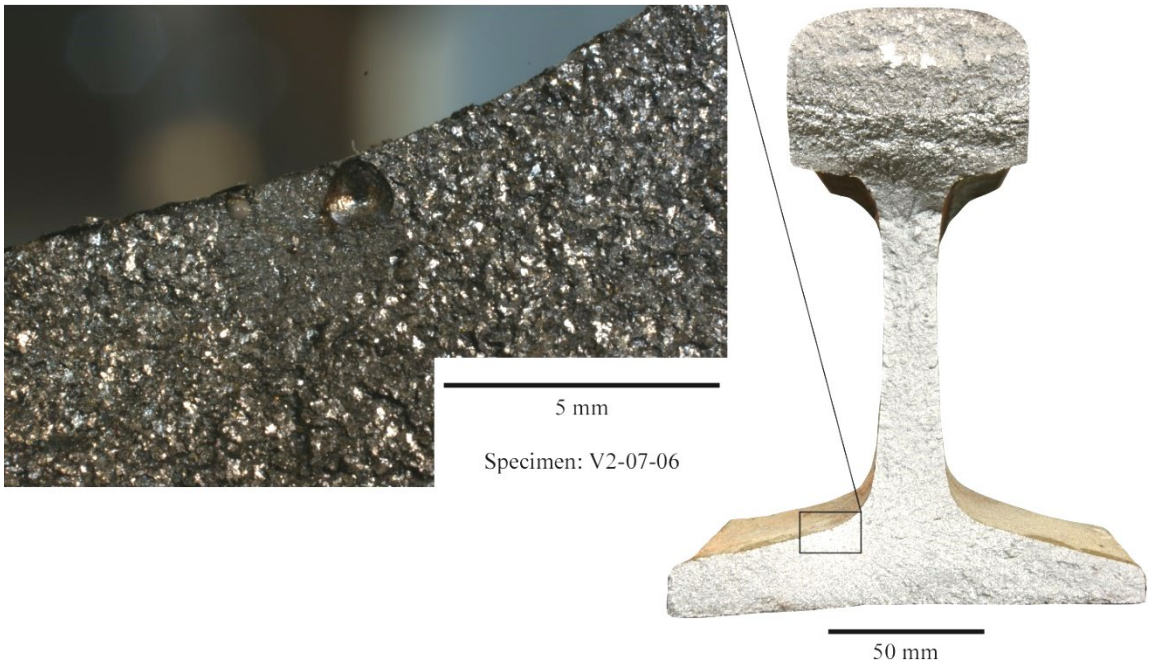

Figure 4.14. Fatigue crack nucleation from a nonmetallic inclusion located in the web-to-base fillet of a thermite rail weld specimen

4.5.3. Influence of Rail Thermal Variations on Fatigue Life

In Section 3, it has been shown that cold rail temperatures caused by winter weather can produce large axial tensile stresses in continuously welded rails which may pull the rail apart. The results of the FE analysis predict regions of high stress concentration located at the rail base corners as well as the web-to-base fillet. In this section, the influence of rail temperature variation on the nucleation of fatigue cracks has been explored. Figure 4.15 illustrates the contour of maximum Findley fatigue parameter over the cross-section of interest for a particular case where the ambient temperature falls 100 ℃ below the rail neutral temperature. The interaction between wheel rolling stress fields and rail thermal stresses is incorporated into the stimulation. The fatigue analysis

predicts a high risk of fatigue damage in the rail base corners and web-to-base fillet. The contribution of thermal stresses seems to be significant mainly due to an increase in the mean stress term.

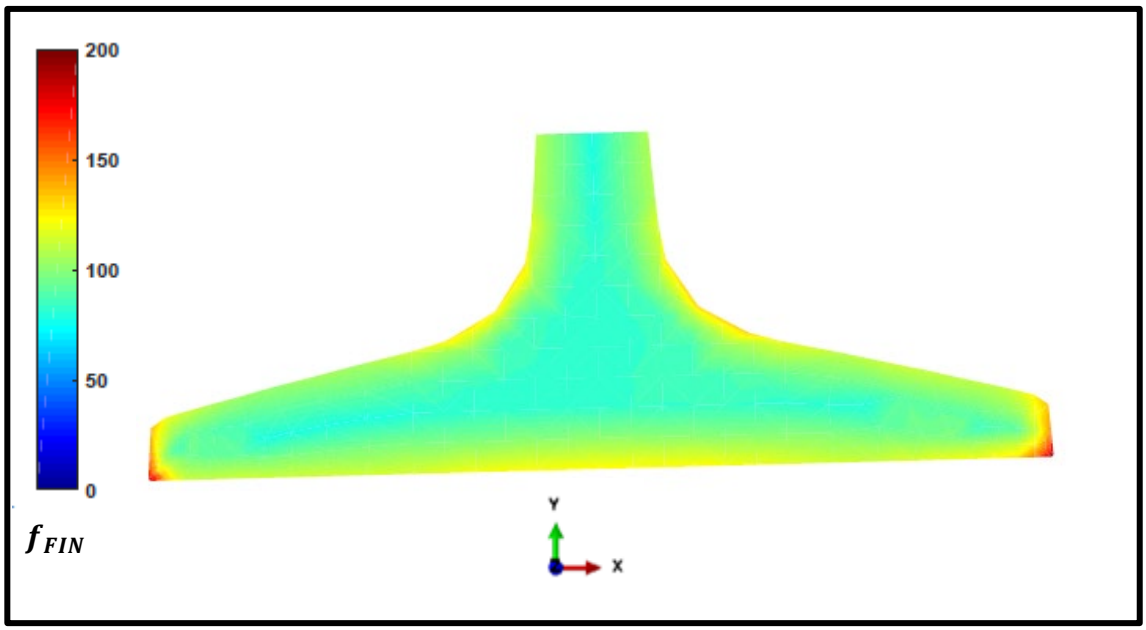

Figure 4.15. Maximum Findley index contour caused by thermal-mechanical loading (MPa)

Table 4.3 summarizes the value of fatigue damage indices along with the direction of approximated cracking planes at three critical locations of the thermite rail weld, as described before. In comparison with the fatigue damage caused by wheel loads, presented in Table 4.1, it can be observed that the Findley fatigue index is amplified by a factor of 3 when the effects of thermal stresses are incorporated into the fatigue analysis. Therefore, the fatigue performance of thermite rail welds is substantially influenced by ambient

temperature changes. Previous studies performed by Skyttebol et al. [44] has also reported a similar effect. In addition, Table 4.3 shows that fatigue cracks tend to nucleate in the transverse plane, perpendicular to the axial tension caused by flexural deformations. Therefore, thermal variations have a small influence on the orientation of approximated cracking planes.

Table 4.3. Summary of possible fatigue crack nucleation sites and cracking planes caused by thermal-mechanical loading

	Location	f_{FIN} (MPa)	$\theta°$	$\phi°$	n_1	n_2	n_3
1	Base Corner	209	20	90	0.00	0.34	0.94
2	Base center	122	10	10	0.17	0.03	0.98
3	Web-base fillet	141	350	160	0.16	-0.06	0.98

Furthermore, fatigue life estimations are summarized in Table 4.4. As seen, cold rail temperatures can tremendously accelerate the formation of fatigue cracks, even if the material is ideally free of any flaws and imperfections. Note that the possibility of fatigue crack nucleation in the web-to base fillet region is about 3 times larger as compared to the rail base center. This might be helpful to address the observation that fatigue fractures in thermite rail welds commonly start in the web-to-base fillet. As a result, fatigue cracks

may grow to failure in a very short period of time if tensile thermal stresses interact with axle loads.

Table 4.4. Summary of fatigue crack nucleation sites and estimated service life associated with thermal-mechanical loading

	Location	f_{FIN} (MPa)	N	Estimate Life (MGT)
1	Base Corner	209	3.20E+05	11
2	Base center	122	1.88E+07	671
3	Web-base fillet	141	6.49E+06	232

4.5.4. Influence of Track Boundary Conditions on Fatigue Life

Effects of the track foundation quality on the stress field in the rail base were studied in the previous section. It has been shown that degraded support conditions can amplify the stresses in the rail base, near the thermite weld. It is also important to note that the rail foundation cannot really resist any tension. In other words, the foundation is not able to pull the rail down in situations where the reverse bending occurs and the rail base tends to move in the upward direction. Therefore, a proper simulation of the track foundation should present the capability to differentiate between compressive and tensile stiffness of the track foundation support. In the present study, six contact pairs are defined

between the rail base bottom surface and top faces of steel tie-plates within the FE simulation. Therefore, the tensile stiffness of the foundation is equal to zero and the rail can move in an upward direction without any constraint. In order to explore the effect of the track foundation stiffness on the fatigue life of thermite rail welds, two cases with linear and bilinear stiffness models are compared. The force-displacement relationship of the track foundation's spring elements is schematically shown in Figure 4.16 for both cases, where F and v correspond to the vertical load and vertical displacement (in the y-axis direction), respectively.

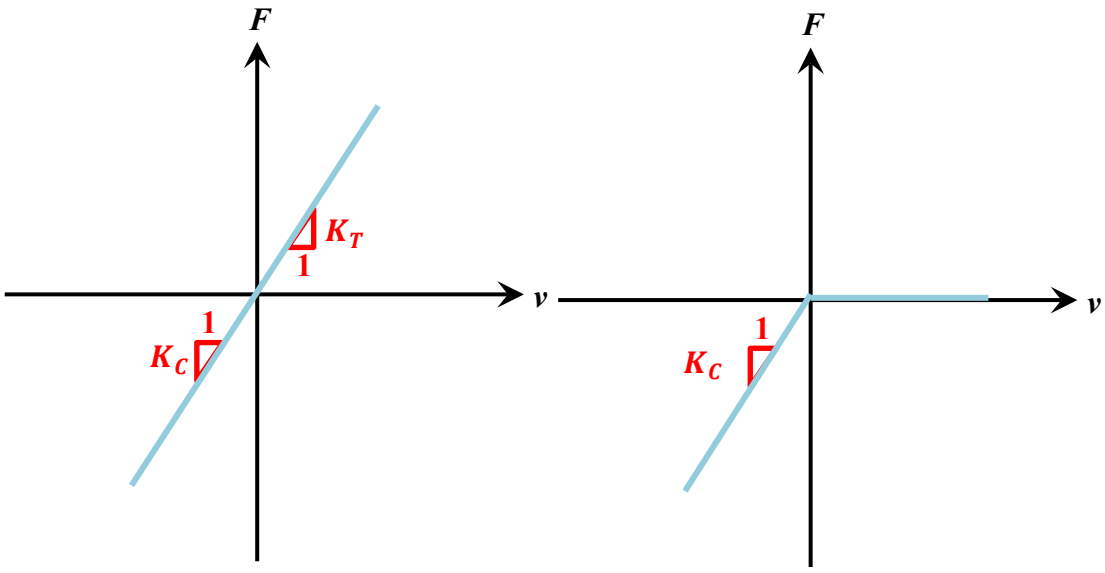

(a) $K_T = K_C = 62.4$ kN/mm **(b) $K_T = 0$**

Figure 4.16. Rail foundation stiffness model: (a) linear springs and (b) bilinear springs

The time history of axial stresses and Findley fatigue parameter is compared for the two models, shown in Figure 4.17. As seen, the linear stiffness model underestimates the peak tensile stress and Findley fatigue damage parameter for about 10 %. Consequently, the assumption of equal stiffness in tension and compression for the track foundation will overestimate the service life of thermite rail welds. Hence, proper simulation of the track foundation is an essential aspect of any track model.

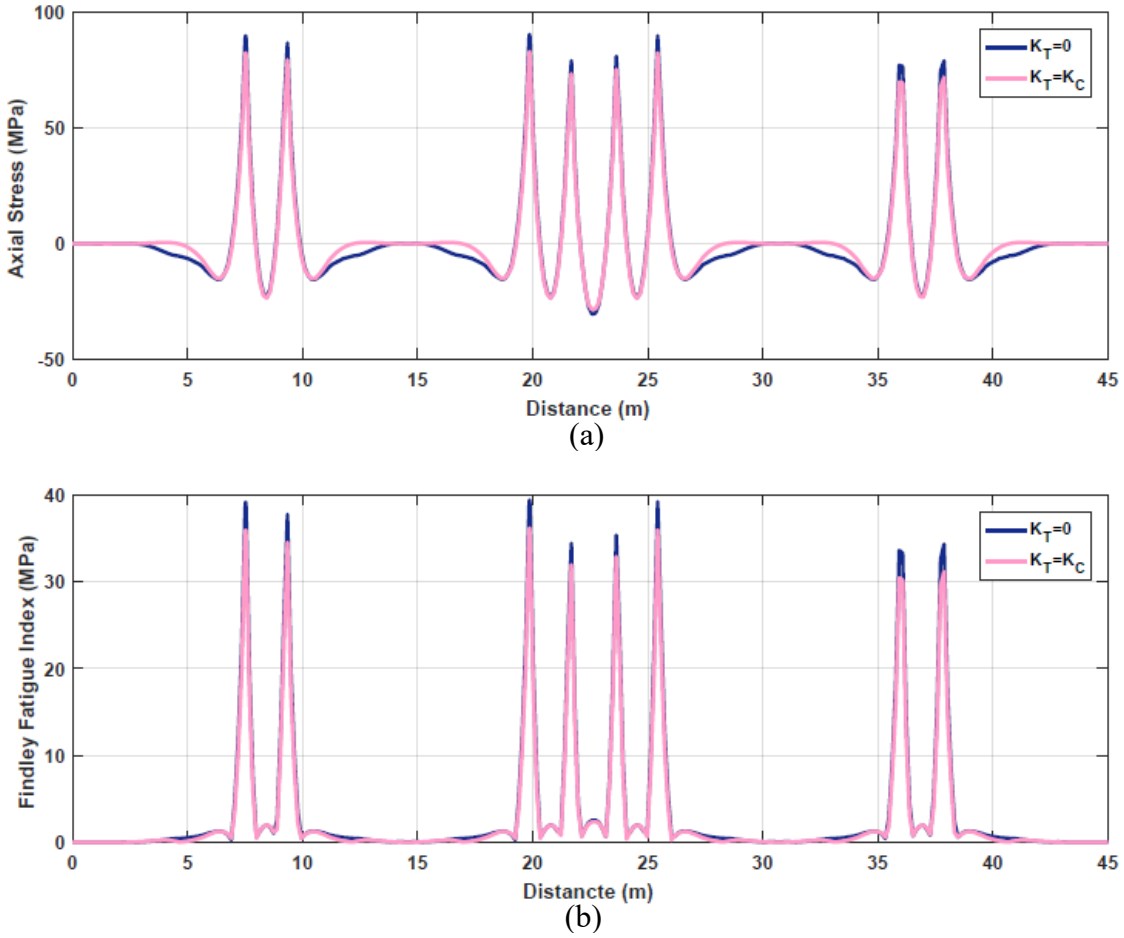

Figure 4.17. Rail track foundation stiffness effects: (a) axial stress and (b) Findley parameter, in the center of the rail base, right next to the thermite weld

4.6 Summary

- A multi-axial critical plane fatigue algorithm is developed in Matlab® to investigate the fatigue behavior in three critical regions of thermite rail welds: base corners, base center, and web-to-base fillet. Findley fatigue parameter is used within the model to predict the fatigue damage at different locations of the rail section, next to the thermite weld. Fatigue life estimates are also made by means of an experimental equation that correlates the Findley fatigue parameter to the rail service life.
- Each wheel passage generates a fatigue cycle.
- The results of the fatigue analysis suggest that fatigue cracks are more likely to nucleate from rail base corners, under wheel rolling stresses. Rail base center is the next critical location to start the fracture. The possibility of fatigue crack initiation in the web-to-base fillet is smaller than the other two locations.
- Fatigue cracks in the web and base region of thermite rail welds tend to initiate in a transverse plane, perpendicular to bending stresses. Therefore, mode I cracking dominates, which is the most critical mode of fracture.
- If the material is "defect-free", a large number of cycles is required for the fatigue cracks to initiate in the web and base region of thermite rail welds, since the stress level is typically small. However, the interaction of other stress fields (such as thermal stresses) can significantly accelerate the fatigue crack formation and early growth.

- Cold rail temperatures caused by winter weather may generate very large tensile stresses in continuously welded rails, which subsequently reduces the service life of thermite rail welds to a short time. The influence of thermal variations is found to be more considerable in the web-to-base fillet region of rail welds.
- Proper simulation of track foundation is necessary for an accurate fatigue prediction. It is important to note that rail track foundations usually cannot resist tensile stresses.

5. NEAR FIELD BEHAVIOR OF PLANAR IMPERFECTIONS

5.1 Introduction

Field observations indicate that under train heavy axle load operations, thermite rail welds are preferential locations for nucleation of fatigue defects when compared to base metal or electric flash-butt rail welds. Despite substantial advancements in material properties and periodic non-destructive inspections, some of the weld defects can be missed and consequently become a hidden threat to the track integrity. Pre-existing defects and metallurgical discontinuities are regarded as potential sites from which fatigue cracks are most likely to initiate and eventually break the rail apart.

In this section, the examination of stress fields at the periphery of planar fatigue defects is carried out. Small, half-penny shaped, surface defects are implemented at critical locations of thermite rail welds. In addition, the influence of pre-existing defects on the fatigue performance of thermite rail welds is assessed and compared to the fatigue nucleation life in a "defect-free" material, as presented in Section 4.

5.2 Computer Simulation of Planar Defects

Experimental observations show that fatigue cracks nucleate as planar defects. The size, shape, and orientation of defects can strongly influence the structural response of any component subjected to a cyclic loading. This study is focused on the implementation of small, half-penny shaped, surface defects with rounded edges into critical locations of the rail, next to the thermite rail weld, from which most of the field failures are observed to

initiate. The geometry of a penny-shaped defect is helpful in stress analysis since it represents an idealized shape of a sharp crack to overcome stress singularities at the crack-tips (Sih [88]). Sack [89] and Sneddon [90] are among the pioneers to study 3D aspects of the stress state around a penny-shaped defect.

As shown in Figure 5.1, fatigue defects commonly trigger from pre-existing imperfections in the heat affected zone (HAZ) of the rail where the state of residual stresses and material properties are highly fluctuated. Also, the results of the fatigue analysis indicate that in rail base and web regions, fatigue defects tend to form in a transverse plane, perpendicular to flexural stresses. Thus, in the current study, defects are transversely oriented in the rail HAZ, next to the weld. Defects are implemented one at a time so that their stress fields do not interact with one another.

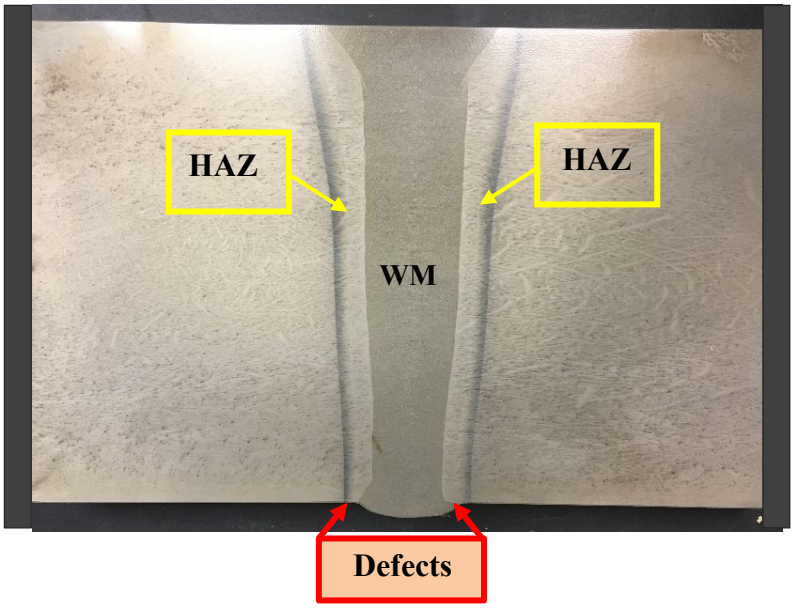

Figure 5.1. Formation of defects in the rail HAZ, right next to the thermite weld

The shape of the defect, illustrated in Figure 5.2, is of the form of a half-penny having a diameter of 2.00 mm with rounded edges -"blunt" tip - having a root radius of 0.2 mm. Note that 2.00 mm is considered as the smallest size of a defect that can be detected by visual inspection. Figure 5.3 represents the mesh pattern around the defect in a transverse plane passing through the tip. The mesh size at the blunt tip is very small - about 0.1 mm - to precisely capture the stress field near the defect. The material is expected to behave elastically in the defect region.

Figure 5.2. Geometry of the implemented half-penny shaped fatigue defect

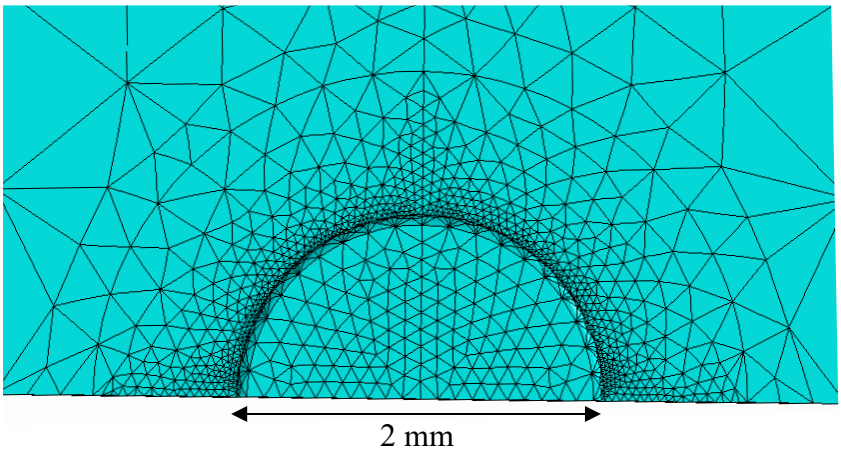

Figure 5.3. Mesh pattern near the defect

As discussed earlier, most of the thermite rail weld service failures are observed to initiate either from web-to-base fillet or rail base center. For this reason, formation of a defect in two critical sites is to be examined: (1) center of the web-to-base fillet (Figure 5.4.a), (2) center of the rail base (Figure 5.4.b).

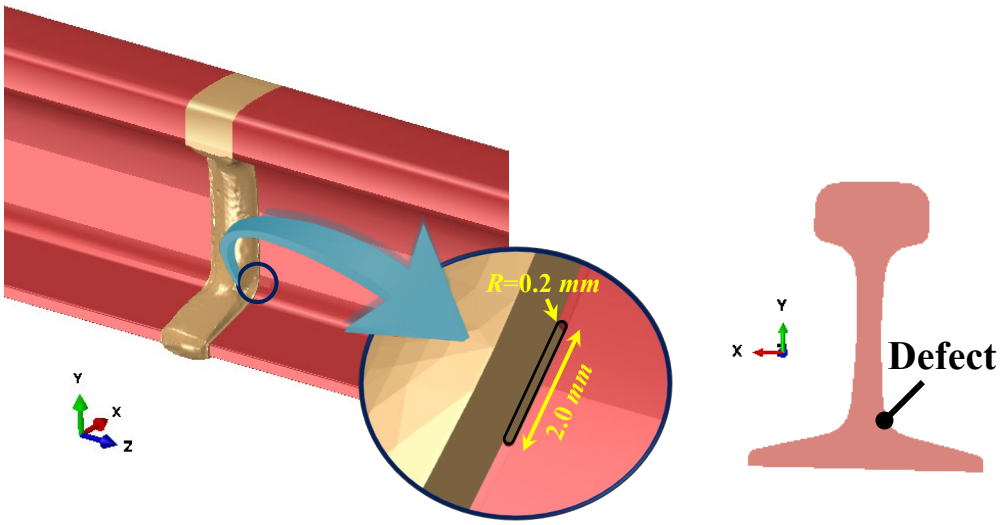

(b) Center of the web-to-base fillet

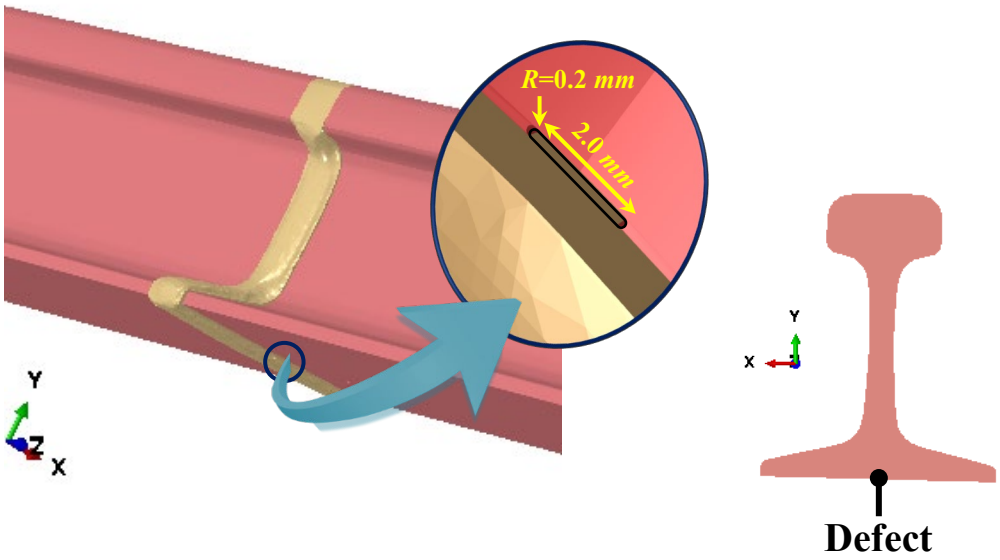

(a) Center of the rail base

Figure 5.4. Location of implemented small planar defects

5.3 Fatigue Analysis

In general, rail fatigue models are aimed for two fundamental goals. First, to determine the number of axles of a certain weight that can pass before a fatigue defect forms in the rail, assuming that there is no pre-existing defect (nucleation stage). Examples of nucleation models are provided in Section 4. Second, to address the propagation characteristics of the defect in terms of the number of passing axles, when a well-defined fatigue defect is implemented into the rail. In fact, the idea is to predict the time required for a detectable fatigue defect to propagate to form a dominant crack that can cause a catastrophic rail break (propagation stage). Specific examples of propagation models include Skyttebol et al. [41], Seo et al. [91], Desimone and Beretta [92], and Bartera et al. [93]. Although some models incorporate both capabilities, most of them only focus on either the nucleation stage or propagation stage.

In the present study, fatigue defect nucleation in a "defect-free" material was thoroughly explored in Section 4. It has been shown that it can take a long period of time for fatigue defects to nucleate in the base or web region of thermite rail welds, mainly because of relatively small stress fields that are generated by the wheel rolling in the rail foot. Thermal stresses caused by cold winter weather, however, were found to considerably accelerate the process. In this section, on the other hand, fatigue nucleation life from pre-existing defects is to be investigated. Small planar defects are implemented to the critical locations of the rail, next to the thermite weld, and the multi-axial fatigue algorithm is utilized to assess the fatigue life near blunt edges of the defect.

5.4 Results and Discussion

Small surface defects are implemented, one at a time, to the computational model of the rail, right next to the thermite weld. FE analysis is performed, using ABAQUS/CAE®, to capture stress fields near defects, caused by wheel axle loads. Then, time histories of the stress tensor are used as an input for the high cycle fatigue model to estimate the number of axle load cycles required for a detectable fatigue defect to propagate. The results are compared to nucleation life in the "defect-free" material to better understand how fast a fatigue crack can initiate from pre-existing flaws.

5.4.1 Stress Fields at Periphery of Defects

The evolution of von-Misses stresses in the vicinity of a defect is studied for the two critical cases shown in Figure 5.4. Figure 5.5 and Figure 5.6 illustrate the contour of von-Mises stresses near the web-to-base fillet defect and rail base defect, respectively. These figures correspond to an increment of time when the wheel load is right on top of the section (mid-cycle). von-Mises stress values near the blunt tip of the defect can be compared to those of a "defect-free" material shown in Figure 5.7.

For the case with a planar defect in the web-to-base fillet center, Figure 5.5 represents two small zones of high stress concentration near blunt tips of the defect on the rail surface, next to the weld. In this figure, the projection of von-Mises stresses into the vertical plane is shown on the top, while the projection of stresses into a transverse cut passing through the defect tip is presented on the bottom. A peak value of about 400 MPa

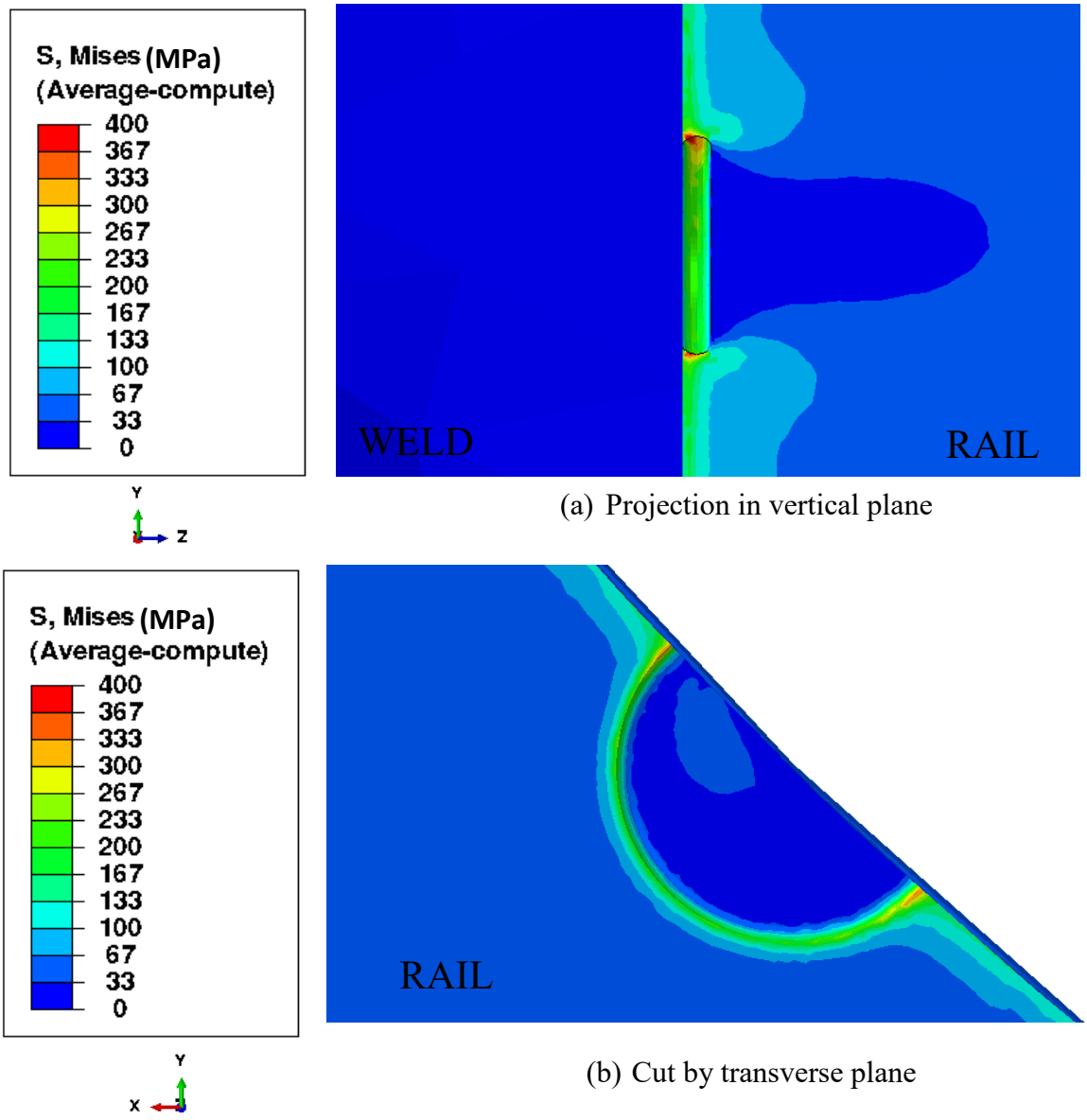

Figure 5.5. Contour of von-Mises stress at the periphery of a small planar defect located in the web-to-base fillet (MPa)

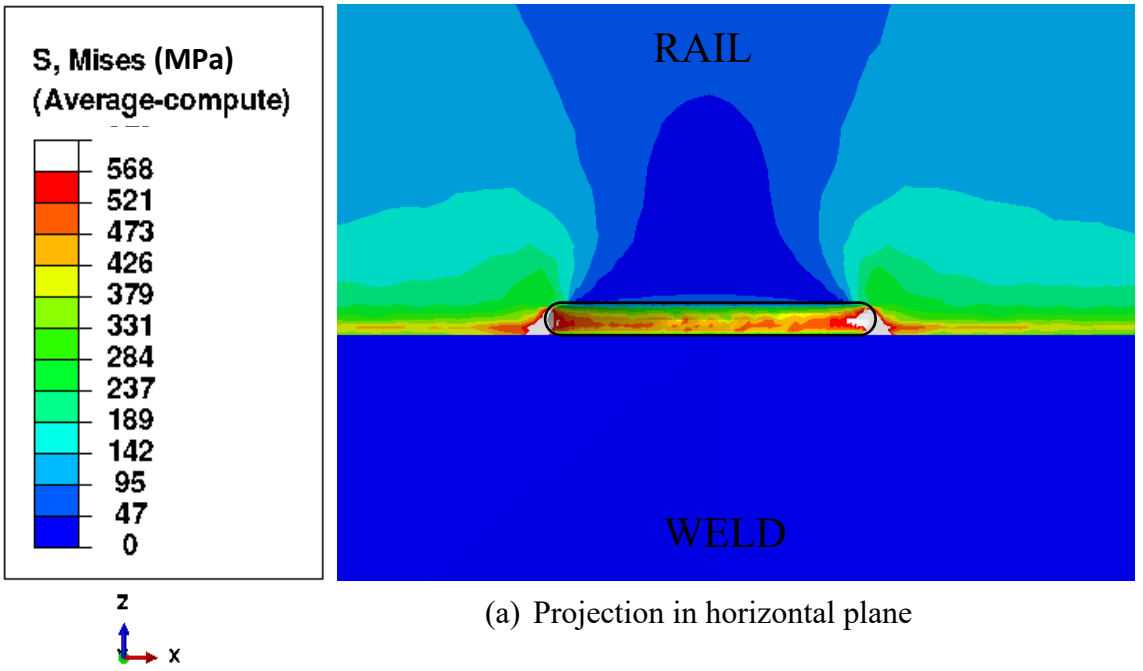

(a) Projection in horizontal plane

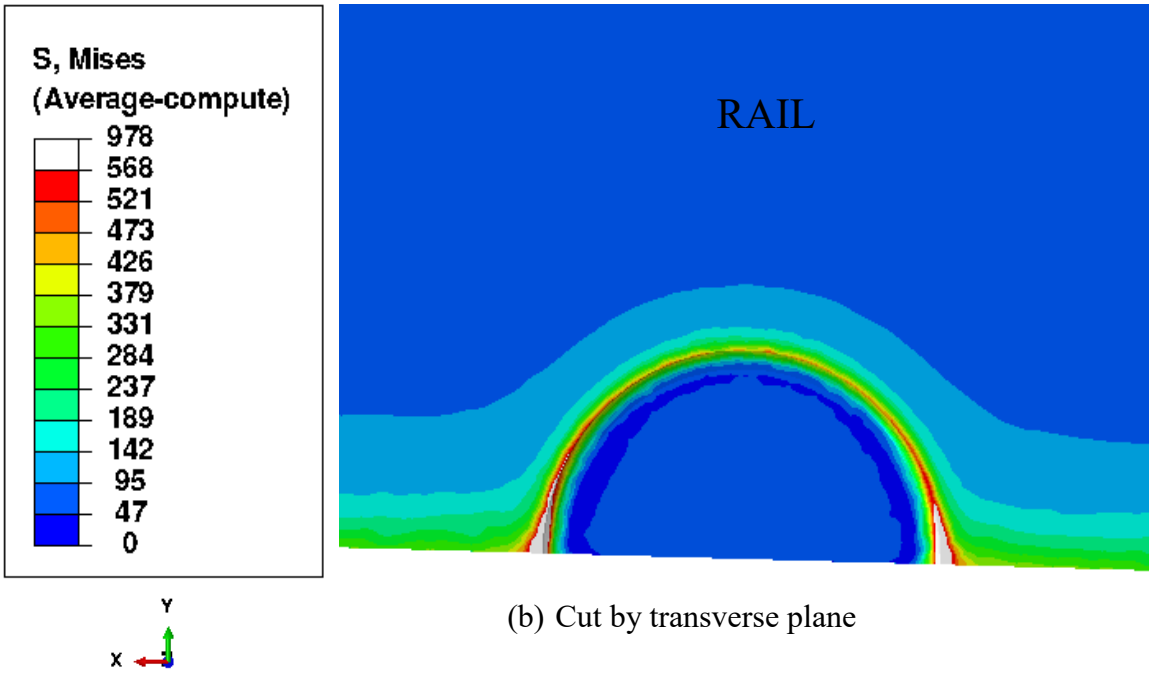

(b) Cut by transverse plane

Figure 5.6. Contour of von-Mises stress at the periphery of a small planar defect located in the rail base-center (MPa)

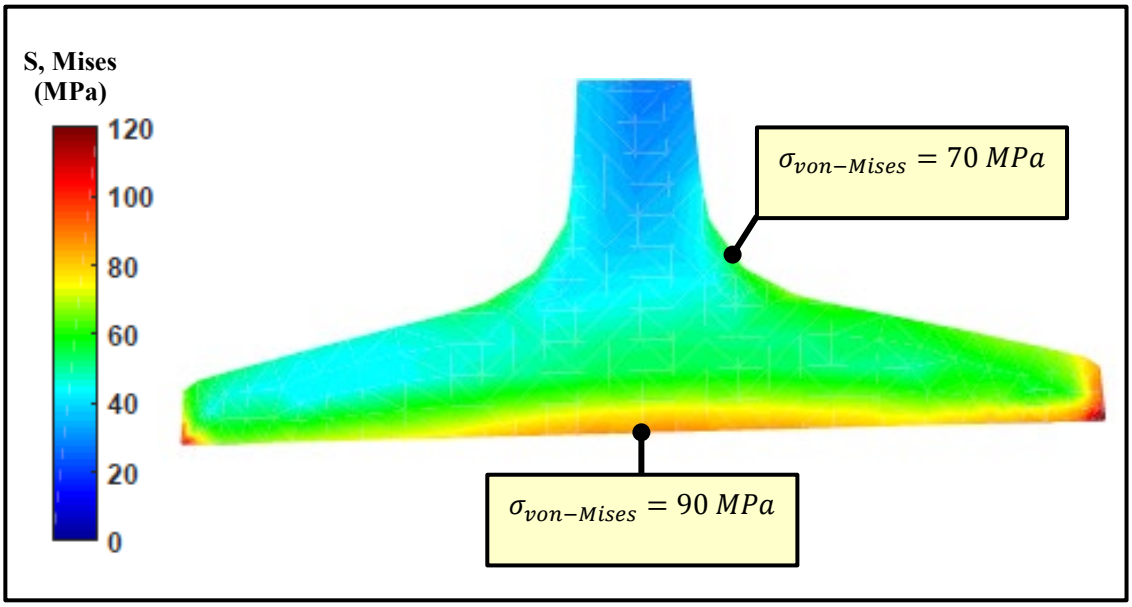

Figure 5.7. Contour of von-Mises stresses caused by the wheel loading in a "defect-free" material, (MPa)

is observed near the tip, on the surface. Therefore, it can be inferred that the defect acts as a stress concentrator which intensifies the stresses by a factor of 5.

Similar evolutions of effective stresses can be observed near the defect which is located in the base center, illustrated in Figure 5.6. However, the peak value of stress at the blunt tip of the defect is very large to the extent that it passes the yield strength limit of the thermite rail weld (568 MPa). Therefore, small localized plastic zones, with a radius of about 0.15 mm, will form near blunt tips which are shown in white in Figure 5.6. Severe stress concentrations may result from the fact that opposite faces of the base-center defect are subjected to large tensile stresses, caused by rail flexure, which make the crack to grow in mode I.

5.4.2 Fatigue Assessment at Periphery of Defects

The multi-axial critical plane fatigue algorithm developed in Matlab® is employed to assess the fatigue behavior in the vicinity of a surface defect that is initiated in the rail foot. The model uses Findley fatigue index to compute the fatigue damage. FE analysis is performed to calculate the time history of three-dimensional stress fields in the rail at the periphery of the defect. The solution does not consider interaction among defects or defect size effects. Since the solution depends on the elastic material behavior, if the von-Mises stress at any point on the periphery of a defect exceeds 568 MPa, then local stress fields at that defect are considered invalid for the fatigue nucleation life assessments.

Table 5.1 shows the estimated fatigue nucleation life near the blunt tip of a defect which is implemented in the center of the web-to-base fillet. Also, a comparison has been made between the fatigue nucleation life in a "defect-free" material, and the life to initiate incipient fatigue cracks from a pre-existing imperfection. As seen, the track service life is reduced to 5 MGT solely due to the presence of a small defect in the web-to-base fillet region of the rail. The fatigue life is even smaller if the defect is present in the rail base where flexural tensile stresses are at the peak. As mentioned earlier, the von-Mises stress will exceed the yield limit when a defect is located in the center of the rail base (see Figure 5.6). Therefore, the crack will continue to grow and fracture-mechanics based approaches are needed to predict the crack propagation.

Hence, the presence of defects in thermite rail welds will significantly deteriorate the integrity of the track. Consequently, regular inspection of the weld is necessary to prevent catastrophic rail breaks that can cause train derailments. In addition, it can be

inferred that fatigue nucleation and early growth may consume over 90% of the service life of high strength thermite rail welds and the life in the propagation stage is expected to be minimal.

Table 5.1. Assessment of fatigue performance near a defect located in the center of the web-to-base fillet

	Fatigue nucleation in defect-free material	**Fatigue nucleation from a pre-existing defect**
f_{FIN} **(MPa)**	40	234
N	9.14E+10	1.39E+05
MGT	3265832	5

5.5 Suggestions for Improving Fatigue Behavior of Thermite Rail Welds

This study shows that pre-existing defects are the major cause of the poor fatigue performance in the web and base region of thermite rail welds. Therefore, eradicating the weld defects (porosity and nonmetallic inclusions) would substantially improve the fatigue performance of thermite rail welds. In this regard, the manufacturing of the refractory sand molds needs to be modified, especially in the web-to-base fillet area, to reduce the formation of pores and trapped inclusions.

In addition, the results of the fatigue analysis suggest that it may only take a short period of time for fatigue cracks to propagate from detectable defects and cause catastrophic rail breaks. Therefore, regular inspection of web and base regions of thermite rail welds will enhance the track integrity and reduce the possibility of train derailments caused by broken welds.

Furthermore, the application of post-welding treatments such as Ultrasonic Impact Technology® (UIT) may be beneficial to improve the fatigue performance of termite rail welds. UIT seeks to minimize effects of stress risers at critical weld geometries by imparting localized compressive stresses to the weld collar-to-rail transition along the web, web-to-base fillet, and the base of the thermite weld.

5.6 Summary

- Small, half-penny shaped, surface defects with rounded edges are implemented to two critical locations of thermite rail welds from which most of the service failures are observed to initiate in the field: web-to-base fillet, and rail base center. Defects do not interact with each other.
- Stress fields at the periphery of defects, caused by wheel axle loads, are examined. High stress concentration zones are identified near the blunt tip of the defect. The magnification of stresses is larger when a defect is present at the rail base, next to the thermite weld.
- The fatigue nucleation life of incipient cracks which emanate from pre-existing defects is studied. It has been shown that the time required for fatigue cracks to

initiate from pre-existing defects is very short as compared to the fatigue crack nucleation life in a nominally "defect-free" material. Hence, it can be inferred that the presence of defects will significantly reduce the service life of thermite rail welds.

- It may take only a short period of time for fatigue cracks to initiate from detectable defects that are present in the web and base regions of the rail and cause failure. Regular inspection is the key to prevent such rail breaks that can result in catastrophic train derailments.

6. CONCLUSIONS AND FUTURE WORK

6.1 Conclusions

- In the rail foot, remote from the wheel-rail contact interface, the material behaves elastically. Therefore, high cycle fatigue failure is expected.
- Wheel rolling-contact effects are negligible in the rail foot region, and thus, each wheel can be replaced by a vertical concentrated load to save computational time and resources.
- The external geometry of the thermite weld collar acts as a stress-riser that magnifies stress fields in the weld zone, specifically next to the weld.
- Proper simulation of the track support is necessary to ensure the reliability of the simulation. Degraded support conditions can magnify the stress fields in the rail base by a factor of 2. Also, it is important to note that track foundations typically cannot resist tensile stresses. Otherwise, tensile stress fields in the rail base may be underestimated.
- Each train wheel passage generates a fatigue cycle in the foot region of thermite rail welds.
- The fatigue model of this study suggests that fatigue cracks are more likely to nucleate from rail base corners, under wheel rolling loads. Rail base center is the next critical location to start the fracture. The possibility of fatigue crack initiation in the web-to-base fillet is less than the other two critical locations.

- The fatigue model of this study predicts fatigue defects in the foot region of thermite rail welds tend to initiate in a transverse plane, perpendicular to the tensile axial stresses caused by flexure. Therefore, mode I cracking dominates, which is the most damaging mode of fracture.
- The fatigue model of this study estimates long fatigue-life for the foot region of thermite rail welds, under wheel loading, if the material is "defect-free". Therefore, the occurrence of premature service failures that are observed to initiate in the base and web region of rail is potentially attributed to either the presence of metallurgical discontinuities and weld imperfections or the formation of tensile thermal stresses. Note that the contribution of welding residual stresses may be damaging in the web-to-base fillet area where tensile residual stresses are probable. Hence, applying compressive stresses around the weld collar might improve the fatigue behavior of thermite welds.
- Cold rail temperatures resulting from winter weather can generate very large tensile stresses in continuously welded rails when the rail temperature falls too low. Axial tensile stresses caused by cold rail temperature are found to significantly accelerate the fatigue process in the rail foot. The influence of thermal variations seems to be more crucial in web-to-base fillet region of rail welds.
- The presence of small surface defects in the foot region of the rail HAZ, next to weld, is found to be the major cause of the poor fatigue performance in thermite rail welds. The fatigue nucleation life of incipient cracks which emanate from

pre-existing defects is shown to be very short as compared to the fatigue crack nucleation life in a nominally “defect-free” material. The stress field at the periphery of a defect is largely magnified. Results show a zone of high localized stress concentration near the blunt tip of the defect, especially for the case of a base-center defect where flexural tensile stresses are the largest.

- It may take only a short period of time for fatigue cracks to initiate from detectable defects that are present in the web and base regions of the rail and cause failure. Regular inspection is the key to prevent rail breaks which can result in catastrophic train derailments.

6.2 Future Work

An updated data set from fatigue experiments on pearlitic rail still is required to improve the reliability of the fatigue-life relation that correlates the Findley fatigue parameter to the fatigue life of the rail. In particular, the normal coefficient that represents the material sensitivity to the tensile-based damage mechanism has to be re-examined.

Actual fatigue-life data from field tests on thermite-welded rails is needed to validate, and consequently improve, the fatigue algorithm that is developed in this study.

The influence of residual stresses resulting from the welding procedure and/or rail fabrication process on the fatigue behavior of thermite rail welds should be incorporated into the fatigue analysis.

Measurements of the material discontinuities and imperfections in web, base, and web-to-base fillet regions of thermite rail welds can provide a valuable database to understand the nature of weld defects that form in the critical regions of the weld where most of the service failures are reported to occur. This data will help to improve the welding procedure to eliminate, or reduce, the formation of weld defects. This can also help to calibrate the fatigue simulations and improve the fatigue-life estimates.

REFERENCES

[1] Dick C.T., Barkan C.P.L, Chapman E.R., Stehly M.P., "Multivariate Statistical Model for Predicting Occurrence and Location of Broken Rails," Transportation Research Record 1825, Paper No. 03-3680, pp. 48-55, 2014.

[2] Hart R. N., "Thermit welding process," Lindsay Publications, Inc., Bradely, 1987.

[3] Gibert F., "Thermite-Welding of Rails: Old Recipe for Modern Track," Rail International, Vol 19, No 5, pp. 8-11, May 1988.

[4] Cheesewright, P.R., "The improvement of thermite weld reliability," Rail Technology: proceedings of a seminar, pp. 305, C.O. Frederick and David John Round ed., Nottingham, July 1983.

[5] Liu X., Saat M.R., Barkan C.P.L., "Analysis of Causes of Major Train Derailment and Their Effect on Accident Rates," Transportation Research Record: Journal of the Transportation Research Board, No. 2289, Transportation Research Board of the National Academies, Washington, D.C., pp. 154–163, 2012.

[6] Aldrich M., "The Peril of the Broken Rail: The Carriers, the Steel Companies, and Rail Technology," Technology and Culture, Vol. 40, pp. 263-291, 1999.

[7] Kristan, J., 'Thermite weld evaluations and developments," Railway Track and Structures, Vol 12, pp. 16, 2002.

[8] Lawrence F.V., Ross E.T., Barkan C.P.L., "Reliability of Improved Thermite Welds," IDEA Program Final Report, project HSR-41, Transportation Research Board, National Research Council, September 2004.

[9] Ailes A.S., “Modem Applications of Thermite welding, Part 1: Repairs to Heavy Sections,” Welding and Metal Fabrication, Vol 32, No 9, 1964.

[10] Habashi F., “Metallothermic Reactions - Past, Present and Future,” Res Rep Metals Vol 2, No 1, 2018.

[11] Goldschmidt Thermit Company, “Reactions: A Quarterly Publication Devoted To The Science Of Aluminothermics,” Volume 7, Issue 1, first quarter, 1914.

[12] Belitkus D., “Aluminothermitic production of metal and alloys,” Journal of Metals, Vol 24, 1972.

[13] Samans C.H., Engineering Metals and Their Alloys, New York: Macmillan company, 1949.

[14] Goldschmidt H., Vautin, C., "Aluminium as a Heating and Reducing Agent," Journal of the Society of Chemical Industry, Vol 6, No 17, pp. 543–545, 1898.

[15] Steele R.K., “Field welding of rails,” Association of American Railroads Technical Center, Chicago, Report Number R-618, 1985.

[16] Sih G.C., Tzou D.Y., “Rail-End Bolt Hole Fatigue Crack in Three Dimensions,” Theoretical and Applied Fracture Mechanics, Vol 3, pp. 97–111, 1985.

[17] Mayville R.A., Hilton P.D., “Fracture Mechanics Analysis of Rail-End Bolt Hole Crack,” Theoretical and Applied Fracture Mechanics, Vol 1, pp. 51–60, 1984.

[18] Lonsdale C.P., "Thermite Rail Welding: History, Process Developments, Current Practices and Outlook for the 21st Century," September 1999.

[19] Archdeacon H.C., “The Track Cyclopedia,” Simmons-Boardman Books, Omaha, NE, pp. 170, 1985.

[20] Hauser, D., "Welding of Railroad Rails-A Literature and Industry Survey," Rail Steels-Developments, Processing and Use, (ASTM Special Technical Publication 644), Edited by D.H. Stone and G.G. Knupp, pp. 118-144, American Society for Testing and Materials, Philadelphia, PA., 1978.

[21] Masubuchi K., "Review of Rail Welding," Proceedings of railroad rail welding, Memphis, Nov.29-30,1983.

[22] Abbott H.L., "Flash Welding of Continuous Welded Rail," Rail Technology: proceedings of a seminar, Charles O. Frederick and David I. Round, ed. Nottingham, pp. 41, July 1983.

[23] Moin, E., "Flash Butt Welding of Premium rails and Stick Weld Repair of Rail End Batters," Proceedings of Railroad Rail Welding, Memphis, November 1983.

[24] Oishibashi, Hirotsugu, Katsuyoshi Ueyama and Muneyuki Ohara, "Gas Pressure Welding of Rails in Japan," Proceedings of Railroad Rail Welding, Memphis, November 1983.

[25] Meric, Cevdet and Turgut Engez, "Understanding the Thermite Welding Process," Welding Journal 1, pp. 33, 1999.

[26] Hay W., William. Railroad engineering, 2nd edition, New York: John Wiley & Sons, 1982.

[27] Lonsdale C.P., Lewandowski JJ., "Fracture toughness of thermite rail weld steel," 39th MWSP Conf. Proc., ISS, Vol, XXXV, Indianapolis, pp. 1083, 1998.

[28] Thermit® Welding Procedures. NJ: Orgo-Thermit, Inc., 2001.

[29] Chen Y., Lawrence F.V., Barkan C.P.L , Dantzig J.A., “Heat transfer modelling of rail thermite welding,” Proceedings of the Institution of Mechanical Engineers: Journal of Rail and Rapid Transit, Part F, Vol 220, pp. 207-217, 2006.

[30] Chen Y., Lawrence F.V., Barkan C.P.L , Dantzig J.A., “Weld defect formation in rail thermite welds,” Proceedings of the Institution of Mechanical Engineers: Journal of Rail and Rapid Transit, Part F, Vol 220, pp. 373-384, 2006.

[31] Dick C.T., “Factors Affecting the Frequency and Location of Broken Railway Rails and Broken Rail Derailments,” MS Thesis, University of Illinois at Urbana-Champaign, 2001.

[32] Sawley K., Reiff R., “Rail Failure Assessment for the Office of the Rail Regulator,” Pueblo: TTCI, AAR, 2000.

[33] Myers J., Geiger G.H., Poirier D.R., “Structure and Properties of Thermite Welds in Rails,” Welding Research Supplement, pp. 258-268, August 1982.

[34] Pickering F.B., “Physical Metallurgy and the Design of Steels,” London: Applied science publishers, LTD, 1978.

[35] Schroeder L.C., Poirier D.R., ‘The mechanical properties of thermite welds in premium alloy rails,” Materials Science and Engineering, 63, pp. 1-21, 1984.

[36] Key A.J., “The Thermit® process for rail welding,” Metal Construction, pp. 419-422, 1984.

[37] Schroeder L. C., Poirier D. R., “Thermite Rail Welds; The Process, Mechanical and Metallurgical Properties, and Possible Improvements,” Railroad Rail Welding, Proceedings of the Rail Welding Symposium, Memphis, TN, Railway Systems and

Management Association, Northfield, NJ, pp. 21-59, November 1983.

[38] Pavlina E.J. and Van Tyne C.J., “Correlation of Yield Strength and Tensile Strength with Hardness for Steels,” J of Materials Engineering and Performance, Vol 17, pp. 888-893, 2008.

[39] Webster P.J., Mills G., Wang X.D., Kang W.P., Holden T.M., “Residual Stresses in Alumino-Thermic Welded Rails,” Journal of Strain Analysis, Vol 32, pp. 389-400, 1997.

[40] Webster P. J., Wang X. D., Mills, G., “Problems with railway rails,” In NATO Advanced Research Workshop on Measurement of Residual Stress Using Neutron Diffraction, Oxford, pp. 517–524, March 1991.

[41] Skyttebol A., Josefson B.L., Ringsberg J.W., “Fatigue crack growth in a welded rail under the influence of residual stresses,” Eng Fracture Mechanics, Vol 72, pp. 271–85, 2005.

[42] Khodabakhshi B., Paradowska A., Ibrahim R., Mutton P., “Measurement of Residual Stresses in Aluminothermic Rail Welds Using Neutron Diffraction Technique”, Materials Science Forum, Vol 777, pp. 237-242, 2014.

[43] Chen Y., “A Heat Transfer Modeling Study of Rail Thermite Welding,” Ph.D. Dissertation, University of Illinois at Urbana-Champaign, 2004.

[44] Kapoor A., "A re-evaluation of the life to rupture of ductile metals by cyclic plastic strain," Fatigue Fract Engng Mater Struct, Vol 17, pp. 201-219, 1994.

[45] Fry G.T., “A fatigue model for thermite rail welds,” Ph.D. Thesis, University of Illinois at Urbana-Champaign, 1995.

[46] Ekh M., Johansson A., Thorberntsson H., Josefson B.L., "Models for cyclic ratchetting plasticity - Integration and calibration," Journal of Engineering Materials and Technology, Trans ASME, Vol 122, pp. 49-55,2000.

[47] Jiang Y., "Three-dimensional elastic-plastic stress analysis of rolling contact," Journal of Tribology, Trans ASME, Vol 124, pp. 699-708, 2002.

[48] Tangtragulwong P., "Optimal railroad rail grinding for fatigue mitigation," Ph.D. Dissertation, Department of Civil Engineering, Texas A&M University, 2010.

[49] Norfolk Southern Railroad private communication (taken from [8]).

[50] Lawrence F.V., Cyre J.P., and Barkan C.P.L., "Improved Reliability of Thermite Field Welds Used on High Speed Rail Lines," IDEA Program Final Report, project HSR-24, Transportation Research Board, National Research Council, September 2003.

[51] Johnson K.L., "Contact mechanics," Cambridge: Cambridge University Press, 1987.

[52] Jiang Y., Sehitoglu H., "Rolling contact stress analysis with the application of a new plasticity model," Wear, Vol 191, pp. 35-44, 1996.

[53] Sluz A., Kish A., Read D., "Factors Affection Neutral Temperature Changes in Continuous Welded Rail," AREMA conference proceedings, 1999.

[54] Zerbst U., Lundén R., Edel K.-O., Smith R.A, "Introduction to the damage tolerance behaviour of railway rails – a review," Engineering Fracture Mechanics, Vol 76, pp. 2563-2601, 2009.

[55] ABAQUS/CAE® 6.14, Dassault Systemes Simulia Corp., Providence, RI, 2014.

[56] Desai C.S, Siriwardane A.M., "Numerical models for track support structures,"

Journal of Geotechnical Engineering Division, ASCE 108, pp. 461–480, 1982.

[57] Kiani M., "Multi-Scale Fatigue Damage Life Assessment of a Railway While Using a Critical-Plane Model," Ph.D. Dissertation, Texas A&M University, College Station, Texas, 2017.

[58] Ekberg A., Kabo E., "Fatigue of railway wheels and rails under rolling contact and thermal loading - an overview," Wear, Vol 258, pp. 1288-1300, 2005.

[59] Ringsberg J., Bjarnehed H., Johansson A, Josefson B., "Rolling contact fatigue of rails - finite element modelling of residual stresses, strains and crack initiation," IMechE, Part F, J. Rail Rapid Transit, Vol 214, pp. 7-19, 2000.

[60] Bower A.F., Johnson K.L., "Shakedown, residual stress and plastic flow in repeated wheel-rail contact," Rail quality and maintenance for modern railway operation: International Conference on Rail Quality and Maintenance for Modern Railway Operation, Kluwer Academic Publishers, pp. 239-252, 1992.

[61] Fry G.T, "A modified rail thermite welding procedure," Master's Thesis, University of Illinois, Urbana, 1992.

[62] Li D., White D., Ahmadian M., El-Sibaie M., "Distribution of Dynamic Wheel/Rail Forces Under Heavy Axle Loads," FRA Report, December 1998.

[63] Love A. E. H., "A treatise on the mathematical theory of elasticity," Cambridge University Press, 1927.

[64] Bannantine J., Comer J., Handrock J., "Fundamentals of metal fatigue analysis," Upper Saddle River, NJ: Prentice Hall, 1990.

[65] Smith R. A., "The wheel-rail interface - some recent accidents," Fatigue and Fracture

of Engineering Materials and Structures, Vol 26, No. 10, pp. 901-907, 2003.

[66] Ekberg A., "Rolling contact fatigue of railway wheels," Ph.D. Thesis, Department of Solid Mechanics, Chalmers University of Technology, Goteborg, 2000.

[67] Ekberg A., Marais J., "Effects of Imperfections on Fatigue Initiation in Railway Wheels," Journal of Rail and Rapid Transit, Vol 214, pp. 45-54, 2000.

[68] Kiani M., Fry G.T., "Fatigue analysis of railway wheel using a multiaxial strain-based critical-plane index," Fatigue & Fracture of Engineering Materials & Structures, Vol 41, pp. 412-424, 2018.

[69] Gutscher D., AAR Rail Welding Research – Recent Developments, Transportation Technology Center Inc.

[70] Garud Y.S., "Multiaxial fatigue- A survey of the state of the art," Journal of Testing and Evaluation, Vol 9, pp. 165-178, 1981.

[71] Jiang Y., Hertel O., Vormwald M., "An experimental evaluation of three critical plane multiaxial fatigue criteria," International Journal of Fatigue, Vol 29, pp. 1490-1502, 2007.

[72] Karolczuk A., Macha E., "A review of critical plane orientations in multiaxial fatigue failure criteria of metallic materials," Int J Fracture, Vol 134, pp. 267-304,2005.

[73] Findley W.N., "A theory for the effect of mean stress on fatigue of metals under combined torsion and axial load or bending," Journal of Engineering Industry, Trans ASME, Vol 81, pp. 301-306, 1959.

[74] Socie D.F., "Critical plane approaches for multiaxial fatigue damage assessment," American Society of Testing and Materials, ASTM STP 1191. Ann Arbor, MI, pp. 7–

36, 1993.

[75] Kaufman R.P., Topper T., "The influence of static mean stresses applied normal to the maximum shear planes in multiaxial fatigue," Biaxial/Multiaxial Fatigue and Fracture, Parma, Italy: Elsevier and ESIS, pp. 123-143,2003.

[76] Dang Van K., Cailletaud G., Flavenot J.F., Le Douaron A., Lieurade, H.P. "Criterion for high cycle failure under multiaxial loading," In: Biaxial and multiaxial fatigue, London, UK: Mechanical Engineering Publications, pp. 459-478, 1998.

[77] Socie D.F, Marquis G.B., Multiaxial fatigue, Warrendale, PA: Society of Automotive Engineers, 2000.

[78] Brown M.W., Miller K.J., "A theory for fatigue failure under multiaxial stress-strain conditions," Proceedings of the Institute of Mechanical Engineers, Vol 187, pp. 745-755, 1973.

[79] Fatemi A., Socie D.F., "A critical plane approach to multiaxial fatigue damage including out-of-phase loading," Fatigue & Fracture of Engineering Materials & Structures, Vol 11, pp. 149-165, 1988.

[80] Marquis G.B., Socie D.F., "Multiaxial fatigue," In: Comprehensive Structural Integrity, pp. 221–252, 2007.

[81] Mcdowell D.L., Stahl D.R., Stock S.R., Antolovich S.D., "Biaxial path dependence of deformation substructure of type-304 stainless-steel," Metall trans A – Phys Metall Mater Sci, Vol 19, pp. 1277-1293, 1988.

[82] Hayhurst D.R., Leckie F.A., McDowell D.L., "Damage growth under nonproportional loading," ASTM STP, Vol 853, pp. 688-699, 1985.

[83] Iwafuchi K., Satoh Y., Toi Y., Hirose S., “Fatigue property analysis of rail steel based on damage mechanics,” Quarterly Report of RTRI, Vol 45, pp. 203-209, 2004.

[84] Scutti J.J., Pelloux R.M., Fuquen-Moleno R., “Fatigue behavior of a rail steel,” Fatigue Fract Eng Mater Struct, Vol 7, pp. 121-135, 2007.

[85] Ahlström J., Karlsson B., “Fatigue behaviour of rail steel--a comparison between strain and stress controlled loading,” Wear, Vol 258, pp. 1187-1193, 2005.

[86] Stadlbauer W., Werner E., “Zyklisch-plastisches Verhalten von un- und niedriglegierten Kohlenstoffstählen (in German),” BHM Berg- und Hüttenmännische Monatshefte, Vol 144, pp. 356-361, 1999.

[87] Fry G.T., Fatigue bending tests of rail steels (Internal communication), 2018.

[88] Sih G.C., Handbook of stress intensity factors, Bethlehem, Pennsylvania: Institute of Fracture and Solid Mechanics, Lehigh University, 1973.

[89] Sack R.A., “Extension of Griffith's theory of rupture to three dimensions,” in Proceedings of Physical Society, London, Vol 58, 1946.

[90] Sneddon I.N., “The distribution of stress in the neighborhood of a crack in an elastic solid,” in Proc. Roy. Soc., London, Vol 187, 1946.

[91] Jungwon Seo, Seokjin Kwon, Hynukyu Jun, Donghyeong Lee, “Fatigue crack growth behavior of surface crack in rails,” Procedia Engineering, Vol 2, pp. 865-872, 2010.

[92] Desimone H., Beretta S., “Mechanisms of mixed mode fatigue crack propagation at rail butt-welds,” International Journal of Fatigue, Vol 28, pp. 635-642, 2006.

[93] Bartera S., Molenta L., Goldsmitha N., Jones R., “An experimental evaluation of fatigue crack growth,” Engineering Failure Analysis, Vol 12, pp. 99-128, 2005.